Enhancing projections of sea-level rise with changing seasonality for the Northwest European Shelf for 2023 to 2053.

DAISY FREDA JOSEPHINE LEE-BROWNE

Enhancing projections of sea-level rise with changing seasonality for the Northwest European Shelf for 2023 to 2053

Abstract

Sea-level rise is a primary damaging aspect of climate change, with potentially major consequences for coastal communities globally. In response to this, there has been a significant research effort into past and present patterns of sea-level change over multiple temporal and spatial scales to inform projections of future sea-level rise. While numerous studies have concentrated on global sea-level projections, there is a demand for more focused projections at the regional level. Existing work that seeks to project regional sea-level change has typically been limited by the complexity of regional climatic and atmospheric processes, and the difficulty of resolving these processes at relevant spatial scales within climate models. Finding alternative methods to resolve components at small enough temporal and spatial scales is therefore relevant to furthering our ability to project regional sea-level change. In this thesis, an approach is proposed and carried out to make projections of sea-level change for the Northwest European Shelf (NWES) between 2023-2053 at seasonal time steps and quantify the uncertainties related to each component of the projection. A novel aspect of the approach is the use of observed atmospheric-oceanic relationships to quantify the seasonal component of sea-level change, which, for the NWES, is strongly related to the North Atlantic Oscillation. Projections were made for 11 tide gauge locations across the NWES. Results show a set of robust projections that predict seasonal amplitudes between ± 0.1 m to ± 0.4 m. Across the 11 sites, projections are in line with SLC from observed sea-level data and existing projections of dynamic sea-level change. The uncertainties on the projections reflect uncertainty associated with the data used, assumptions within the methodology, and inherent variability present in the climate system. Overall, the approach demonstrated in the study is a novel way of projecting sea-level change over fine temporal and spatial scales.

Enhancing projections of sea-level rise with changing seasonality for the Northwest European Shelf for 2023-2053

Daisy Lee-Browne

Thesis submitted for the degree of MSc by Research

Department of Geography

Durham University

November 2023

Table of Contents

List of Figures

List of Tables

List of Equations

List of Abbreviations

AGCM	Atmospheric General Circulation Model
AMOC	Atlantic Meridional Ocean Circulation
AR	Assessment Report
CESM	Community Earth System Model
CMIP	Coupled Model Intercomparison Project
CRU	Climate Research Unit
DSLC	Dynamic sea-level change
ECMWF	European Centre for Medium-Range Weather Forecasts
ENSO	El Niño Southern Oscillation
ERA5	ECMWF Reanalysis v5
GCM	General Circulation Models
GMSL	Global mean sea level
HAMSOM	Hamburg Shelf Ocean Model
IB	Inverse Barometer
IOD	Indian Ocean Dipole
IPCC	Intergovernmental Panel on Climate Change
KNMI	Royal Netherlands Meteorological Institute
MMLEA	Multimodel Large Ensemble Archive
MSL	Mean sea level
NAO	North Atlantic Oscillation
NWES	Northwest European Shelf
PSMSL	Permanent Service for Mean Sea Level
RCM	Regional Climate Model
RCP	Representative Climate Pathway
RLR	Revised Local Reference
ROMS	Regional Ocean Models
SE	Standard error
SLA	Sea-level anomaly
SLC	Sea-level change
SSP	Shared Socioeconomic Pathway
SST	Sea surface temperature
TG	Tide gauge
UKESM	UK Earth System Modelling
VLM	Vertical land motion

Statement of Copyright

Acknowledgments

Firstly, I would like to thank Dr Luke Jackson, Dr Sophie Williams and Professor Pippa Whitehouse for their incredible guidance, patience and knowledge throughout the completion of this thesis. Luke – your genuine enthusiasm for science is infectious and working with you over the last two years or so has been an amazing experience. You have truly shaped my interest in sea-level and climate science and I cannot thank you enough for your unrelenting support in what has been a challenging but rewarding year. Sophie – your knowledge, shared experience and belief in me has been invaluable throughout this year, thank you. Pippa – from sitting in your 1st year lectures to now, I feel very lucky to have worked with you and you have taught me so much, within and outside of academia.

A massive thank you goes to my incredible friends for being so supportive throughout this process. Finally, thanks go to my family for their love and everything they have done to support me, this year and always.

Chapter 1: Introduction

1.1 Importance of sea-level rise

Sea-level rise (SLR) over the 20th and 21st centuries is a major consequence of anthropogenic climate change (Fox-Kemper *et al.*, 2022). The rate of global mean sea level (GMSL) rise over the 20th century is estimated at around 1.6 ± 0.4 mm year^{-1}, and this rate is expected to accelerate in the future as rates of ice sheet melt increase with rising global temperatures (Nerem *et al.*, 2018; Dangendorf *et al.*, 2019). Regional sea level is also changing, but differs from the global rate due to local climatic and oceanographic processes, such as modes of climate variability and dynamic variations in ocean circulation (Stammer *et al.*, 2013; Kopp *et al.*, 2015; Gregory *et al.*, 2019). The resulting economic and social impacts of SLR on coastal communities and ecosystems will be costly, predominantly through increasingly frequent and catastrophic inundation as a result of tidal flooding and storm surges on top of a rising baseline sea level (Vousdoukas et al., 2018).

Predicting how sea level is going to change in the future, both globally and regionally, is critical to managing the effects of SLR for exposed coastlines. Existing projections of GMSL suggest different rates of SLR depending on the rate at which greenhouse gas emissions rise over the next century and beyond. The global projections provided as part of the most recent Intergovernmental Panel on Climate Change (IPCC) Assessment Report 6 (AR6) project rising GMSL based on different socio-economic scenarios, termed Shared Socio-economic Pathways (SSPs). In AR6, the SSPs are paired with the radiative forcing scenarios established in AR5, termed Representative Concentration Pathways (RCPs) to give projections for a socio-economic and radiative forcing combination (Eyring *et al.*, 2016). These projections are consistent with those from the Special Report on the Ocean and Cryosphere in a Changing Climate (SROCC), which projected likely GMSL rise of 0.41 (0.26–0.56) m and 0.81 (0.58–1.07) m under RCP2.6 and RCP8.5 respectively, over the same period (Oppenheimer *et al.*, 2019). AR6 projections are higher than those of AR5, which projected likely GMSL rise of 0.41 (0.25–0.58) m under RCP2.6 and 0.71 (0.49–0.95) m under RCP8.5 (Church *et al.*, 2013). Alongside the process-based projections provided in IPCC assessment reports, there are a range of other global and regional projections available that use a variety of methodologies and approaches. This includes implementations of process-based methods to make probabilistic projections (Grinsted *et al.*, 2015; Jackson and Jevrejeva, 2016; Le Bars *et al.*, 2017) and possibilistic projections (Le Cozannet *et al.*, 2017), as well as use of the semi-empirical approach (Kopp *et al.*, 2016; Mengel *et al.*, 2016; Jackson *et al.*, 2018).

The majority of these projections currently focus on decadal timescales with an emphasis on end-of-century and multi-century horizons. Although numerous components of sea-level change (SLC) respond over long time periods (e.g. thermal expansion, ice sheet melt), it is clear that atmosphere-ocean interactions also drive sea-level variability on much shorter timescales (Boening *et al.*, 2012; Ferrero *et al.*, 2021). This variability can be largely attributed to fluctuations in large-scale climate oscillations such as the El Niño Southern Oscillation (ENSO), the North Atlantic Oscillation (NAO) and the Indian Ocean Dipole (IOD). The sea-level signals resulting from these oscillations can have significant amplitudes and have the potential to persist over multiple months (Miles *et al.*, 2014). Within projections, these signals contribute to amplified levels of seasonal SLC and significant uncertainty in the short term. The uncertainty contribution is demonstrated in recent projections of SLC for the UK coastline, which show that over the next decade, uncertainty from internal variability will dominate over uncertainties arising from emission scenarios and model structure (Palmer *et al.*, 2018). At sub-annual to multi-annual timescales when climate forcing plays a lesser role in sea-level projection uncertainty than natural variability, it is therefore important to characterise the drivers of internal variability so that short-term projections can be improved (Marcos *et al.*, 2017; Carson *et al.*, 2019).

1.2 Projecting seasonal sea-level change

At present, there is a gap between short-term weather forecasts spanning days to weeks and climate projections spanning decades to centuries. Current projection methods and frameworks struggle to make projections of sub-annual to multi-annual SLC, mainly because the current generation of Global Climate Models (GCMs) operate at spatial resolutions typically too coarse to capture the fine-scale climate and ocean processes that operate at sub-annual timescales (Jevrejeva *et al.*, 2020). The result is that seasonal variations are not included in annual to decadal projections or the uncertainties. Modelling studies have only recently begun to address this issue, and one of the primary approaches has been to use dynamic downscaling. This technique uses a regional climate model (RCM) to refine the output of a GCM at a higher spatial resolution, which helps resolve climate processes and sea-level variability at the appropriate spatial scale to make seasonal projections of SLC (Tinker *et al.*, 2018, 2020). Examples include downscaled simulations of ocean dynamic sea-level change (DSLC) on the NWES (Hermans *et al.*, 2020, 2022).However, using models in this way is computationally expensive and the output is still subject to uncertainties associated with the representation of physics within the model.

The limitations associated with using large-scale climate models means alternative approaches to making projections of future seasonal SLC have been developed. They typically involve data-driven methods which use time-series analysis and machine learning (Krivec *et al.*, 2021; Nieves *et al.*, 2021; Song *et al.*, 2023). Another approach, proposed by this study, involves taking a sea-level 'budget' approach and using it to generate region-specific projections. By isolating the relevant sea-level components for a particular region at their various timescales and combining them to formulate a projection at a sub-annual level, a short-term projection of sea level can be generated, along with the uncertainties of each component. As the focus here is on sub-annual timescales and changes linked to climate oscillations, the relevant components will change from region to region depending on the dominant climate oscillation and the resulting physical atmospheric-oceanic processes driving SLC in that region. The approach used in this study utilises several sources of data, including existing projections of SLC alongside observations of sea level from tide gauge (TG) data or from satellite altimetry. These data sources can be used, in combination with observed relationships between sea level and climate variables, for multiple locations within a region, to estimate future changes in SLC.

The proposed approach draws on existing methods of making projections. By isolating the physical components relevant to a region and utilising observed atmospheric-oceanic relationships, the method draws on the concepts of process-based and semi-empirical approaches. Process-based models, such as the GCMs used within Coupled Model Intercomparison Project (CMIP) projections, simulate appropriate components of sea level and combine them within a sea-level model to produce a projection, whilst the semi-empirical approach combines statistical models with observed relationships to estimate future changes.

The budget-based method described below is used to make projections for the Northwest European Shelf (NWES) region. The NAO has been shown to be the dominant driver of sub-annual to decadal sea-level variability over the NWES through an extensive amount of research (Wakelin *et al.*, 2003; Dangendorf *et al.*, 2013; Tinker *et al.*, 2020), and there is also good data availability from TGs. These factors make the NWES an appropriate region in which to make projections using this novel approach. Projections are made for the 30-year period from 2023-2053 to address the effect of seasonality during a period where there is less scenario-dependence within projections.

1.3 Thesis Aims and Objectives

1.3.1 Aim

The aim of this study is to use the proposed sea-level 'budget' approach to make projections of SLC at seasonal time steps, and quantify the uncertainties related to each component in the budget for the period 2023-2053.

1.3.2 Research objectives

The aim will be achieved through the following objectives:

1. Assess the impact of data gaps and low data availability in tide gauge records on identifying relationships between sea level and the NAO, using the long tide gauge record from Den Helder.
2. Analyse and quantify the relationship between sea level and the NAO over the observational period 1950-2021.
3. Define and project the relevant sea-level components and their uncertainties using a combination of modelled and observed data sources to produce seasonal projections of SLC across the NWES.

1.4 Study area

The NWES region is a large area of shallow, temperate water which consists of multiple seas and channels including the North Sea, the English Channel, the Malin/Hebrides Shelf seas, the Irish Sea and the Bay of Biscay. The shelf region is mostly between 100 and 150 m in depth and meets the adjacent North Atlantic via a steep shelf gradient, resulting in oceanographic conditions that are very different between the Atlantic Ocean and the shelf (Huthnance *et al.*, 2022). Some areas of the NWES are dominated by large tidal variability. The shelf is dominated by semidiurnal tidal constituents (M2 and S2), whilst the tidal range differs across the shelf (Uehara *et al.*, 2006). The UK coastline, Irish Sea and Celtic Sea experience macrotides (tidal range exceeding 4 m). This includes areas with some of the largest tides globally, such as Avonmouth in the Bristol Channel which has a spring tidal range of >14 m (Pelling *et al.*, 2013). The western side of the North Sea is meso-tidal (between 2 m and 4 m range) and the eastern side of the North Sea, including the Norwegian coastline and the German Bight, is micro-tidal with a reduced range of less than 2 m (Gerkema, 2019).

A large number of TG records are available for the NWES region; for the purpose of this study 11 were selected to cover the main sub-regions across the shelf (Figure 1.1 and Table 1.1).

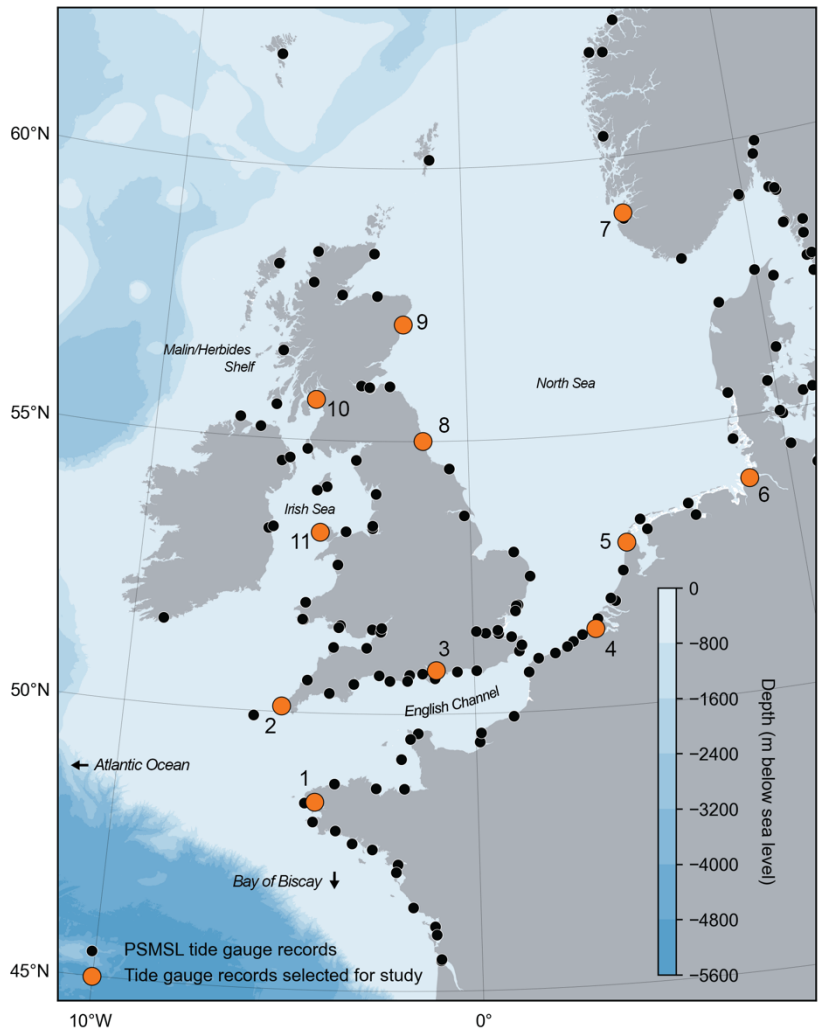

Tide gauge	PSMSL ID	Number on map
Brest	1	1
Newlyn	202	2
Portsmouth	350	3
Vlissingen	20	4
Den Helder	23	5
Cuxhaven2	7	6
Stavanger	47	7
North Shields	95	8
Aberdeen I	361	9
Millport	755	10
Holyhead	5	11

Figure 1.1: The study area and location of tide gauges in the NWES. Tide gauges used in the study are numbered and named in the table, along with their respective PSMSL ID number.

NWES region	Tide gauges in region
Atlantic margin/Bay of Biscay	1, 2
Malin/Hebrides shelf	10
Irish Sea	11
English Channel	3
North Sea	4, 5, 6, 7, 8, 9

Table 1.1: NWES sub-regions and the corresponding tide gauges in each region.

Sub-regions were identified using regions loosely defined in existing studies that use the NWES as a study location (Wakelin *et al.*, 2012; Legge *et al.*, 2020), based on variations in shelf bathymetry and changes in the dominant physical processes (Neill *et al.*, 2016). The shelf slope is steep in the south around the Bay of Biscay and becomes less steep north towards the Malin/Hebrides shelf (Huthnance *et al.*, 2022). Both the Bay of Biscay and Malin Seas are open to the shelf boundary with the Atlantic Ocean. The English Channel increases in depth towards the shelf edge and connects the North Sea and the Bay of Biscay. The North Sea is shallower in the south and southeast (depth less than 50 m below 55°N) and deeper to the north (Uehara et al., 2006).

The NWES is an area where regional changes in sea level have been well-studied, over multi-annual and sub-annual timescales. At the multi-annual timescale there are a number of studies focused on mean sea level (MSL) variations throughout the 20th century, along specific coastal stretches. For instance, Wahl *et al.* (2013) used 30 TG records to estimate an average MSL rise of 1.5 ± 0.1 mm/yr in the North Sea from 1900 to 2011. Similarly, Woodworth *et al.* (2009) estimated a MSL increase of 1.4 ± 0.2 mm/yr along the UK coastline over 1901-2009.

Sea-level variability at multi-decadal time steps has also been analysed; Frederikse and Gerkema (2018) quantified low-frequency variations present in seasonal deviations from annual MSL over decadal timescales for the North Sea, using monthly sea-level data from 33 TGs. They found variability was stronger over winter and autumn than in spring and summer driven primarily by changes in wind and atmospheric pressure. These changes were largely linked to large-scale atmospheric patterns, such as the NAO and the Scandinavia Pattern. Across the region, multi-decadal seasonal variability was found to be of a similar magnitude to long-term trends in MSL. Earlier research has also suggested that a proportion of decadal-scale variability that affects the NWES is a response to a large coherent signal present along the European Atlantic coastline (Sturges and Douglas, 2011; Calafat *et al.,* 2012). This signal has been shown to be linked with wind-stress driven coastally trapped waves, which are a major contributor to the propagation of the signal into the North Sea. The amplitude of decadal fluctuations is generally shown to be smaller than that of higher-frequency bands at ± 15 cm (Frederikse and Gerkema, 2018), but can still cause MSL to exceed global MSL for several years at a time.

Variability on shorter timescales typically expresses stronger spatial patterns and higher magnitudes relative to MSL than longer, decadal scale variability. The southeastern region of the North Sea in particular experiences large variability of up to ± 60 cm for intra and interannual timescales (Dangendorf

et al., 2014) and between 20-29 cm for the annual MSL cycle (Dangendorf *et al.*, 2012). Wind stress is the biggest driver of variability in this region (Wakelin *et al.,* 2003). Variability is smaller in amplitude along the UK and Norwegian coastlines and is more dominantly linked to changes in pressure rather than wind stress (Wahl *et al.,* 2013). Overall, high-frequency variability on the NWES is atmospherically driven, with a much lower contribution from steric change (Chen *et al.*, 2014).

Large sections of the NWES coastline are highly vulnerable to the effects of rising sea levels. The coastal zone around mainland Europe and parts of the UK coastline includes extensive regions of very low topographic gradients which creates ideal conditions for inundation and further exposure to coastal hazards. These low coastal zones are heavily populated and economically important; as well as the ~50 million people who live in the low elevation coastal zone (McEvoy *et al.*, 2021) a significant amount of Europe's economic assets are situated on the flood plain. The number of ports at risk from inundation levels higher than 1 m is projected to increase by 80% between 2030 and 2080 (European Commission *et al.*, 2018), with the amount of cargo handled also set to increase (Christodoulou *et al.*, 2019). Recent research into the cost of coastal flooding shows that whilst it will be the larger European economies of the UK, Germany, France, the Netherlands and Belgium that will experience the largest proportion of flood damage by the end of the century (Vousdoukas et al., 2020). For smaller European countries such as Denmark, Norway and Ireland, coastal flooding could be more significant in terms of economic health, with damage potentially costing up to 5% of national GDP by 2100 (Vousdoukas et al., 2018).

The most notable examples of existing responses to SLR are from the Netherlands and the UK. Both countries have invested in large scale protection projects, such as the Thames Estuary 2100 Project (UK) and Delta Programme (Netherlands), both of which include barrier projects such as the Thames and Maeslant barriers that have protected the floodplain behind them since their construction in the 1970s-1980s (Ranger *et al.*, 2013; Van Alphen, 2016). When it comes to future planning, the risks that SLR poses to coastlines means sea-level projections are increasingly incorporated into coastal adaptation planning. In a global survey of coastal practitioners, 87% of respondents within Europe were using SLR projections in planning (Hirschfeld *et al.*, 2023). Seasonal forecasting systems are also being developed to try produce accurate predictions of short-term water levels which incorporate seasonal and interannual sea-level anomalies as well as storm surges (Miles *et al.*, 2014; McIntosh *et al.*, 2015).

Chapter 2: Literature Review

The following chapter reviews key areas of existing sea level change literature. The first section covers global and regional SLC over the 20th century up to present. The second section focuses on SLC over the NWES and reviews the specific drivers of variability, including the NAO. The third section reviews current sea level projections and methodologies.

2.1 Global to regional sea-level change

2.1.1 Global sea-level change

Constraining changes in global mean sea level (GMSL) over the instrumental era is important for understanding how anthropogenic climate change is affecting sea level. Estimates of GMSL have been made using various techniques, which helps to inform and predict future change. Reconstructions of GMSL are typically made using long tide gauge records with 100+ years of data and more recent (~30 year) satellite altimetry data. Different approaches to making the reconstruction produce varying estimates of GMSL, but all estimates indicate GMSL has been rising since at least 1900. Church and White (2011) estimate a SLR rate from 1900 to 2009 of 1.7 mm ± 0.2 mm yr^{-1} by combining spatial patterns from TG and satellite altimetry data. Subsequent estimates have varied; Hay et al. (2015) give a lower rate of 1.2 ± 0.2 mm yr^{-1} for 1901-1990 based on an approach that uses TG data alongside the spatial fingerprints of components estimated from model ensembles. The reconstruction from Dangendorf et al. (2019) also uses spatial fingerprints but it extends to 2015 to give a rate of 1.6 ± 0.4 mm yr^{-1}.

An understanding of the driving mechanisms behind both global and regional changes in sea-level is crucial when quantifying past changes and looking to project future patterns. On the global scale, the primary components can be represented by the following equation:

$$\mathrm{GMSL}(t) = \mathrm{GMSL}_{barystatic}(t) + \mathrm{GMSL}_{thermosteric}(t) \quad (1),$$

where at any point in time *t*, GMSL is the sum of the barystatic (mass) and thermosteric (volume) components. The barystatic component reflects the addition of water mass to the ocean from ice sheets, glaciers, ice caps (Bamber et al., 2018; Zemp et al., 2019), as well as changes in terrestrial water storage

(Humphrey and Gudmundsson, 2019), whilst the thermosteric component is attributed to changes in ocean density as the oceans warm and expand (Cheng and Zhu, 2016).

The approach of trying to reconcile the sum of the contributions from these individual components with observed GMSL is often referred to as 'closing the sea-level budget' and it is key to understanding the drivers of SLC (Figure 2.1). Several studies have attempted to close the global budget. Initial studies could not close the budget within the estimated uncertainties (Moore *et al.*, 2011; Gregory *et al.*, 2013) because certain components were underestimated e.g., the ice-sheet contributions (Miller and Douglas, 2004), and the TG-derived rate of GMSL was overestimated (Jevrejeva *et al.*, 2017). Frederikse et al. (2020) have since reconciled the budget within appropriate uncertainties using a probabilistic framework, and the budget is now considered to be closed for the period 1900-2020.

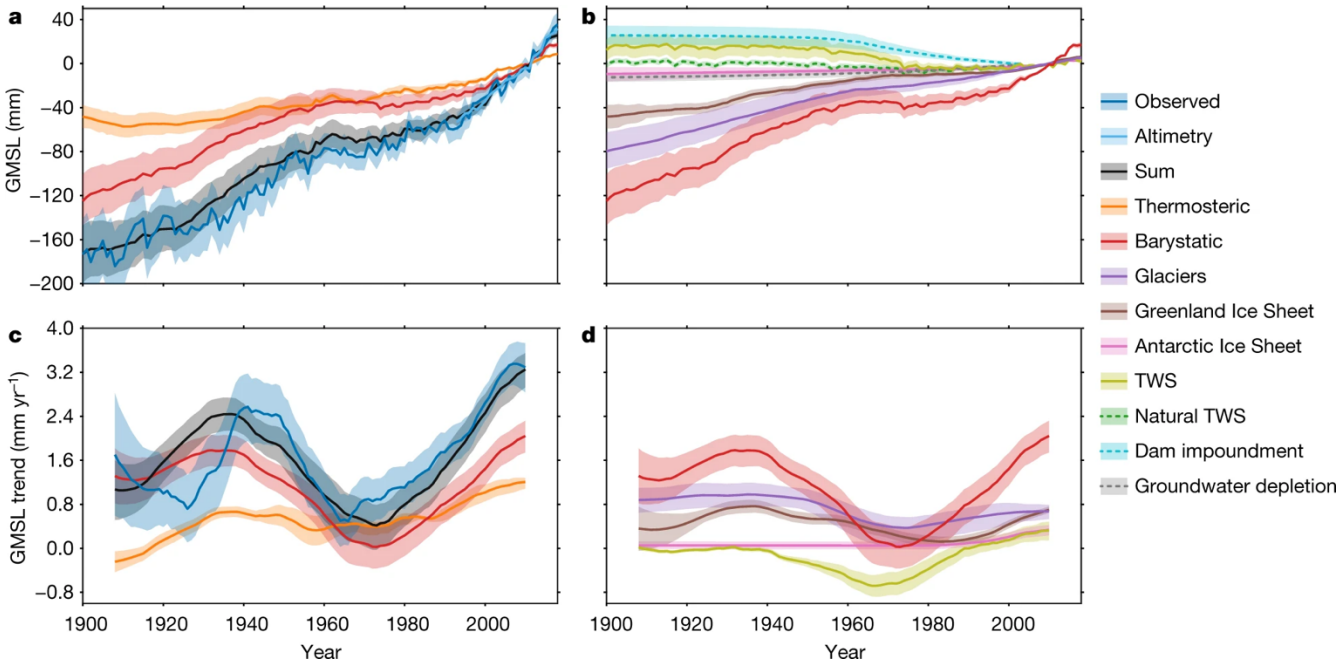

Figure 2.1: (From Frederikse et al., 2020) a) Observed GMSL, and the estimated barystatic and thermosteric contributions and their sum. b) The barystatic contribution and its individual components. The TWS term is the sum of groundwater depletion, water impoundment in artificial reservoirs and the natural TWS term. c) 30-year-average rates of observed GMSL change and of GMSL change as a result of the different contributing processes. d) 30-year-average rates of GMSL change due to the barystatic contribution and its individual components. The shaded regions denote 90% confidence intervals. The values in a) and b) are relative to the 2002–2018 mean.

A challenge when estimating GMSL, and also regional change, is the lack of sea level data available worldwide. Satellite altimetry provides continuous, global measurements of sea surface height but is only available from the start of the satellite era in 1993. Prior to this, TGs are the primary source of historical sea level data, but there are a number of challenges associated with using this data to calculate GMSL

(Hamlington and Thompson, 2015). There is a major bias in the distribution of TG stations, with a greater number in the Northern Hemisphere versus the Southern Hemisphere. The global network is also fairly sparse until the second half of the 20th century. Given that TGs are located on the coastline, estimates of GMSL derived from TG data do not reflect change in the ocean interior. TG records are also prone to containing large gaps where data is not recorded, either from malfunction, storms, or because the TG stops being maintained. These limitations mean that GMSL estimates based solely on TG data are subject to considerable uncertainties. To address this challenge, a more robust approach involves reconstructing 20th-century SLC by integrating model outputs with TG and satellite altimetry data (Hamlington *et al.*, 2011; Hay *et al.*, 2015). This combined methodology reduces the impact of uncertainties associated with individual data sources.

2.1.2 Regional sea-level change

SLC is not a globally uniform process (Church and White, 2011). Regional patterns exist due to climatic and oceanic mechanisms which operate over shorter timescales (i.e. sub-annual to decadal) and smaller areas than those at the global scale, which introduces localised conditions of SLC. Regional SLC at location *x* over time *t* can be expressed as:

$$\mathrm{RSL}(x,t) = \mathrm{SL}_{IS/LWS}(x,t) + \mathrm{SL}_{DSL}(x,t) + \mathrm{SL}_{VLM}(x,t) + \mathrm{SL}_{HF}(x,t) \quad (2),$$

where RSL is regional sea-level, $\mathrm{SL}_{IS/LWS}(x,t)$ is mass changes from ice sheets, glaciers and land water storage, $\mathrm{SL}_{DSL}(x,t)$ is change associated with steric variability and ocean dynamics, $\mathrm{SL}_{VLM}(x,t)$ is change from vertical land motion (VLM) processes and $SL_{HF}(x,t)$ is higher-frequency variability associated with astronomic tides, storm surges, wave set-up and wave run-up. The contributions from land-based ice masses, ice sheets and land water storage are usually considered using the regional signature or fingerprint created by gravitational, rotational and deformational changes as a result of redistributions of land ice and water. VLM is typically split into glacial isostatic adjustment (GIA) and non-GIA components, such as tectonics and sediment compaction (Frederikse *et al.*, 2019). Certain components will be more dominant depending on the region in question. For example, regional rates of SLC are higher than the global mean on the eastern US coastline due to GIA (Roy and Peltier, 2015). Higher rates are also observed around Greenland and in the Southern Ocean Greenland (Stammer *et al.*, 2013).

Atmospheric forcing is a primary driver of sub-annual to multi-annual change in both climate and ocean systems at a regional scale. It is a form of natural climate variability, where variability can be defined as the difference between the mean state of the climate system over time and the state of the system at a particular point in time (Hurrell *et al.*, 2003). In simple terms, this describes fluctuations above and below the mean state of the climate system. One of the main sources of atmospheric forcing for sea level in many regions is large-scale climate oscillations. The integrated nature of ocean-atmosphere systems means variations in these oscillations propagate into changes in sea level. The most dominant oscillation globally is ENSO, which affects climate and sea level directly over large parts of the Pacific Ocean and indirectly further afield. The climatic effects are so large that ENSO activity can create SLC up to 20-30 cm above/below the mean within the Pacific (Becker *et al.*, 2012) and global changes up to 2 cm (Nerem *et al.*, 1999). The NAO similarly dominates sub-interannual climate and sea level over the North Atlantic (greater detail on this matter is provided in section 2.2.1.

As with GMSL, work has also been done to define and close sea-level budgets at a regional scale. This is challenging, because the individual regional patterns of SLC are made up of highly dynamic components, making it difficult to accurately capture their interactions within a budget framework (Slangen *et al.*, 2012, 2014; Royston *et al.*, 2020). However, progress in this area has been made using machine-learning techniques to further improve the ability to close sub-basin sea-level budgets (Camargo *et al.*, 2023).

2.2 Sea-level change over the NWES

2.2.1 The NAO

The NAO is the primary mode of climate variability that will be focused on in this study. It is characterised as a north-south dipole of atmospheric surface pressure differences between the Icelandic Low and the Azores High which oscillates between two phases (positive and negative) and drives climatic changes over the North Atlantic and Europe (Figure 2.2) (Hurrell, 1995). The NAO index can be defined using multiple methods but it is typically derived from the normalized sea-level pressure differences between a northern station (e.g. Iceland) and a southern station (e.g. Gibraltar or Ponta Delgada).

Positive NAO phases occur when the pressure difference between the two stations is large and results in strong westerly winds over the North Atlantic and Europe, bringing stormy and wet conditions to Northern Europe (Hurrell *et al.*, 2003). Negative phases occur when the pressure difference is low. It is primarily a winter phenomenon, as this is when the greatest pressure difference exists between the two atmospheric centres and perturbations are at their largest amplitude (Hurrell, 2003), but the NAO index can be defined for all seasons.

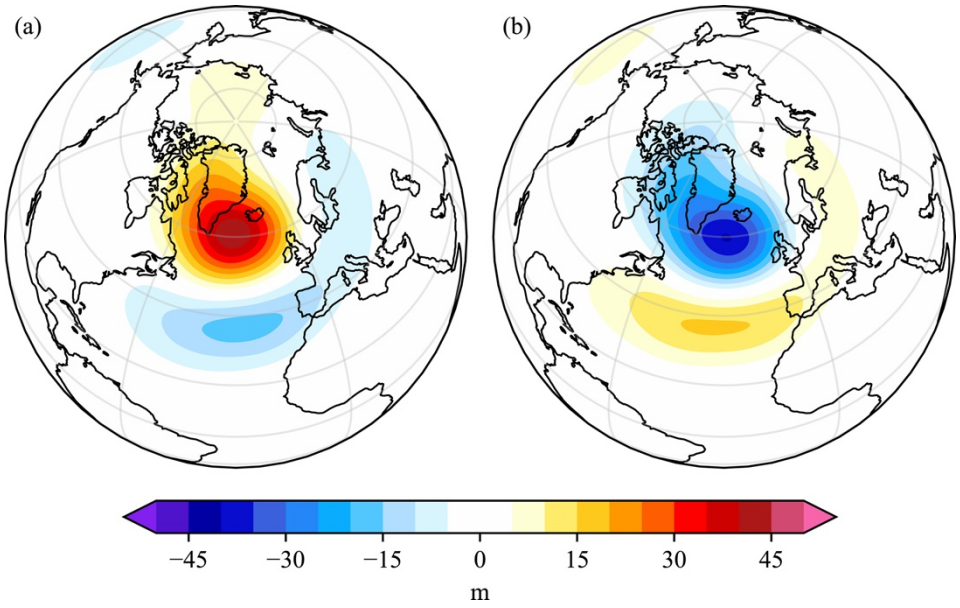

Figure 2.2: (From Skinner et al., 2022) Boreal winter (November to April) (a) negative North Atlantic Oscillation (NAO−) and (b) NAO+ Z500 anomaly composites over the period 1985–2014 in HadGEM3-GC3.1-MM.

The NAO drives changes on a range of timescales and is interrelated with other large-scale components of the North Atlantic climate system. As well as variations in wind strength and direction, moisture transport and surface pressure that are induced by NAO activity over sub- to multi-annual timescales, research involving climate models has shown a connection between the NAO and the Atlantic meridional overturning circulation (AMOC) which operates over decadal timescales (Eden and Jung, 2001; Kim *et al.*, 2023). In this case, the NAO influences AMOC variations through air-sea fluxes of heat and water, which in turn alter density gradients in the subpolar North Atlantic and induce changes in the AMOC (Delworth and Zeng, 2016). The NAO can also be associated with the Arctic Oscillation (AO), with the NAO sometimes characterised as a regional expression of the AO (Freitas *et al.*, 2022).

Over the 20th century, the NAO has shown a strong trend towards more positive phases than negative phases, first shifting towards more positive phases in the 1920s, with another period of strong positive

phases from the mid-1960s to the mid-1990s (Visbeck *et al.*, 2001; Pinto and Raible, 2012). Climate change has been suggested as one of the forcing mechanisms for this trend; studies using atmospheric general circulation models (AGCMs) suggest that increasing CO_2 concentrations and increasing sea surface temperatures (SST) coincide with increases in the winter NAO index (Gillett *et al.*, 2003; Dong *et al.*, 2011). Related studies looking at temperature also suggest there is evidence that anthropogenically-induced climate change will alter large-scale atmospheric circulation (e.g., McKenna and Maycock, 2021; McKenna et al., 2021a).

2.2.2 Relationship between sea level and the NAO

The NAO has a varied spatial relationship with sea level over the NWES. There is a strong spatial pattern in the correlations between sea level and the NAO for parts of the NWES in wintertime (when the NAO is at its strongest). Correlations are positive (>0.8) for the North Sea and the northern shelf seas such as the Shetland Trench and Malin Sea, and negative (<-0.7) for the southern areas such as the English Channel and into the Atlantic Ocean (Wakelin *et al.*, 2003). Notably, sensitivity of sea level to the NAO reaches up to 96 mm/unit NAO in the southeast North Sea for the period 1955-2000 (Wakelin *et al.*, 2003). Other studies observe similar patterns. For instance, in the German Bight TGs demonstrate a very strong positive correlation between the NAO and mean sea level during winter, accounting for 30-35% of the observed fluctuations (Dangendorf *et al.*, 2012). Studies conducted for the UK coastline reveal smaller correlations between the NAO and MSL (Woodworth *et al.*, 2007), and a negative relationship for some North Sea and English Channel TGs (Yan *et al.*, 2004). Longer timescales also exhibit significant correlations between the NAO and decadal sea level variations on the European Atlantic coast and in the Mediterranean Sea (Calafat *et al.*, 2012). These findings demonstrate the complex and varied relationship between the NAO and MSL even just across the NWES seas.

Studies utilizing a combination of models and observed sea level and atmospheric indicators have identified wind stress as the primary mechanism of NAO-related atmospheric forcing on the NWES (Tsimplis *et al.*, 2006; Richter *et al.*, 2012), with thermosteric changes having a negligible impact (Chen *et al.*, 2014). Wind-driven variability tends to dominate in shallow shelf seas such as the North Sea (Roberts *et al.*, 2016) and is more predicable than variability that originates in oceanic processes (Miles *et al.*, 2014). The switch from positive to negative correlations around the English Channel can also be attributed to atmospheric forcing, originating from pressure via the IB effect (Dangendorf *et al.*, 2014).

2.3 Making sea-level projections

2.3.1 Projections of global sea-level change

Significant research effort has been put into improving projections of future SLC, the result of which is a whole suite of published projections made using various methods, as well as papers dedicated to improving the modelling of different components (Slangen *et al.*, 2023). Evidence of this is in the substantial progress made in both the methods used and the science produced through the iterations of IPCC reports. Between AR5 and AR6, the main developments have been: 1) the use of information from CMIP6 models (Eyring *et al.*, 2016) to make projections which are forced by SSP scenarios (O'Neill *et al.*, 2014); 2) differences in how certain components are modelled, mainly the glacier and ice sheet contributions for global projections; 3) the inclusion of low confidence projections in AR6, mainly considering the deep uncertainty surrounding the potential contribution from the Antarctic ice-sheet (DeConto *et al.*, 2021); and 4) improvements to the resolution of regional sea-level projections.

The IPCC's process-based projections underpin a large number of regional and national assessments and decision-making (Nicholls *et al.*, 2014). The process-based approach draws on the idea of the sea-level budget (see section 2.1.1), where projections are built from combining sea-level components with other climate information within climate models. The components that are generally included in the calculation of projected total GMSL rise over time (t) are thermosteric expansion (T), ice mass from glaciers (GIC_i), the Greenland Ice Sheet ($GrIS$), the Antarctic Ice Sheet (AIS) split into East ($EAIS$) and west ($WAIS$), and changes in land water storage $\left(LWS_j\right)$ (Jevrejeva *et al.*, 2019):

$$GMSL(t) = T(t) + \sum_i GIC_i(t) + GrIS(t) + WAIS(t) + EAIS(t) + \sum_j LWS_j(t) \quad (3)$$

2.3.2 Projections of regional sea-level change

The complex nature of regional SLC makes projecting regional changes tricky. When making projections up to 2100 and beyond, regional sea-level projections at locations x, over time t can be typically represented as:

$$\mathrm{RSL}(x,t) = \mathrm{T}(t) + \mathrm{DSL}(x,t) + \sum_i F_i(x)\mathrm{GIC_i(t)} + \mathrm{F_{GrIS}(x)GrIS(t)} + \mathrm{F_{WAIS}(x)WAIS(t)}$$

$$+ \mathrm{F_{EAIS}(x)EAIS(t)} + \sum_{\mathrm{j}} \mathrm{F_{LWS_i}(x)LWS_j(t)} + \mathrm{Bkgd(x,t)}$$

(4),

where relative sea level ($RSL(x,t)$) is the sum of: thermosteric expansion (T); the dynamic sea level contribution ($DSL(x,t)$); the contribution from the different glacial regions and land water storage scaled to the normalised gravitational, rotational and deformational fingerprint for the location in question ($F_{GIC_i}, F_{WAIS}, F_{EAIS} and F_{LWS_J}$); and localised background processes ($Bkgd$), for example GIA or sediment compaction (Jevrejeva *et al.*, 2019).

Regional projections of SLC are receiving more attention; the increased emphasis on regional climate change in AR6 is an example. As already touched on in section 1.1, there are a number of approaches to making regional projections, all of which have to carefully consider how components and their uncertainties are combined. Regional projections have been previously produced for the NWES region, ranging from projections of total SLC to projections of individual components. One of the most comprehensive assessments of projected SLC comes from the 2018 report of United Kingdom Climate Projections (UKCP18), which includes projections of changes in MSL, extreme water levels and the UK wave climate for 40+ coastal TG sites (Palmer *et al.*, 2018). The general pattern for the UK coastline is greater SLR projected for southern sites, with values close to global mean projections, and lower SLR for northern sites, lower than the global mean. The report also provides downscaled model simulations under RCP5-8.5 to predict changes in storminess.

To further the ability of models to resolve processes at a fine enough spatial scale to produce regional projections, work is being done on modelling individual sea-level and climate components. Dynamical downscaling as a method is one of the most effective ways of modelling components at the required spatial scale (Rummukainen, 2010). This approach has been applied in the NWES region to various sea-level and climate processes, including ocean circulation (Mathis *et al.*, 2018), extreme sea level (Palmer *et al.*, 2018; Howard *et al.*, 2019) and DSLC (Hermans *et al.*, 2020, 2022). The latter studies highlight the differences between original and downscaled GCM output; Hermans *et al.* (2020) finds that the difference in the projected change in the amplitude of the seasonal sea-level cycle can be greater than 0.3 mm/year for downscaled output versus raw GCM output. When considering the magnitudes of seasonal

SLC, this is could translate into a considerable difference over time. These studies show that steps are being made towards better quantifying future sub-annual SLC.

Given the importance of the NAO to climate and sea-level changes in the NWES region, it is surprising that potential future changes in the NAO and other modes of climate variability have remained relatively unexplored compared with other areas of sea-level research (Cusinato *et al.*, 2021). Out of the climate modes, the NAO has been well-studied in terms of multi-model analyses (Davini and Cagnazzo, 2014; Wang *et al.*, 2017; Bracegirdle *et al.*, 2018). The main reason for a lack of research on future behaviour of climate modes is due to difficulties in representing the modes within climate models. In CMIP models, simulation of the NAO is achieved through the modelling of components such as sea-level pressure (SLP), wind patterns and temperature. As these interactions occur on very fine spatial and temporal scales, it is unsurprising that current GCMs struggle to effectively simulate the finer features of the NAO, even when downscaled. However, there has still been progress in the simulation of the mode through different generations of CMIP models. Models within CMIP5 struggled to accurately simulate the physical processes linked to the NAO, such as jet stream variability and high-latitude pressure variations, leading to misinterpretations of the NAO output (Davini and Cagnazzo, 2014). In the transition from CMIP5 to CMIP6, Cusinato et al. (2021) reported that CMIP6 models demonstrate an improved ability to represent NAO features compared with CMIP5. In a study that compared historical CMIP6 output from UKESM1 with observational data, general aspects of the North Atlantic climate system were well-simulated, including good simulation of the NAO structure, and the ensemble spread of the NAO covered the observed NAO indices (Robson *et al.*, 2020). However, this study also highlighted spatial patterns of the NAO that were too zonal, with centres of action confined to overly small areas when compared with observed indices. The improvements between CMIP generations indicate models are getting closer to resolving the finer-scale features of the NAO.

2.3.3 Uncertainty

There are multiple approaches to computing uncertainty on climate and sea-level projections. The IPCC framework articulates projection uncertainty through precise language concerning confidence and likelihood. Typically, projections are presented at specific confidence levels for the median, the 17th-83rd percentile (*likely range*), and the 5th-95th percentile (*very likely range*), corresponding to probabilities of at least 66% and 95%, respectively (Fox-Kemper *et al.*, 2022). To extend uncertainties beyond these ranges, a probabilistic method can be used. This approach uses the probability density

functions (PDFs) of individual components to quantify the probability of a given sea level and construct uncertainty outside of the 'likely' or central ranges (Jevrejeva *et al.*, 2019). A key feature of studies that use the probabilistic approach is the introduction of non-Gaussian uncertainty into the tails of ice sheet contributions from Antarctica and Greenland. This produces projections of low-probability, high-impact ranges of future SLC (Kopp *et al.*, 2014; Grinsted *et al.*, 2015; Jackson and Jevrejeva, 2016).

A common feature of all projections, local to global, is that uncertainty grows over time (Slangen *et al.*, 2023). Within this general pattern, the relative contributions of uncertainty from different components changes over time, as revealed by separating the individual sources of uncertainty within CMIP projections (Hawkins and Sutton, 2011). Three main sources of uncertainty are identified that apply to scenario-based projections produced from a multi-model ensemble (Hawkins and Sutton, 2009). The first source is uncertainty originating from internal, unforced variability, which represents the chaotic and unpredictable aspect of the climate system within the model. Second is uncertainty attributed to structural differences between climate models, resulting from different model setups and tuning. These differences affect how models respond to forcing and simulate aspects of the climate system. The last main source is scenario uncertainty, linked with the radiative forcing or emissions scenario that a projection is being made under. The contribution to total uncertainty from each of the three components for various global TG locations from Palmer et al. (2020) is shown in Figure 2.3. All locations show the same general pattern of uncertainty dominance from natural variability up to around 2040, then beyond ~2050 contributions from the forcing scenario and modelling uncertainty are dominant. Model uncertainty related to mass loss from the Antarctic Ice Sheet is a critical source of 'deep uncertainty', particularly towards the end of the century, as experts cannot agree on a conceptual model or probability distribution that appropriately constrains future contributions from the ice sheet (Oppenheimer *et al.*, 2019).

In contrast, uncertainties in the short-term (~30 years) mainly originate from internal climate variability, which is an important consideration for this study. At a regional scale, the sources contributing to internal variability in different regions will vary. The uncertainty associated with modelling large-scale climate oscillations, for example, will differ between the NAO, ENSO and other oscillations. The complex nature of these oscillations makes them hard to accurately depict in model output, and this complexity is a reason that uncertainty related to representing climate variability in models dominates short-term uncertainty (Feliks *et al.*, 2021). There is also the question of the degree to which the spread in model output reflects structural differences between models versus internal variability (McKenna and Maycock, 2021). There are only a small number of models within the CMIP generations which are truly

independent; CMIP6 and previous CMIP generations are made up of individually named models, but many models share the same base model, provided by larger modelling centres (Leduc *et al.*, 2016). Examples of base models include the UK Earth System Model (UKESM) developed by the Met Office Hadley Centre and the Community Earth System Model (CESM) developed by the National Centre for Atmospheric Research (NCAR). The sharing of base models involves sharing conceptual frameworks and source code, as well as baseline frameworks (Masson and Knutti, 2011; Knutti *et al.*, 2013; Brands, 2022), and the result is that models within CMIP6 range from fully independent to effective replicas (Merrifield *et al.*, 2023). The interrelation of models means there are a limited number of model realisations that truly have different initial conditions and responses to the same forcing (McKenna and Maycock, 2021).

In summary, SLC has been well-studied over past and future time periods, and at global to local spatial scales. There are significant challenges associated with accurately quantifying regional SLC, mainly due to the complexity of identifying and then modelling the processes that drive climatic and oceanic change for areas such as the NWES. Progress has been made in the ability to project regional-scale sea-level in particular, but there is scope for further development in this area.

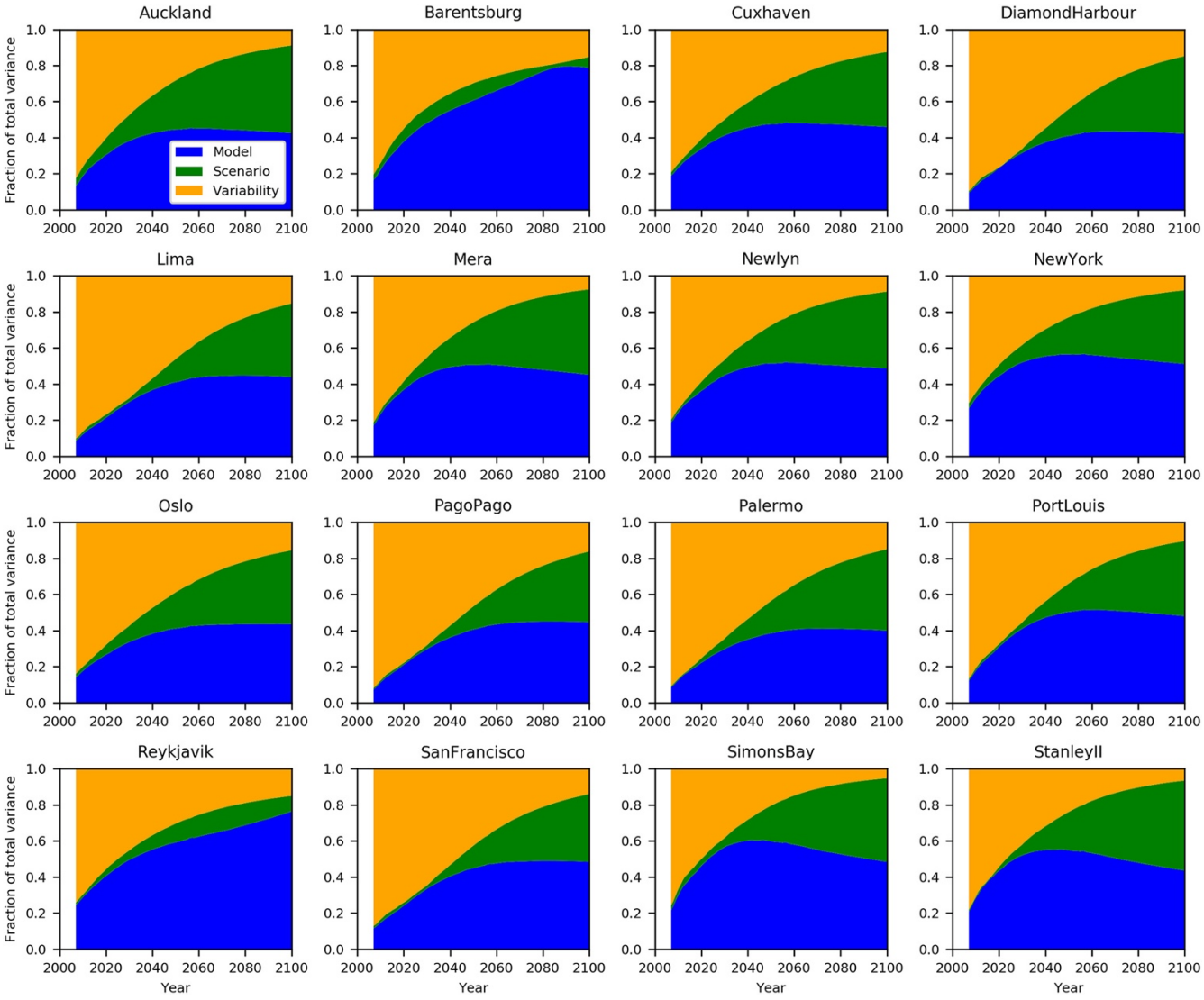

Figure 2.3: (From Palmer et al., 2020) Assessment of the fraction of total variance of sea-level change explained by model, scenario, and variability, following Hawkins and Sutton (2009) as indicated in the figure legend for Auckland.

Chapter 3: Methodology

This chapter outlines the methods used to firstly analyse sea level and the NAO over the observational period, and secondly, make projections of sea level using a budgetary approach. Section 3.1 details the datasets used. Section 3.2 details how regional NWES TG data was obtained and processed to analyse the seasonal cycle. Section 3.3 describes the approach used to assess how record completeness affects analysis of the relationship between sea level and the NAO, which addresses Objective 1. Section 3.4 describes how the relationship between the seasonal cycle and the NAO index is analysed, addressing Objective 2. Section 3.5 then covers the approach used to calculate a projected NAO index. Finally, Section 3.6 describes the process of making sea-level projections at a seasonal time scale. Sections 3.5 and 3.6 both address Objective 3.

3.1 Datasets

3.1.1 Tide gauge data

Monthly mean sea level values from eleven TG records were acquired from the PSMSL database (Holgate *et al.*, 2013) for this study (Figure 1.1). Each record was provided in revised local reference (RLR) form; RLR records are all reduced to a common datum by PSMSL to provide consistency between station records in the database. TGs were chosen both for data availability, and to ensure all regions of the NWES were covered by at least one data point. Each record chosen had over 70 years of data available and over 80% completeness, with the exceptions of Portsmouth (60 years of data available) and Le Havre (68% completeness). As a number of TG records, do not provide data for 2022, particularly around the UK coastline, all data was retrieved up to 2021.

3.1.2 ERA5 sea-level pressure data

The sea-level pressure (P_a) data used in this study to make the inverted barometer correction was the ERA5 reanalysis product produced by the European Centre for Medium-Range Weather Forecasts (ECMWF) (Hersbach *et al.*, 2017), downloaded from the Royal Netherlands Meteorological Institute (KNMI) Climate Explorer website (https://climexp.knmi.nl/selectfield_rea.cgi). ERA5 is the latest reanalysis dataset from ECMWF, produced by fitting weather models to historical measurements to provide a long-term dataset that is spatially and physically consistent in terms of atmospheric evolution through time. The data is available from 1950 to present day. To make the correction at each of the 11

TGs, a P_a time series was retrieved at monthly time steps between January 1950 and July 2021 (for consistency with the TG data, see section 3.1.1) and on 0.25° by 0.25° longitude-latitude grids for each gauge. As the data are gridded, each P_a time series was obtained for a defined box to the nearest 0.25° N and W of the coordinates of the TG.

3.1.3 NAO index

The NAO index used in this study was the monthly NAO index available from the Climatic Research Unit (CRU), University of East Anglia, which was downloaded for the period between 1950 and 2021. The CRU index is a normalised station-based index, calculated by taking the difference in sea-level pressure anomalies between two fixed stations in Gibraltar and southwest Iceland (Jones *et al.*, 1997) (http://www.cru.uea.ac.uk/cru/data/nao/nao.dat). An uncertainty to be considered when using a station-based index is that the stations are fixed in space, whilst the centres of action of the NAO (i.e., centres of the pressure field) shift in space over annual timescales. This means the effect of interannual movements on the pressure field are not captured at either station and are therefore not accounted for within the NAO index, which is an assumption to highlight.

3.1.4 CMIP6 sea-level projections

The sea-level projections used are the regional sea-level projections from AR6, downloaded from the NASA-IPCC sea-level projections tool (https://sealevel.nasa.gov/ipcc-ar6-sea-level-projection-tool), referred to herein as CMIP6-SLPro. These projections were produced using output from CMIP6 models, driven by the SSP scenarios outlined in AR6 (Eyring *et al.*, 2016). The NASA sea-level projection tool provides projections for individual TG locations from 2020 to 2150 at decadal time steps. All projections are provided at a medium confidence level (as defined in AR6) for five SSP scenarios, relative to a 1995-2014 baseline. The median and 17th-83rd percentile projections were downloaded for each of the 11 TG locations specified in section 1.4, all for the SSP2-4.5 scenario. The length of the projection period in this study (2023-2053) means the choice of SSP scenario is negligible. There is a degree of scenario divergence towards 2053 in the median and percentile projections, but as the objectives of the study are to examine natural variability, the deviation in warming scenario is less critical.

3.1.5 CMIP6 sea-level pressure data

CMIP6 sea-level pressure (SLP) data, subsequently referred to as CMIP6-SLPres, was obtained from the KNMI Climate Explorer website. Monthly data was obtained for a southern box (90°W–60°E, 20°N–

55°N) and a northern box (90°W–60°E, 55°N–90°N). The ensemble mean output from all 41 available models was downloaded for the SSP2-4.5 scenario.

3.2 Tide gauge data preparation

To analyse the seasonal component of sea level, each TG time series needed correcting for a number of signals. First, the long-term mean SLR signal was removed by detrending each time series using linear regression (Figure 3.1b) to give a detrended and demeaned time series of mean sea level (MSL). The annual sea-level cycle was then estimated and removed from each MSL series using an empirical approach (Pezzulli *et al.*, 2005; Dangendorf *et al.*, 2012). The annual cycle was isolated by calculating the median MSL value for each month separately over all available years in the time series. For example, the median value was calculated for all the January's in the series, then the February's etc. This gave the average annual cycle, which was subtracted from each month in the MSL series to give the anomaly from the average annual cycle (Figure 3.1c, annual component shown in red), which is the annually corrected MSL time series. Additionally, using the empirical approach can make it harder to distinguish interannual fluctuations of the annual cycle from longer-term variations in sea level (Pezzulli *et al.*, 2005). However, for the present study, the empirical method is suitable, as the focus is on the shorter seasonal component, and the issue of unaccounted interannual variations is less important.

The final correction applied to each MSL series was the inverted barometer (IB) correction. The IB response (η^{ib}) refers to changes in sea level in response to changes in surface atmospheric pressure. On timescales longer than a few days, full adjustment results in a 10 mm depression in the ocean surface for a 1 mb increase in barometric pressure. This can differ regionally and on longer timescales, where the regional effect of the IB effect can vary between <1 cm in the tropics and up to 2-3 cm at higher latitudes (Ponte, 2006). Making this correction is important when examining seasonal cycles, as any sea-level variability related to the IB effect can be misinterpreted as a signal related to ocean circulation or density (Ponte, 2006).

In this study, the correction was made by following the method set out in Piecuch and Ponte (2015) using the P_a data detailed in section 3.1.2. The IB response (η^{ib}) was calculated for each time series according to Ponte (2006):

$$\eta^{ib} = -\frac{P_a - \bar{P}_a}{\rho g}$$

(5),

where $\bar{P}_a$ is the spatial average pressure over the global ocean surface, *r* is a constant reference surface density, and g is acceleration due to gravity. The IB response, which is in mm, could then be subtracted from the annually-corrected MSL series for each TG to give an MSL time series which has been corrected for the long-term trend, the annual cycle and the IB effect (Figure 3.1d).

3.3 Tide gauge record sensitivity analysis

A record sensitivity analysis was undertaken to assess whether TG record length and completeness affected the relationships identified between MSL and the NAO. A large issue with TG records is that record completeness is not uniform in time or space. This is true even in the NWES region, which has some of the longest and most complete records globally. For example, the Brest record from northwest France has 215 years of data and is 89.5% complete, and the TGs along the Dutch coastline, which give data from 1848 onwards, are upwards of 99.8% complete. However, there are many TGs which have less than 30 years of data and contain a variety of gaps; this is particularly problematic around the UK coastline.

3.3.1 Calculating record completeness

As aforementioned, the use of the ERA5 P_a data set in the TG record correction process (described in section 3.2) has an impact on the timescales used in the study. The ERA5 P_a data are only available from 1950 onwards and so 1950 is the earliest year of possible analysis. In the following analysis of record sensitivity, record completeness (%) is determined by identifying the number of missing months of data between January 1950 and November 2021 in each TG time series and then calculating the percentage of complete data in each record (Figure 3.2):

$$TG_{completeness} = \left(\frac{t_{TG}}{(2021 - 1950) * 12}\right) * 100$$

(6),

where t_{TG} is the number of missing months of data in a TG record. As a result of restricting the timescale to 1950-2021, these completeness values differ from the completeness given for each record in the

PSMSL database as PSMSL completeness is calculated over the entire period data are available (which, in many records, can precede 1950).

3.3.2 Calculating the baseline record

To carry out the sensitivity analysis, a 'baseline' record was established using the Den Helder TG record (number 5 in Figure 1.1). This record is 100% complete and spans from 1865-2022. The relationship between MSL and the NAO was determined for Den Helder by calculating Pearson's correlation between the corrected MSL time series and the NAO index for 1950-2021. Correlations were then determined for four separate seasonal periods where monthly data were split into winter (December, January and February), spring (March, April and May), summer (June, July and August) and autumn (September, October and November). Data gaps informed by the 10 other TGs in the main NWES sub-set, as well as 72 other TG records located in the shelf region (which have data up to 2021), were applied to the baseline record to create 'synthetic records'. For example, the data gaps from the Millport record (number 10 in Figure 1.1 and 55% complete) were applied to the baseline record, so that the missing years of data from the Millport record were removed from the baseline record. This approach was repeated to produce a total of 82 synthetic records as shown in Figure 3.2. Subsequently, the correlation between sea level and the NAO was recalculated for each synthetic record, both for 1950-2021 and for the four seasonal time periods. The deviation in the synthetic correlation coefficient from the baseline correlation coefficient was used to assess the effect of data gaps.

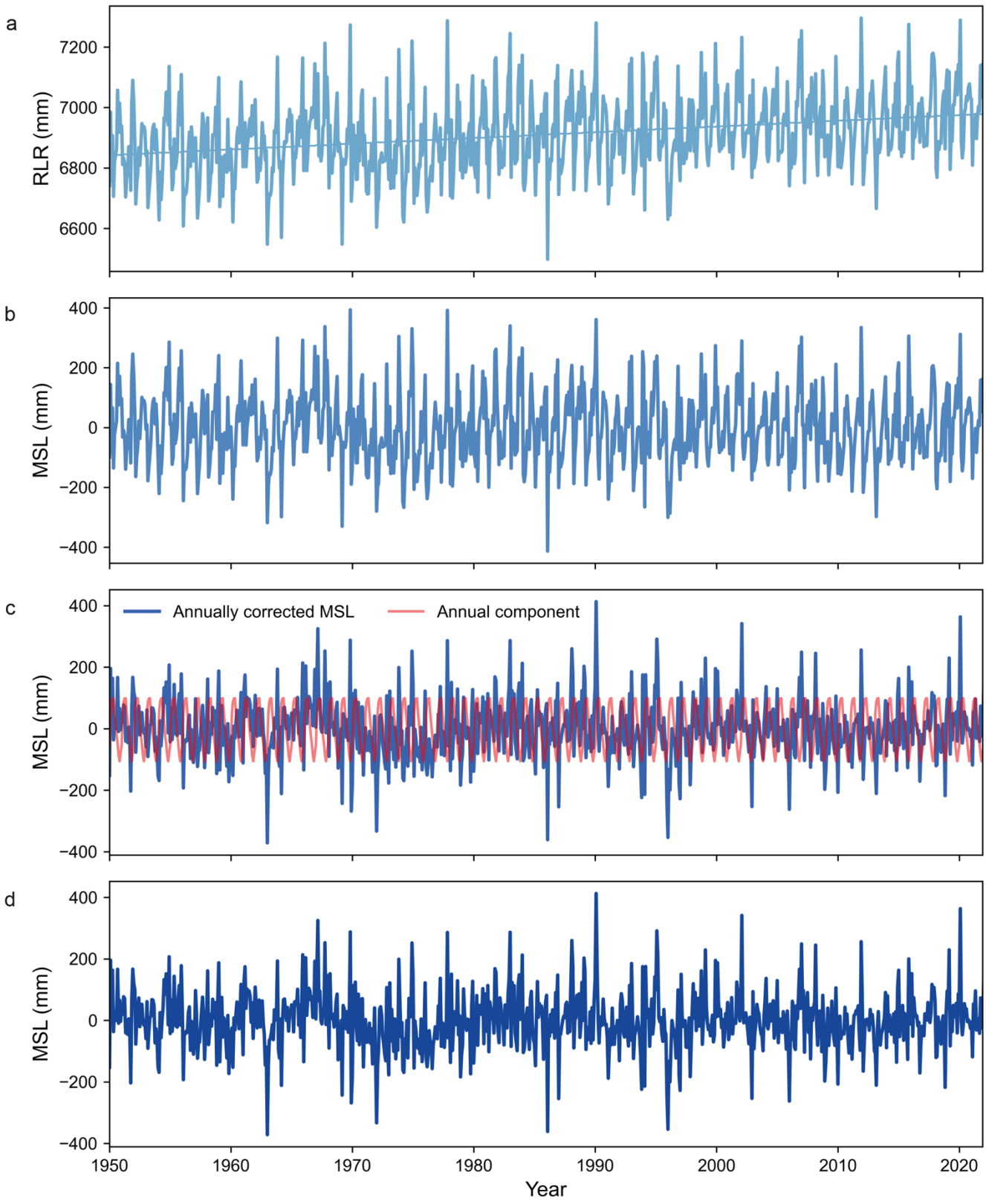

Figure 3.1: Stages of TG data correction for the Den Helder record (23). (a) Monthly RLR water levels from the PSMSL database. (b) RLR data linearly detrended. (c) Mean sea level (MSL) data with annual correction applied. (d) MSL with IB correction applied.

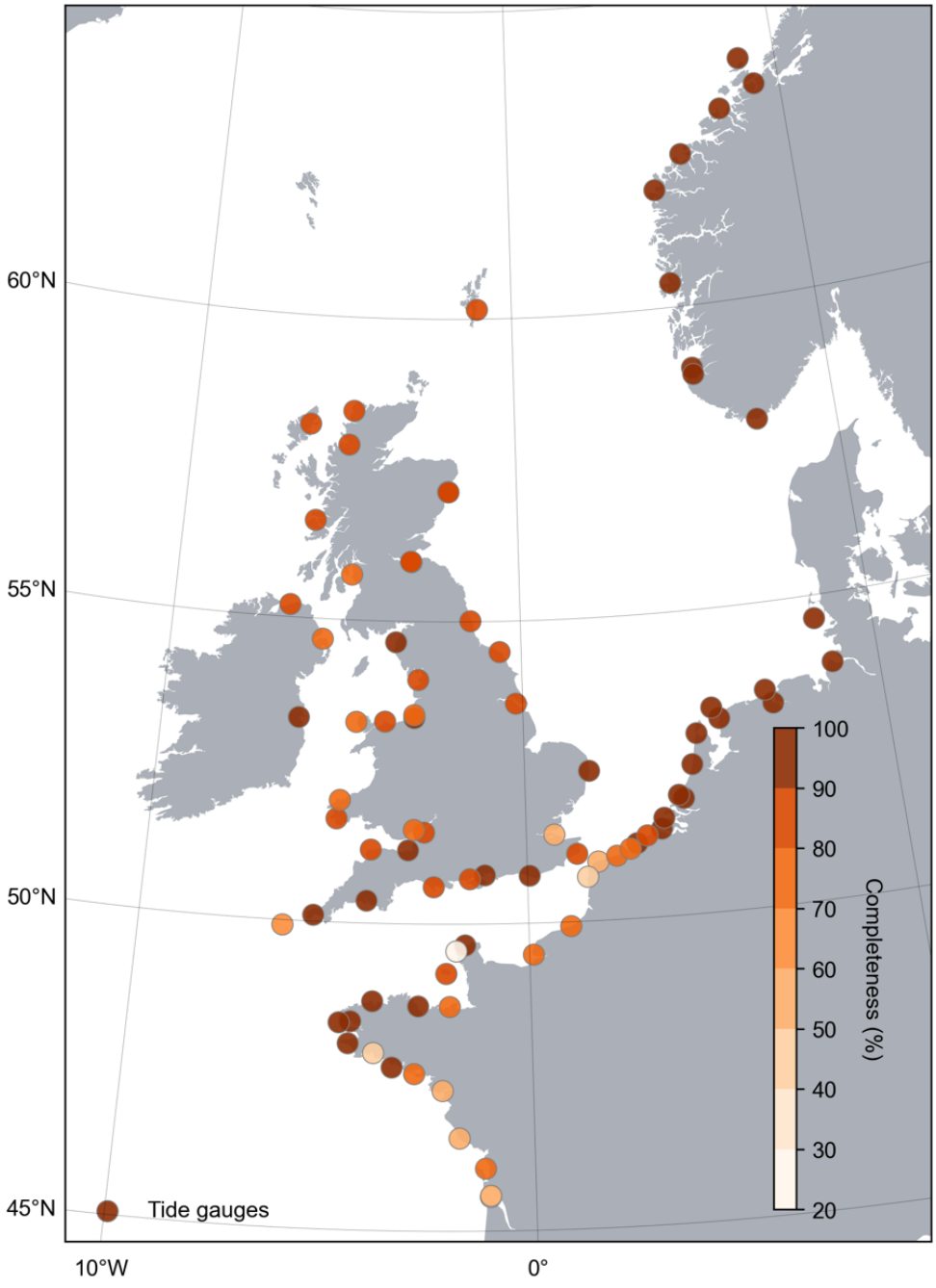

Figure 3.2: Record completeness at 82 tide gauges. Completeness is calculated as per section 3.3.1.

3.4 Correlation analysis

3.4.1 Calculating the seasonal cycle

To capture the effect of the NAO on sea level, a multi-seasonal correlation analysis was conducted. First, the seasonal cycle of sea level was established in each TG time series using an empirical approach by averaging time series individually to estimate the seasonal component. As discussed in 2.2.1, the NAO is primarily a winter phenomenon, but the index can be determined for every month of the year (Barnston and Livezey, 1987), making analysis of the index possible for multiple seasons. Corrected TG time series were used as per the correction process described in section 3.2. For consistency between data sets, the monthly NAO index was also detrended linearly.

The monthly time series were transferred into four seasonal time series to give one time series for winter, one for spring etc., for each gauge. The records were divided into three-month windows as per section 3.3.2. In the winter time series, months were grouped so that December values come from the previous year to the January and February values e.g., the last three values in the winter time series are December 2020, January 2021 and February 2021.

Seasonal means ($\overline{\mathrm{x_{s,y}}}$) were then computed for each year by calculating the three-month mean for each year in the four time series:

$$\overline{\mathrm{x_{s,y}}} = \left(\sum_{\mathrm{m = month\ 1}}^{\mathrm{m = month\ 3}} \mathrm{MSL_{m,y}} \right) / \mathrm{n}$$

(7),

where $MSL_{m,y}$ refers to the MSL value for the specific month and year and n refers to the number of months in the range month 1 to month 3. For the winter series the yearly seasonal mean was calculated using the December value from the previous year, as above.

3.4.2 Correlation analysis between sea level and the NAO

The following analyses were carried out for each TG specified in section 1.4. Using the seasonal time series defined above, the interaction of sea level and the NAO could then be analysed using Pearson's correlation and linear regression models, following the approach in Wakelin et al. (2003). Correlation coefficients were computed between sea level and the NAO index for each season over two separate time

periods: 1950-2021 and 1993-2021. The latter period was used to reflect future comparison between using TG data and satellite altimetry data. To assess the significance of the computed Pearson correlation coefficients, a significance level of 95% ($\alpha = 0.05$) where p-values were computed and compared against the 0.05 threshold.

The corrected MSL values in each seasonal time series were also regressed with detrended seasonal NAO index values over the same two time periods to give a regression coefficient in cm/unit NAO for each season. Measuring the sensitivity of sea level to the NAO index by using the slope of the regression line carries the assumption that sea level is a linear function of the NAO index.

3.5 Calculating a projected NAO index

A key part of producing NAO-induced projections of seasonal SLC was calculating an NAO index for the period 2023-2053. This was carried out using CMIP6-SLPres data as described in section 3.1.5, and by following the CRU method of calculating an NAO index (Jones *et al.*, 1997) to produce an index at seasonal time steps. A full description of the method used and of the adjustments made is available in Appendix A.

3.6 Projecting sea-level components

3.6.1 The MSL sea-level component from CMIP6-SLPro

In order to make projections of SLC at a seasonal (three-month average) time scale, it was necessary to interpolate the CMIP6-SLPro from their original decadal time scale. Both the median (50th percentile) and 17th-83rd percentile projections were interpolated linearly, giving MSL sea-level projections for each TG location at quarterly time steps.

The uncertainty on the MSL projection was calculated as an estimate of two standard errors of the median projection, using the 17th and 83rd percentiles:

$$2SE = \left((q_{83rd} - q_{50th}) + (q_{50th} - q_{17th})\right)/2 * 1.96 \quad (8)$$

3.6.2 Projecting the annual sea-level component

The annual sea-level component was projected at each TG using the annual cycle calculated in the observed MSL series in section 3.2. The component was converted from a monthly time scale to a seasonal time scale by calculating three-month averages as described in section 3.3.2. This step was necessary so that all components in the projection were at the same seasonal time steps. The annual component was then added to the MSL projection to give a projected annual cycle.

Uncertainty on the annual component was quantified by calculating the standard error of each month of the year across the MSL series. Three-month averages of these standard errors were calculated to keep time scales consistent.

3.6.3 Projecting the NAO-induced sea-level component

Projections of NAO-induced SLC (hereby referred to as NAO-SL) were produced for each TG location. This required two components: 1) the projected NAO index as detailed in section 3.5 and 2) season-specific sea-level/NAO coefficients as calculated in section 3.4.2 and displayed in Table 3.1. At each time step, SLC induced by the NAO was computed as the product of the NAO index ($NAO_{m,y}$) and the corresponding sea-level/NAO coefficient, resulting in SLC values in mm:

$$SLC_{NAO_{m,y}} = coefficient * NAO_{m,y} \quad (9)$$

To account for uncertainty on this component, two main sources of uncertainty were identified. The first was the standard error of the sea level/NAO coefficient. The second source was model uncertainty arising from use of the 41 CMIP6 ensemble members. This type of uncertainty occurs because different models give differing responses to the same inputs due to differences in model parameterisation (Deser *et al.*, 2012; Little *et al.*, 2015). The calculation of the model uncertainty is described in Appendix A.

3.6.4 Summing of the components

As a final step, total seasonal sea-level change at each TG location (SLC^{i}_{total}) at month and year *t* over the projected period was calculated as:

$$SLC^{i}{}_{total}(t) = SLC^{i}{}_{median}(t) + SLC^{i}{}_{annual}(t) + SLC^{i}{}_{NAO}(t)$$

(10),

where $SLC^{i}{}_{total}$ is the sum of the interpolated CMIP6-SLPro MSL projection ($SLC^{i}{}_{median}$), the annual component calculated in 3.6.2 ($SLC^{i}{}_{annual}$) and the NAO-SL component calculated in 3.6.3 ($SLC^{i}{}_{NAO}$).

3.6.5 Propagating uncertainties

To compute the total uncertainty of all components, the individual uncertainties were added in quadrature. Doing so assumes all uncertainties follow a normal distribution and are independent from each other, and this may not be the case with the uncertainties being dealt with here; uncertainty due to natural variability is present in both the NAO-SL component and the MSL component, making it likely these sources are not entirely independent of each other. This assumption is recognised, and quadrature is used in line with the linear summation of the projected sea-level components to gain an empirical estimate of the total uncertainty. Total projection uncertainty for each TG location (σ^{i}_{total}) over time *t* is therefore made up of uncertainty from each component in equation 10:

$$\sigma^{i}_{total}(t) = \sqrt{\sigma^{i^2}_{MSL}(t) + \sigma^{i^2}_{annual}(t) + \sigma^{i^2}_{nao}(t)}$$

(11)

3.6.6 Components not included in the projections

There are components that influence seasonal SLC that were not included in the projections. Firstly, interannual to decadal variations that are unrelated to NAO activity were not explicitly included. A significant proportion of decadal-scale variability that affects the NWES has been shown to be a response to a large coherent signal present along the European Atlantic coastline propagating into the North Sea (Sturges and Douglas, 2011; Calafat *et al.,* 2012). This source of variability was not accounted for as an individual component, but the signal may be present within the MSL component. Another component that is also present in the MSL projection and was not calculated individually is DSLC. The omission of these specific components means that the projections might not fully capture all potential fluctuations in seasonal SLC. As such, while these projections provide valuable insights, potential end-users would need to use them with an understanding of the constraints and in conjunction with other data sources and local knowledge to make more informed decisions regarding coastal management and planning.

Tide gauge	PSMSL ID	Coefficient (mm/unit NAO)	SE	Coefficient (mm/unit NAO)	SE	Coefficient (mm/unit NAO)	SE	Coefficient (mm/unit NAO)	SE
		Winter		**Spring**		**Summer**		**Autumn**	
Brest	1	-16.48	6.49	-7.39	5.54	-11.90	3.63	-19.90	6.12
Holyhead	5	17.80	5.55	2.20	6.00	-7.65	5.48	3.26	8.60
Cuxhaven 2	7	78.10	9.52	18.11	10.98	1.73	5.78	27.16	9.30
Vlissingen	20	23.18	4.96	0.79	5.54	-7.98	3.83	3.84	4.69
Den Helder	23	42.67	6.05	11.88	6.79	-8.40	4.65	16.04	6.00
Stavanger	47	27.64	4.16	12.10	4.74	-3.04	5.11	18.01	4.31
North Shields	95	13.55	3.88	5.78	4.21	-7.53	3.54	-2.92	4.51
Newlyn	202	-14.25	5.30	-8.74	5.18	-14.70	3.28	-15.76	5.01
Portsmouth	350	-1.58	6.34	-10.38	5.88	-8.28	4.40	2.37	5.80
Aberdeen I	361	27.36	4.74	13.60	5.56	-2.48	5.12	5.38	4.70
Millport	755	26.20	8.98	16.30	6.93	-1.51	7.03	7.83	7.10

Table 3.1: Correlation coefficients and the corresponding standard errors (SE) between corrected MSL and the NAO index for 11 TG locations in each season.

Chapter 4: Results

4.1 Tide gauge record sensitivity

Figure 4.1 relates to Objective 1 and indicates how missing data affects the correlation coefficients between sea-level and the NAO between 1950 and 2021 for the 82 TG records analysed. There is a consistent pattern across all seasons of higher record completeness corresponding to lower coefficient deviation from the baseline. This pattern is most pronounced in winter and summer (Figure 4.1a and c). Winter has the widest range of coefficients, deviating between +0.16 and -0.08 from the baseline record. With the exception of one record in the summer months, all records above 80% completeness give correlations within ±0.05 of the baseline coefficient. Overall, the correlation coefficients do not deviate beyond +0.16 and -0.09 of the baseline.

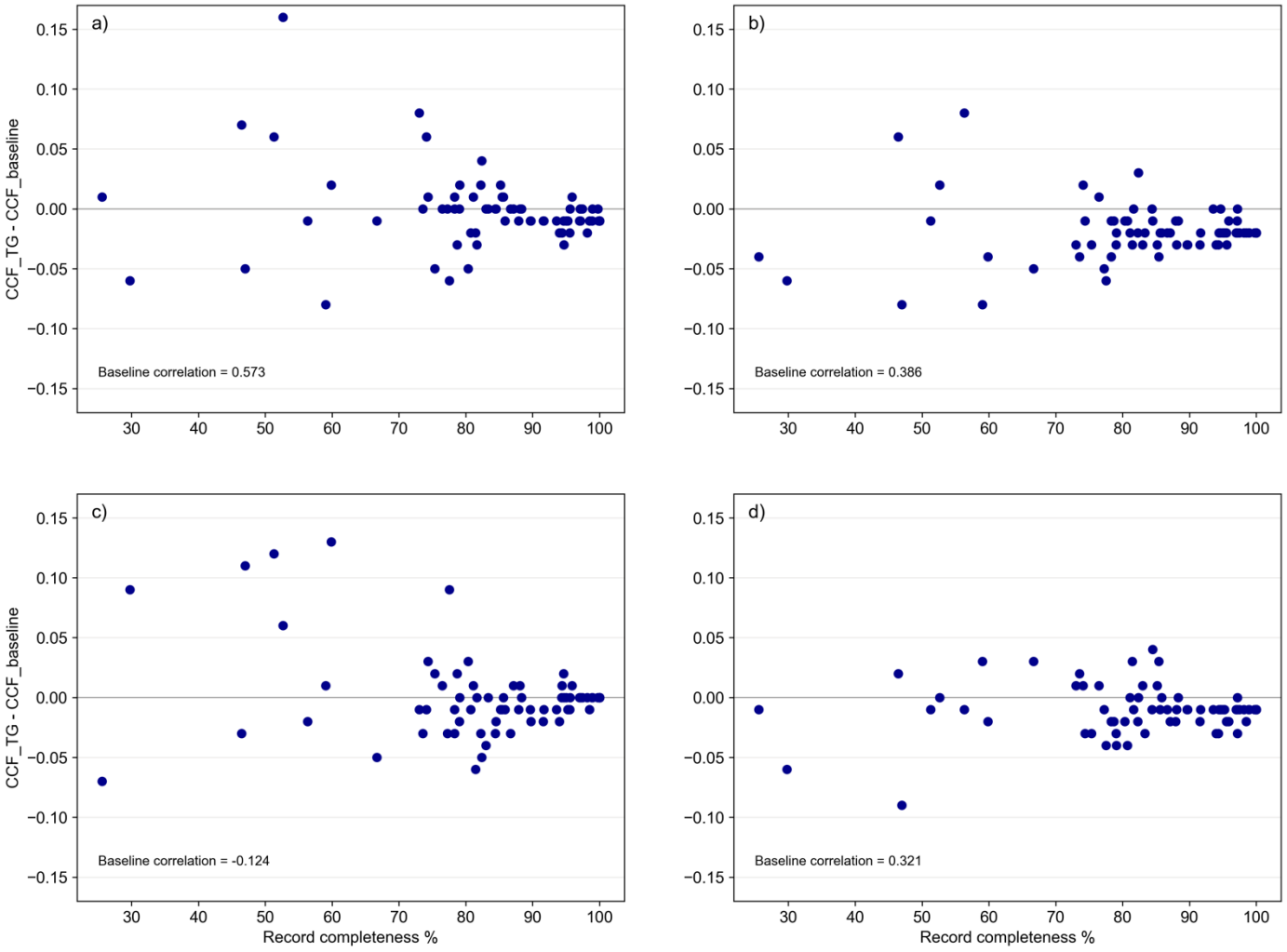

Figure 4.1: Sensitivity of the correlation coefficient between sea level and the NAO to record completeness at 82 TG sites for: a) Winter, b) Spring, c) Summer, and d) Autumn. The data for each season is presented relative to the baseline correlation calculated from the baseline record as detailed in section 3.3.2.

4.2 Correlations between observed MSL and the NAO index

The correlation coefficients between the corrected MSL time series and the NAO index at each TG are presented for the periods 1950-2021 (Figure 4.2) and 1993-2021 (Figure 4.3). These correlations help address Objective 2 and also form the basis of the NAO-SL component, which relates to Objective 3. Particular emphasis is put on correlations observed during winter and summer, as the NAO is more prominent during these seasons (Dangendorf *et al.*, 2014). However, the key trends in correlations for spring and autumn are also explored.

The differences in the spatial patterns of the correlation coefficients are minimal between the two time periods 1950-2021 and 1993-2021. However, there are differences in the strength and significance of the correlations. As expected, the most pronounced spatial correlation patterns between MSL and the NAO index emerge during the winter and summer seasons for both time periods. For 1950-2021, correlations between winter MSL and the NAO index show a clear north-east to south-west spatial pattern (Figure 4.2a): correlations vary from strongly positive in the North Sea and the north-west UK coastline (between 0.2 and 1) to negative through the English Channel and around the south-west NWES region (between -0.2 and -0.4). Only one correlation (Portsmouth, TG 3) is statistically significant (i.e. $p < 0.05$). For most TGs these winter correlations are the strongest out of all seasons for 1950-2021. When comparing the two time periods, positive correlations strengthen in 1993-2021 (Figure 4.3) compared with the correlations in 1950-2021 (Figure 4.3a). 72% of winter correlations for 1993-2021 are statistically significant compared with only one for 1950-2021.

During summer there is an inversion of the winter correlation pattern for the majority of TGs in 1950-2021 and 1993-2021, with most showing negative and significant correlations between MSL and the NAO index (Figure 4.2c and Figure 4.3). The exception to this is the 1950-2021 correlation for Cuxhaven 2 (TG 6), which is low and positive correlation around 0 to 0.2. The strongest negative correlation for summer 1950-2021 is at Newlyn (TG 2) and is between -0.6 and 0.8. During 1993-2021 the correlations become more negative at four TGs, giving a clear north-east to south-west strengthening of correlations (Figure 4.3c). Only one correlation is significant for 1993-2021 compared with eight for 1950-2021.

The correlations for spring and autumn over both time periods do not have as clear of a spatial pattern than the correlations for winter and summer. The spatial pattern of positive and negative correlations is broadly the same for spring and winter, but the spring correlations are generally weaker,

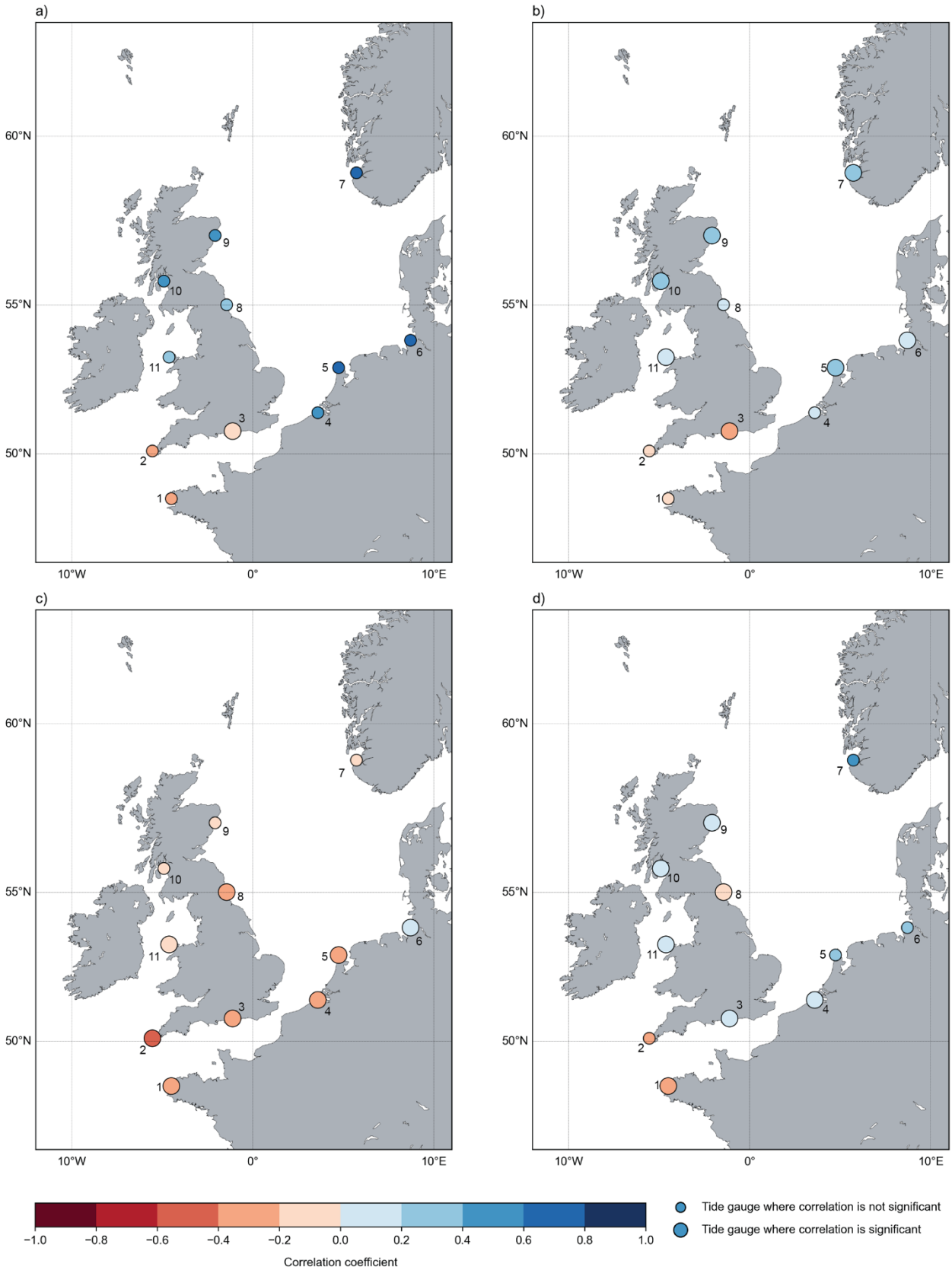

Figure 4.2: Correlation between IB-corrected MSL and the NAO between 1950 and 2021 at individual TG locations for: (a) winter; (b) spring; (c) summer and (d) autumn. Larger circles indicate the correlation at a site is significant.

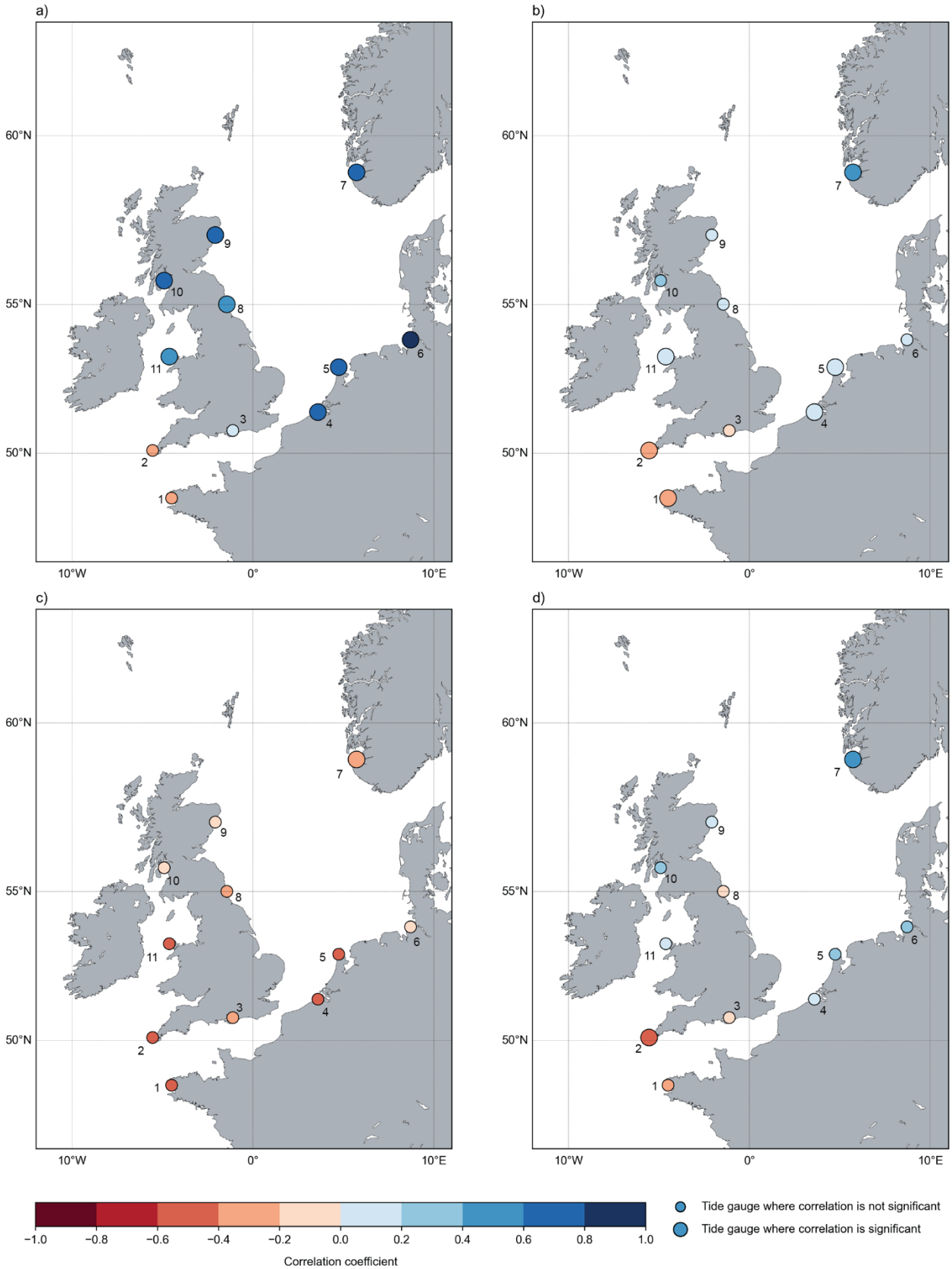

Figure 4.3: Correlation between IB-corrected MSL and the NAO for the satellite era between 1993 and 2021 at individual TG locations for: (a) winter; (b) spring; (c) summer and (d) autumn. Larger circles indicate the correlation at a site is significant.

(Figure 4.2b and Figure 4.3b) as the winter-summer transition is occurring. On average, spring correlations compared to winter are 66% smaller for 1993-2021 and 58% smaller for 1950-2021. From summer to autumn, correlations for TGs in the north and at the upper end of the English Channel turn from negative in summer to weakly positive in autumn, whilst the south-west TGs remain positive (Figure 4.2c-d and Figure 4.3c-d). This pattern is the same for 1950-2021 and 1993-2021. The main difference between observed summer and autumn correlations is changing significance at various TGs between the time periods. For spring 63% and 50% of correlations are significant for the 1950-2021 and 1993-2021 periods respectively, but four of the locations (TGs 3, 6, 9 and 10) for which correlations are significant in 1950-2021 are not significant in 1993-2021. In autumn, again 63% of correlations are significant in 1950-2021 but this drops to only 18% in the 1993-2021 period.

4.3 Sea-level projections

4.3.1 Individual projected sea-level components

The following section presents results linked to Objective 3. The individual components (Equation 10) that make up the total sea-level projections are shown in Figure 4.4-Figure 4.6. Figure 4.4 shows the MSL component, which is the SSP2-4.5 CMIP6 sea-level projection for each location (Fox-Kemper *et al.*, 2022); this is the long-term sea-level trend that underlies the annual and NAO-SL components. All values of SLC outlined here are relative to a 1995-2014 baseline. The MSL pattern is highly consistent between locations, rising from around 0.1 m in 2023 to between 0.2-0.3 m in 2053. The associated uncertainty is also consistent across all the locations, and the envelope widens over time from ± 0.08 m in 2023 to ± 0.2 m in 2053, with a notable change in the rate of increase around 2040.

The projected annual component is periodic over time at each location (Figure 4.5), whilst the amplitude of the cycle differs by site. The projections at Cuxhaven 2 (Figure 4.5c), Den Helder (Figure 4.5e) and Stavanger (Figure 4.5f) all have a peak to trough amplitude of ~ 0.2 m, compared with the projections at Brest (Figure 4.5a) and Portsmouth (Figure 4.5i) that have an amplitude half the size ~ 0.1 m. Compared with the other locations, Brest and Millport (Figure 4.5k) have more asymmetric cycles; the annual cycle for Millport has a fall-rise-fall pattern between the peak and trough of the cycle ,and Brest has two values close to the peak. This asymmetry is accentuated because the annual cycle is averaged to a quarterly (three-month) timescale. The uncertainty on the annual component is relatively small compared with the annual component itself; for example, the winter part of the cycle at Den Helder reaches up to 0.8 m with

an uncertainty of 0.01 m. On average, annual uncertainty in winter is 10% of the amplitude and ~8% in summer.

The NAO-SL sea-level projection is the product of the sea level/NAO regression coefficients by season by site (Table 1) and the projected, seasonally-averaged NAO index (Appendix A, Figure A3). Consequently, any spatial differences in the NAO-SL component are driven by the coefficients. As a result, all locations show a highly fluctuating patterns of SLC with a distinct individual signal (Figure 4.6). Cuxhaven 2 (Figure 4.6c), Den Helder (Figure 4.6e) and Stavanger (Figure 4.6f) have the largest peak to peak amplitudes, because they have some of the highest and lowest coefficients for winter in particular (78.10 mm/unit NAO, 42.67 mm/unit NAO and 27.64 mm/unit NAO respectively). The signal for Holyhead (Figure 4.6b), North Shields (Figure 4.6g) and Portsmouth (Figure 4.6i) are all more muted in comparison, with winter coefficient values of 17.80 mm/unit NAO, 13.54 mm/unit NAO and -1.58 mm/unit NAO respectively. The uncertainty on the NAO-SL component for all TG locations shows consistency over time. However, the individual patterns of uncertainty vary between each location. Cuxhaven 2 (Figure 4.6c) and Den Helder (Figure 4.6e) have the largest uncertainty of ± 1.5 m and ± 0.8 m respectively. Den Helder has a smaller relative difference between summer and winter uncertainty, indicated by a wider central band, whereas Cuxhaven 2 has a much larger seasonal difference shown by the deeper troughs and narrower central band. TGs such as Aberdeen 1 (Figure 4.6j) and Portsmouth (Figure 4.6i) also have uncertainties dominated by large seasonal differences. Similar to the NAO-SL component, the uncertainty for Holyhead (Figure 4.6b), North Shields (Figure 4.6g), and Portsmouth (Figure 4.6i) is smaller, measuring approximately ± 0.25 m, compared to other locations.

4.3.2 Total projected seasonal sea-level change

Projections of total seasonal SLC (Equation 10) and the associated total uncertainty for each TG location (Equation 11) are shown in Figure 4.7. All locations show an oscillating pattern of seasonal SLC, resulting from the annual and NAO-SL components, that trend upwards over time as a result of the MSL projection. Locations with particularly large seasonal amplitudes include Cuxhaven 2 (Figure 4.7c), Den Helder (Figure 4.7e) and Stavanger (Figure 4.7f), which is as expected given the pattern of the projected NAO-SL signal at these locations. Cuxhaven 2 in particular has a large amplitude of ~0.5 m. Cuxhaven 2 and Den Helder also have notable peaks in winter sea level. The projection for Portsmouth (Figure 4.7i) has a seasonal amplitude of ~0.1 m, which is small compared with the other projections. The projections for Holyhead (Figure 4.7b), North Shields (Figure 4.7g) and Portsmouth

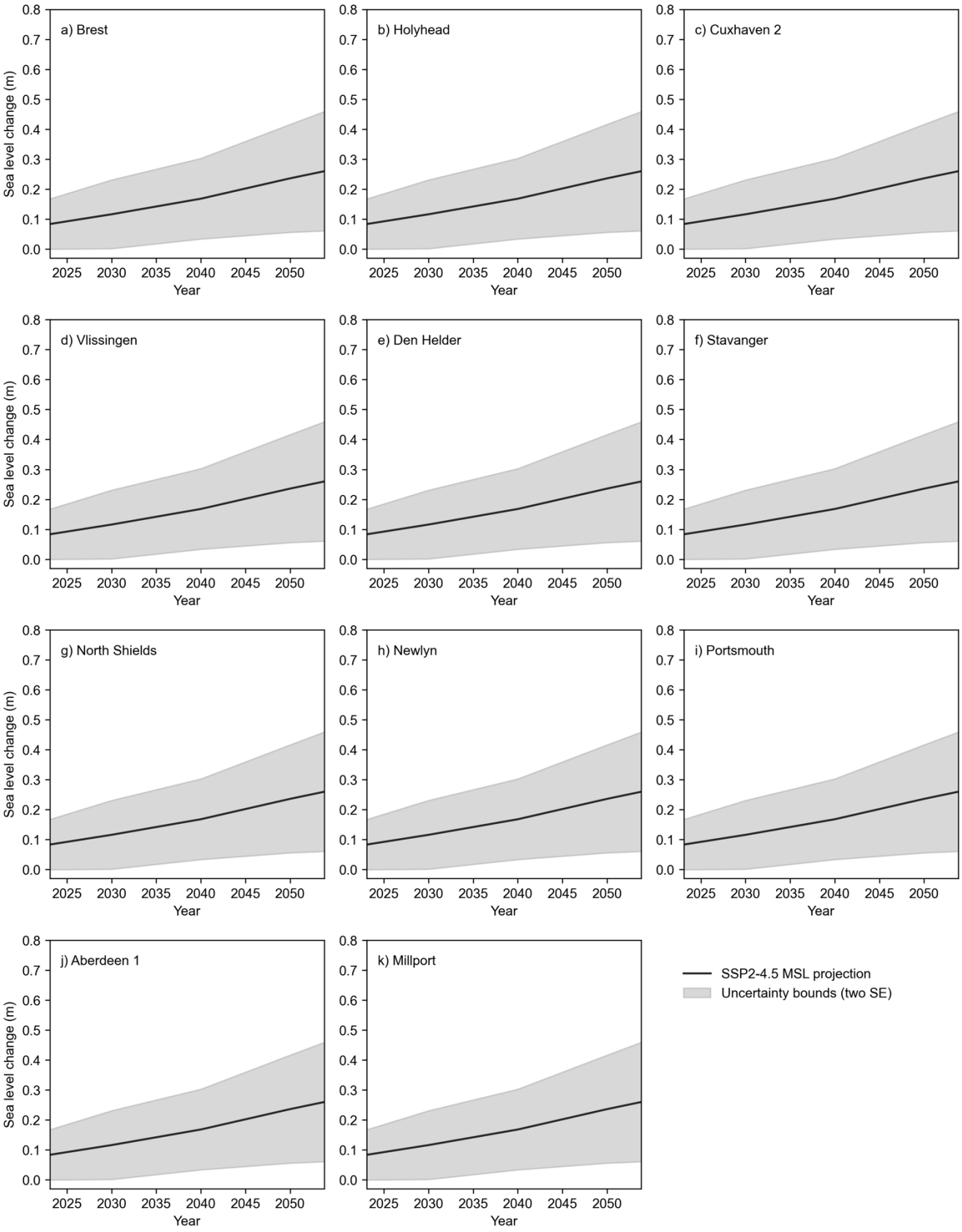

Figure 4.4: The MSL sea-level component (the interpolated SSP2-4.5 sea-level projection) and the associated uncertainty given as two standard errors (SE) for 2023-2053 at each TG location.

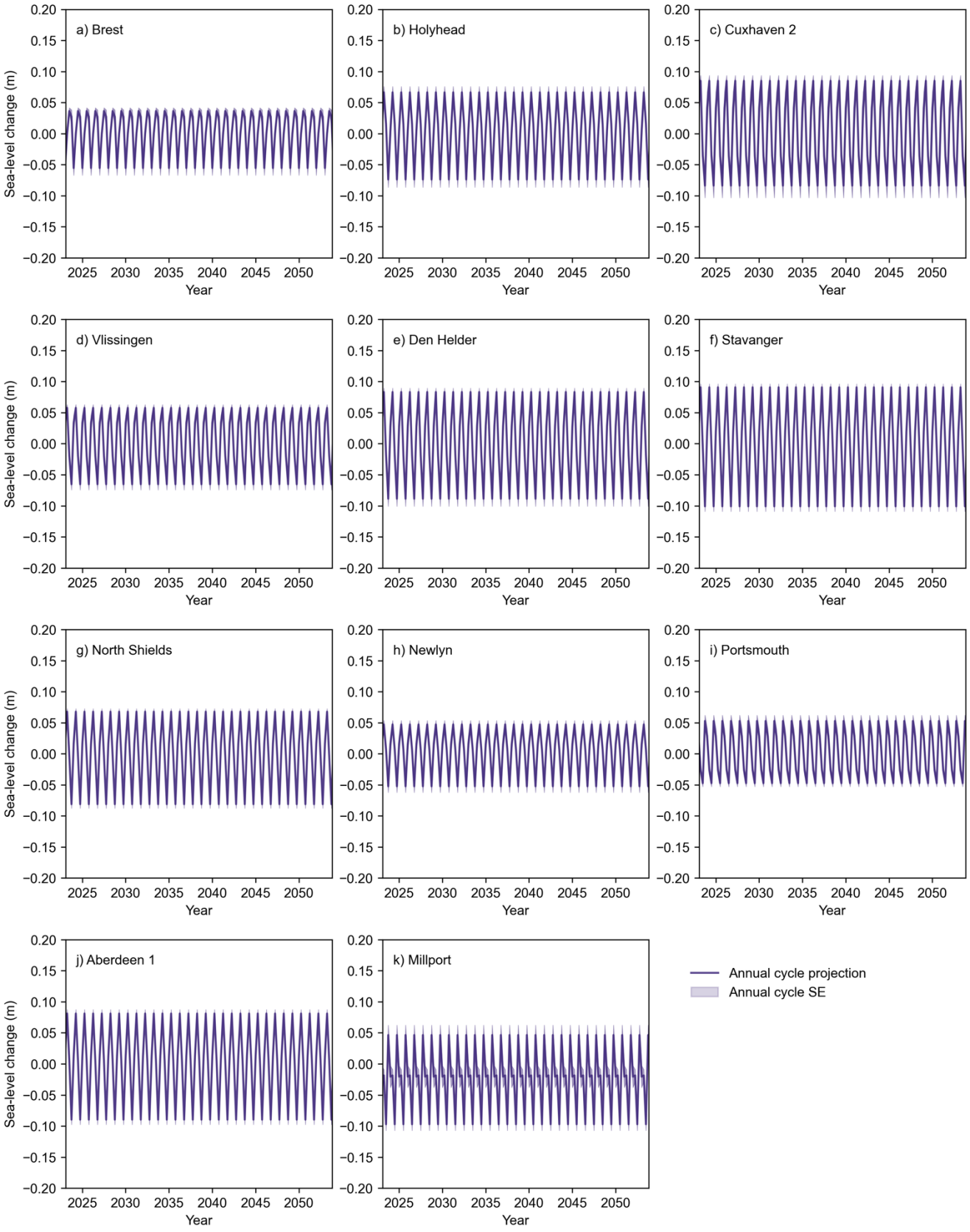

Figure 4.5: The sea-level annual cycle component and the associated uncertainty given as one standard error (SE) for 2023-2053 at each TG location.

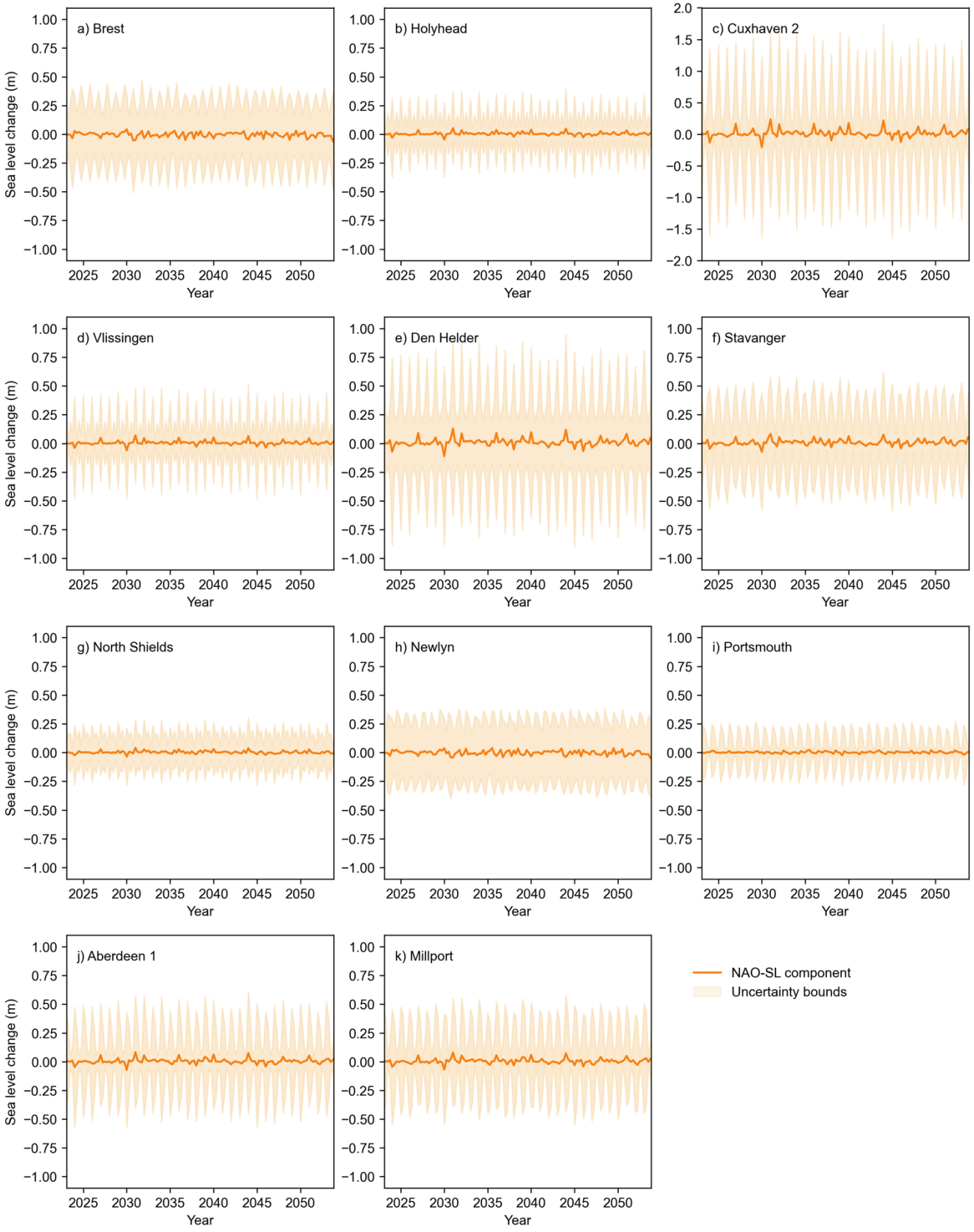

Figure 4.6: The NAO-SL component and the associated uncertainty (coefficient error and model uncertainty) for 2023-2053 at each TG location. Note the different y-axis scale for Cuxhaven 2 (c).

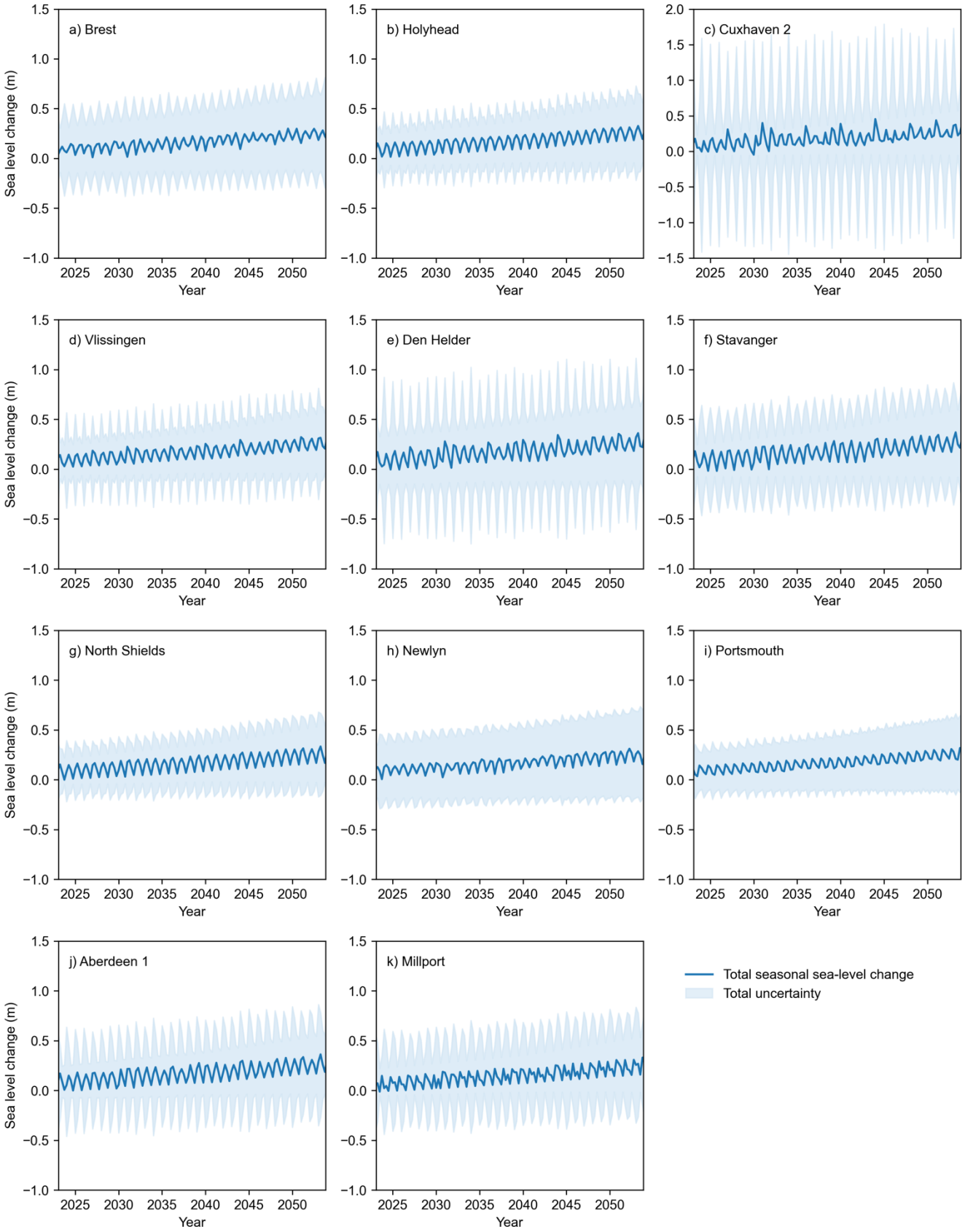

Figure 4.7: Total projected seasonal SLC and the associated total uncertainties for 2023-2053 at each TG location. The MSL, annual and NAO-SL components have been summed to give a sea level projection at seasonal time steps. Note the different y-axis scale for Cuxhaven 2 (c).

(Figure 4.7i) also show a more consistent cyclical pattern compared with the other records, which show more sporadic peaks and troughs throughout time. Over the time period, each of the seasonal projections rise in a manner consistent with the pattern of MSL change (shown in Figure 4.4).

The pattern of total uncertainty differs between locations. The uncertainty on the NAO-SL component displays seasonal variability (Figure 4.6), and this is more extreme for some locations than others. Uncertainties for Holyhead (Figure 4.7b), North Shields (Figure 4.7g), Newlyn (Figure 4.7h) and Portsmouth (Figure 4.7i) are dominated by the linear MSL signal with a muted seasonal uncertainty signal. Conversely, the uncertainty in the Cuxhaven 2 (Figure 4.7c), Den Helder (Figure 4.7e), Aberdeen 1 (Figure 4.7j) and Millport (Figure 4.7k) projections are dominated by seasonal sources. The variance for all locations increases over time in line with the MSL component uncertainty (Figure 4.4). This pattern is particularly noticeable for Holyhead (Figure 4.7b), Vlissingen (Figure 4.7d), North Shields (Figure 4.7g) and Aberdeen 1 (Figure 4.7j).

4.4 Fraction of variance analysis

Figure 4.8 shows the different sources of uncertainty in the seasonal sea-level projections expressed as a fraction of the total uncertainty over 2023-2053. The projection uncertainty shows a similar general pattern over time at each location. Across all sites, NAO-SL uncertainty contributes on average ~80% of total uncertainty in 2023, which falls to 50-60% in 2053 as the relative contribution of MSL uncertainty increases. However, NAO-SL uncertainty varies seasonally, at its greatest fluctuating at ± 50% of total uncertainty for Cuxhaven 2 (Figure 4.8c). The contribution from annual uncertainty remains fairly small and constant over the whole time period.

Around this general trend, there are distinct patterns of projection uncertainty at each TG location. As mentioned above there are spatial differences in the seasonal ranges within the NAO-SL uncertainty. Uncertainty for Brest (Figure 4.8a), Den Helder (Figure 4.8e), and Newlyn (Figure 4.8h) fluctuates less between seasons, while Cuxhaven 2 (Figure 4.8c), Vlissingen (Figure 4.8d), Portsmouth (Figure 4.8i) and Millport (Figure 4.8k) are all dominated by large differences between winter and summer uncertainty.

For some locations NAO-SL uncertainty also remains more dominant over time than others, such as Stavanger (Figure 4.8f) and Cuxhaven 2 (Figure 4.8c) where peak uncertainty from NAO-SL remains at ~70-80% and ~90% of total uncertainty over time. At North Shields (Figure 4.8g) and Holyhead (Figure 4.8b) the peak contribution from NAO-SL uncertainty falls from ~80-60% and from ~75-50% respectively.

In general, annual cycle variance only makes a small contribution to total variance and at all sites the relative contribution of annual cycle uncertainty falls over time. There are also clear individual patterns at each location. At Holyhead, Portsmouth and Millport annual cycle uncertainty makes up a higher proportion (7%, 9% and 8% at the cycle peak in 2023 for the respective TGs) than for Brest, Den Helder and Newlyn, where the contribution to total uncertainty is lower at ~1% at the cycle peak in 2023 for all three sites.

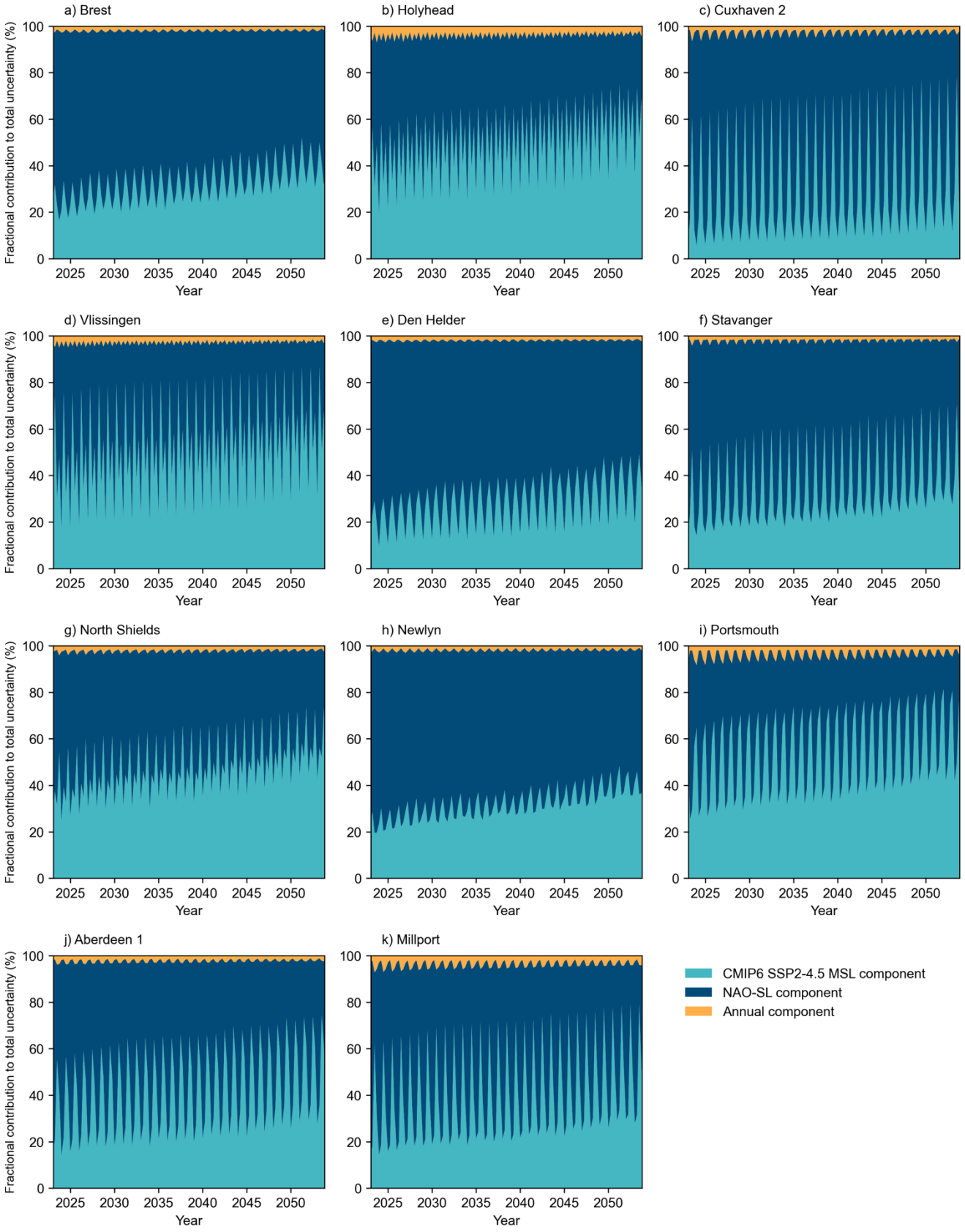

Figure 4.8: Fractional contribution of individual components to total uncertainty in the seasonal sea-level projection at each tide gauge location (a-k).

Chapter 5: Discussion

5.1 Tide gauge record sensitivity

As could be surmised, the record completeness analysis indicates that data gaps in TG records affect correlation coefficients calculated using TG data, but crucially the impact on the coefficients is relatively small. The sensitivity analysis in section 3.3 shows that synthetic coefficients do not vary beyond ± 0.15 of the baseline correlations for any season, with the exception of one record in winter that is + 0.16 of the baseline. These correlation deviations from the baseline are small considering six of the records are <50% complete. However, the analysis does not fully distinguish whether the seasonal differences in sensitivities can fully be attributed to the data gaps, or whether the true differences between seasonal correlation coefficients (see Figure 4.2 and Figure 4.3) are having an influence here too. It is also important to acknowledge that the analysis is based on a singular record (the Den Helder TG), for which the sea-level data shows a strong relationship to the NAO. Were the analysis to be carried out using a record with a stronger or weaker relationship between the NAO and sea level the correlation deviations from the baseline would be different, as the baseline correlation would also be a different value.

Data gaps in TG records have been a persistent challenge in sea-level science as long as TGs have been used to measure SLC (e.g., Church et al., 2004; Mangiarotti, 2007). Typically, the gaps are addressed using reconstruction and interpolation techniques (e.g., Dangendorf et al., 2019) to combat this issue. This analysis of record sensitivity, conducted at seasonal time steps, suggests that at higher-frequency temporal scales, data gaps tend to have a reduced impact on data analysis. This may be attributed to the larger number of data points available at seasonal time intervals, which mitigate the absence of certain data points and means missing data is less consequential to the overall analysis.

A way to take this type of record sensitivity analysis further would be to also account for the distribution of data gaps through records. Some records have gaps at systematic intervals, but others have large periods of missing data, such as Portsmouth and Holyhead. The method used to create the synthetic records does incorporate the individual distribution of gaps present in each TG record used in the analysis, but the distribution is not then quantified and represented as a contributing factor to completeness. Incorporating a quantification of gap distribution alongside the quantification of missing data would be a step towards an even more comprehensive understanding of how TG data gaps affect sea-level analysis. Studies have tackled TG data gaps and more general issues with TG data sets using various approaches. For example, improvements to the TG data available for the UK and Australia

coastlines have been made via verifying records and adjusting for datum errors using metadata from archived sources (Hogarth *et al.*, 2020) and by using a homogenisation technique to detect and correct jumps or steps in data (Hague *et al.*, 2022). A harmonic least-squares procedure was used by (Gil and de Toro, 2005); applying a similar approach to daily-monthly records alongside could be effective.

5.2 Relationships between observed MSL and the NAO

The relationships between observed MSL and the NAO that are highlighted in this study show similarities with patterns observed in previous studies. The spatial pattern, characterized by a transition from positive to negative correlations extending from north-east to south-west, aligns with findings from earlier studies (e.g., Wakelin et al., 2003; Dangendorf et al., 2012). These consistent spatial patterns emphasize the persistent influence of the NAO on MSL in the NWES region.

This study also identifies strong winter correlations between MSL and the NAO index over two extensive time periods, spanning from 1950 to 2021 and from 1993 to 2021, for TGs situated in the North Sea and along the west coast of the UK. Specifically, the correlation coefficients obtained in this study closely resemble those reported in Wakelin et al. (2003). The correlation values range from 0.6 to 0.8+ for TGs in the North Sea in 1950-2021 (Figure 4.2), a range that is in alignment with the 0.7 to 0.8+ correlations identified in Wakelin et al. (2003). This strong connection between sea level and the NAO in the south-east North Sea, which is consistently observed in studies, has been attributed to the positioning of low-pressure systems that are connected to the activity of the NAO. These systems typically track from southern Greenland over the North Sea, creating distinctive strong westerly winds and high MSL variability for this region of the NWES (Ullmann and Monbaliu, 2010).

The NAO-MSL relationship is not limited to the winter and summer seasons. The correlations provided for spring and autumn also give valuable insights into the interaction between the NAO and MSL. These seasons capture the transition from a positive to a negative sign that takes place from winter to summer at all TGs excluding Brest and Newlyn across both time periods and Cuxhaven 2 in 1950. In terms of the correlations, the transition brings weakening positive correlations in spring and switches from negative to positive correlations for many TGs during autumn. There may be an indication of a lag effect of the NAO on sea level, suggested by spring correlations turning weaker but remaining positive for all TGs except Brest, Newlyn and Portsmouth. These three TGs are all located in the English Channel, suggesting as other studies do that the NAO-induced effects of wind-stress versus pressure effects differ spatially

(Dangendorf *et al.*, 2014). Evidence of this could be further investigated by evaluating correlations against wind stress and direction to identify how correlation strength and the sign evolve between winter and summer.

While the relationships between the NAO and MSL are well established during winter and summer months, the significance of these correlations are varied among studies. Some studies find that only specific months, notably December to March, exhibit significant coefficients (e.g., Wakelin et al., 2003; Dangendorf et al., 2012). Conversely, other analyses, such as that by Chen et al. (2014), indicate significant correlations for January and February, but not for December or March at inter-annual timescales. In terms of how the correlation coefficients match up to these findings, it is harder to find a strong agreement or disagreement due to the variation in significance between the two time periods. For instance, only Portsmouth has a significant correlation in winter 1950-2021, but 63% are significant in spring 1950-2021. Conversely, 72% TGs are significant for winter and 55% for spring 1993-2021. The inconsistency between the time periods makes it hard to draw a general conclusion because even though the number of spring correlations is consistent between the time periods, the locations that are significant change.

One distinct metric that does emerge is that 61% of correlations for 1993-2021 are significant compared with only 48% for 1950-2021. This may be attributable to two factors: the influence of the NAO becoming more pronounced in recent years, or disparities in the coverage and quality of data between the two periods. Over the longer time period between 1950 and 2021 there is a greater proportion of data gaps compared to the more recent time period, which may explain the lower number of significant correlations. Missing data results in lower statistical power and makes it harder to detect significant correlations even if they truly exist within the climate system. This is emphasised if data are missing from some seasons more than others, as this will skew the seasonal pattern of correlations at individual TG locations.

5.3 The seasonal projections

This study draws together observational TG data and CMIP6 model projections to quantify future seasonal SLC in the NWES region. Using the budget approach described in section 3.6, projections were constructed for the 11 TG locations from individual sea-level components to build up a picture of

seasonal change, where the NAO was treated as the main driver of seasonal change. In the following sections, the value of the budgetary projection method is assessed, against existing work and as a method in its own right.

5.3.1 Comparison with existing projections

When compared with projections produced using alternative, model-based methods, the projections shown in Figure 4.7 demonstrate feasible ranges of seasonal SLC over the 30-year period between 2023-2053 in the NWES region. Comparison can be made with the projections in Hermans et al. (2022), who present seasonal projections of DSLC from downscaled GCM output for the period 2081-2100 for SSP5-8.5 for the NWES, as well as seasonal sea-level anomalies (SLA) for 1980-2100 (Figure 5.1). The time period and SSP scenario of the DSLC projections differ from those in this study; however, given a lack of seasonal projections for the period up to 2050, a 30-year projection later in the century at seasonal time steps provides the best comparison possible. A DSLC projection specific to Esbjerg is supplied in Hermans et al. (2022), so in order to make a meaningful comparison, the summed annual and NAO-SL components for Cuxhaven 2 (Figure 4.6c) and Stavanger (Figure 4.6f) are evaluated alongside the DSLC projections at Esbjerg.

The projected winter and summer sea-level anomalies (SLA) for Esbjerg in Hermans et al. (2022) have more distinct patterns than spring and autumn over the period 2020-2060 (Figure 5.1b). Between 2020-2030, the SLA for all seasons overlap; however, towards 2060, clearer patterns in winter and summer start to emerge. Winter SLA start trending above the SLA of other seasons and reach up to ~4 cm, whilst still showing large variance above and below 0. The pattern is similar with summer, but the anomalies start trending below those of winter, spring and autumn and reach ~-3 cm by 2060. In comparison, the sign and general trends in the seasonal SLA for Cuxhaven 2 (Figure 5.2a) and Stavanger (Figure 5.2b) align with those in Hermans et al. (2022), but they exhibit different magnitudes. For instance, winter SLA variability at Cuxhaven 2 also have large variance, but they reach up to ~30 cm which is more than three times the maximum SLA reached in the Hermans et al. (2022) projection. Summer SLA at Cuxhaven 2 also have a negative sign similar to SLA at Esbjerg but show much less variation. The variance in the SLA for Stavanger is more similar to the variance in the SLA for Esbjerg, particularly summer. Also, none of the seasonal components in Figure 5.1b show a major change in gradient until after 2050, which is consistent with the gradient of this study's seasonal projections.

The major difference between the SLA in Figure 5.2 and Figure 5.1a is that the former remain relatively constant over time. This is as expected because both the annual and NAO-SL components, as shown in Figure 4.5 and Figure 4.6, exhibit consistent behaviour throughout the study period, unlike the SLA trends in Hermans et al. (2022), which display long-term temporal changes. The differences in magnitude can be attributed to the fact that DSLC and the annual + NAO-SL components do not lend themselves to a true direct comparison. The relationship of the NAO with AMOC and the wider North Atlantic climate system means there are shared physical processes between the two, but NAO is just one contributing factor to DSLC. Another important distinction is the temporal scales of maximum variance: variance in DSLC is predominant in the long-term component, while the NAO-SL component calculated in this study demonstrates strong intra-annual variance. It is noteworthy that despite these differences, the seasonal SLA in both datasets share a similar relative positioning with respect to each other.

5.3.2 Evaluation of projected sea-level change

There are notable spatial patterns among the individual projections across the shelf region. There is a clear increase in both projected SLC and projection uncertainty from the south-west through to the north-east, which is demonstrated in Figure 5.3 for two time slices in 2023 and 2053. For example, total projected SLC for TGs in the North Sea in 2053 (TGs 5-9 in Figure 5.3b) is 0.3-0.4 m compared with 0.2-0.3 m for TGs in the south-west (TGs 1-3). The same pattern is reflected in the uncertainty in Figure 5.3c-d. The higher level of SLC occurring in the north-east of the shelf is likely linked to the effect of the NAO on sea level in this region, particularly as there is negligible difference between the MSL and annual components between any of the TGs. The NAO has been shown to have a particularly strong relationship with seasonal sea level in studies using TG and satellite altimetry data in the German Bight (Dangendorf *et al.*, 2012) and the south-east North Sea (Dangendorf *et al.*, 2014), so it is unsurprising that the largest seasonal signals in the projections are also found in this area of the shelf. This north-east to south-west gradient suggests a corresponding gradient in the NAO and the effect of the oscillation on sea level, which is logical as the NAO-SL component is partly driven by relationships between sea level and the NAO in the TG records, where this gradient over the NWES is visible. There is also a positive comparison to be made again with the seasonal DSLC projections in Hermans et al. (2022). The spatial pattern of winter SLA in Figure 1a in Hermans et al. (2022) is consistent with the spatial pattern in winter SLC in Figure 5.3, which helps verify that way the projected seasonal components have been calculated in this study accurately captures known patterns of NAO behaviour, and by extension seasonal trends within sea level.

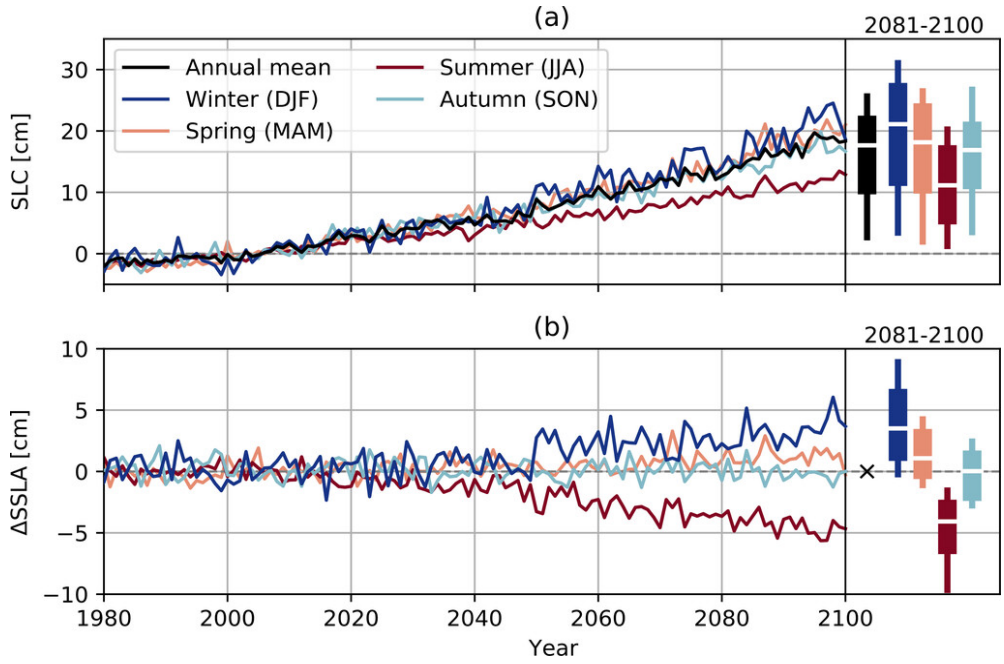

Figure 5.1: Ensemble median projections for Esbjerg of (a) annual mean and seasonal mean DSLC (cm) and of (b) the change in seasonal sea level anomalies (cm) for SSP5–8.5 (relative to 1995–2014). The bars on the right indicate the 50% (horizontal white stripes), 17%–83% (thick bars), and 5%–95% (thin bars) percentiles of the multimodel distributions of the mean change in 2081–2100 (from Hermans et al., 2022).

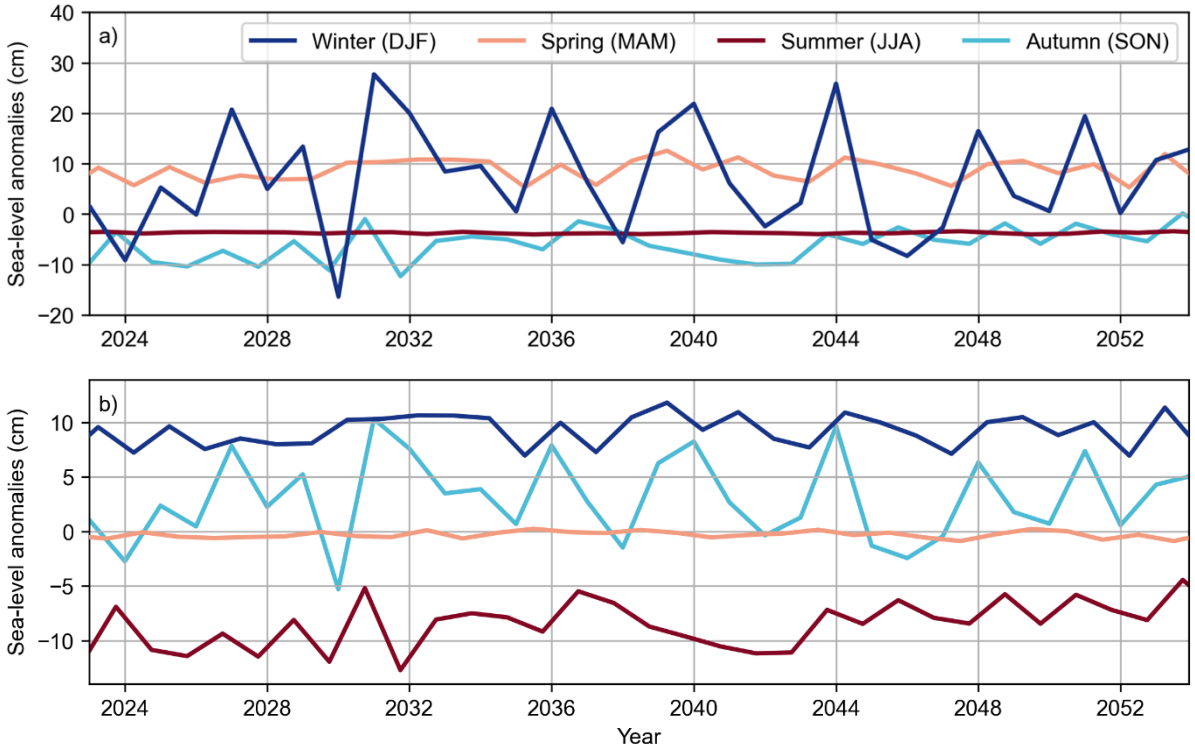

Figure 5.2: Seasonal SLC at Cuxhaven 2 (a) and Stavanger (b) for SSP2-4.5, relative to 1995-2014.

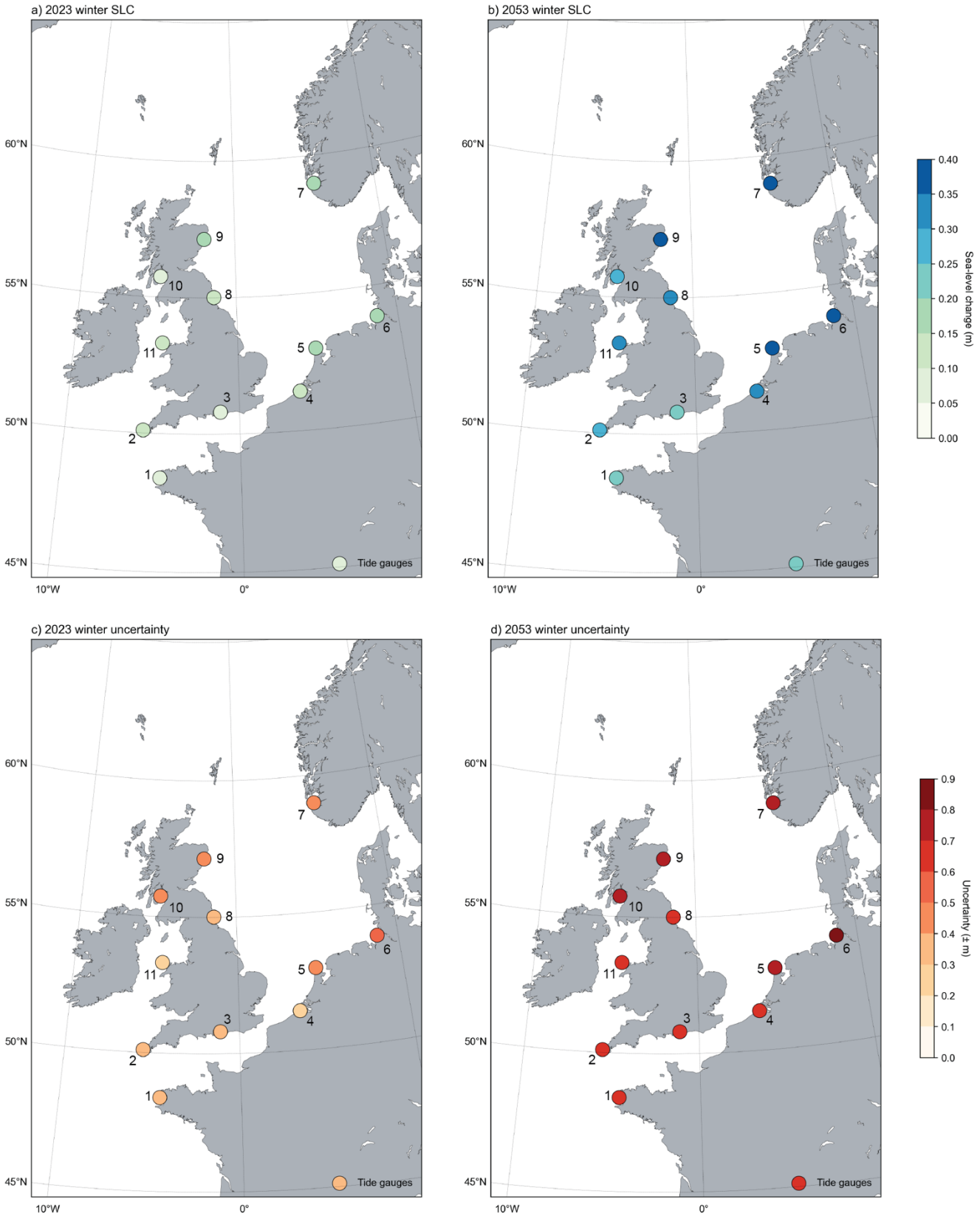

Figure 5.3: Changes in sea-level change (a-b) and total uncertainty (c-d) at coastal tide gauge locations (refer to Figure 1.1 for tide gauge numbers) between 2023 and 2053.

5.3.3 Comparison between observed and projected sea-level change

Figure 5.4 shows how observed MSL from 1950-2020 compares with the seasonal projection and associated uncertainties produced in this study for 2020-2053 at each TG location. Both datasets are relative to a 1995-2014 reference period. In Figure 5.4, it is evident that the amplitude of the seasonal projection (represented by the blue line) is consistently smaller than the amplitude of the observed sea level at all locations, and there are a few reasons that contribute to this. Firstly, the observed MSL time series are at monthly time steps and will therefore capture higher-frequency sea-level signals that the projections, which are at coarser time intervals, cannot replicate. Additionally, the observed MSL series incorporate data from extreme weather events, along with long-term and seasonal behaviour, whereas the projections do not include a component that explicitly represents these extreme events. Given the differences in signals within both data sets, it is encouraging that the seasonal water levels in the projected series do not exceed those in the observed series.

Another observation to note is that the underlying gradient of some projections seems to be greater than the gradient of the historical data, for example the projections for Brest (Figure 5.4a), Stavanger (Figure 5.4f) and Millport (Figure 5.4k). This is entirely connected to the gradient of the SSP2-4.5 MSL projection (Fox-Kemper *et al.*, 2022), and reflects the projected rise in MSL produced in CMIP6 models under the SSP2-4.5 scenario. At the locations specified above, it appears that the rate of projected MSL rise is greater than the rate experienced at the TGs over the last 70 years.

Following on from comparing the central estimate of projected SLC with observed sea level, comparing the projection uncertainties with observed sea level in Figure 5.4 draws out some additional features. The central band of uncertainty which is primarily associated with the MSL component in the projection (identified as the solid area within projection uncertainty in Figure 5.4) accounts for the whole range of SLC observed in the MSL series at multiple locations, such as Holyhead (Figure 5.4b), Vlissingen (Figure 5.4d) and Den Helder (Figure 5.4e). At these locations, the seasonal component in the uncertainty gives an estimate of potential sea-level values between 0.2-1 m outside the range of water levels observed at these locations, which by comparison is a large overestimation. This is even more extreme at locations such as Cuxhaven 2 (Figure 5.4c) and Aberdeen 1 (Figure 5.4j), where the seasonal components of the uncertainty dominate and suggest potential water levels nearly twice that of recorded water levels in the TG series. By contrast, there are locations where the projection and uncertainty give potential water levels well within those already observed, such as North Shields (Figure 5.4g) and Portsmouth (Figure

5.4i). At these locations, the method appears to be effective at providing projections that align closely with the physical processes in those respective regions.

This comparative analysis of observed data with the projections and their associated uncertainty highlights two important observations: firstly, that different components in the projections have varying degrees of importance depending on the location, and secondly that the effectiveness of the method in accurately representing the underlying physical processes can vary significantly from site to site. For instance, the more conservative projection and uncertainty for Portsmouth may be linked to sea-level variability in the English Channel being dominated by the IB effect rather than wind-stress (Dangendorf *et al.*, 2014). As wind stress is the main driver of NAO-SL sea-level variability (Tsimplis *et al.*, 2005), an NAO-dominated projection will not accurately represent the physical processes driving SLC in this region. Additionally, the limited representation of the English Channel in models, even when the output for the region is downscaled, might also contribute to the challenge of accurately simulating fine-scale climate features in this region (Tinker *et al.*, 2020).

5.3.4 Evaluation of the projected NAO index

The projected NAO index used in this study exerts significant influence over the final projection, which makes it important to assess both the method and resulting output of the projection. The approach of using the CRU method on modelled SLP data to produce a projected index appears to be sound. When comparing the modelled NAO index with the observed index over the period of 1950-2020 using Pearson's correlation, the resulting correlation coefficient was low and positive ($r = 0.03$). Similar low and positive correlations between modelled and observed NAO indices have been reported in studies using CMIP5 and CMIP6 generated data (X. Wang *et al.*, 2017; Bracegirdle *et al.*, 2018), which suggests that the modelled NAO index in this study represents a reasonably robust indicator of future NAO patterns within the limits of the method used to calculate it.

When evaluating the method used to project the NAO index, the first consideration to make is how CMIP6 models resolve SLP and the wider North Atlantic climate system, which includes climatic features such as the NAO and AMOC which vary on intra-annual and interannual time scales. As outlined in section 2.2.1, the simulation of the NAO, and subsequently the components the oscillation, within

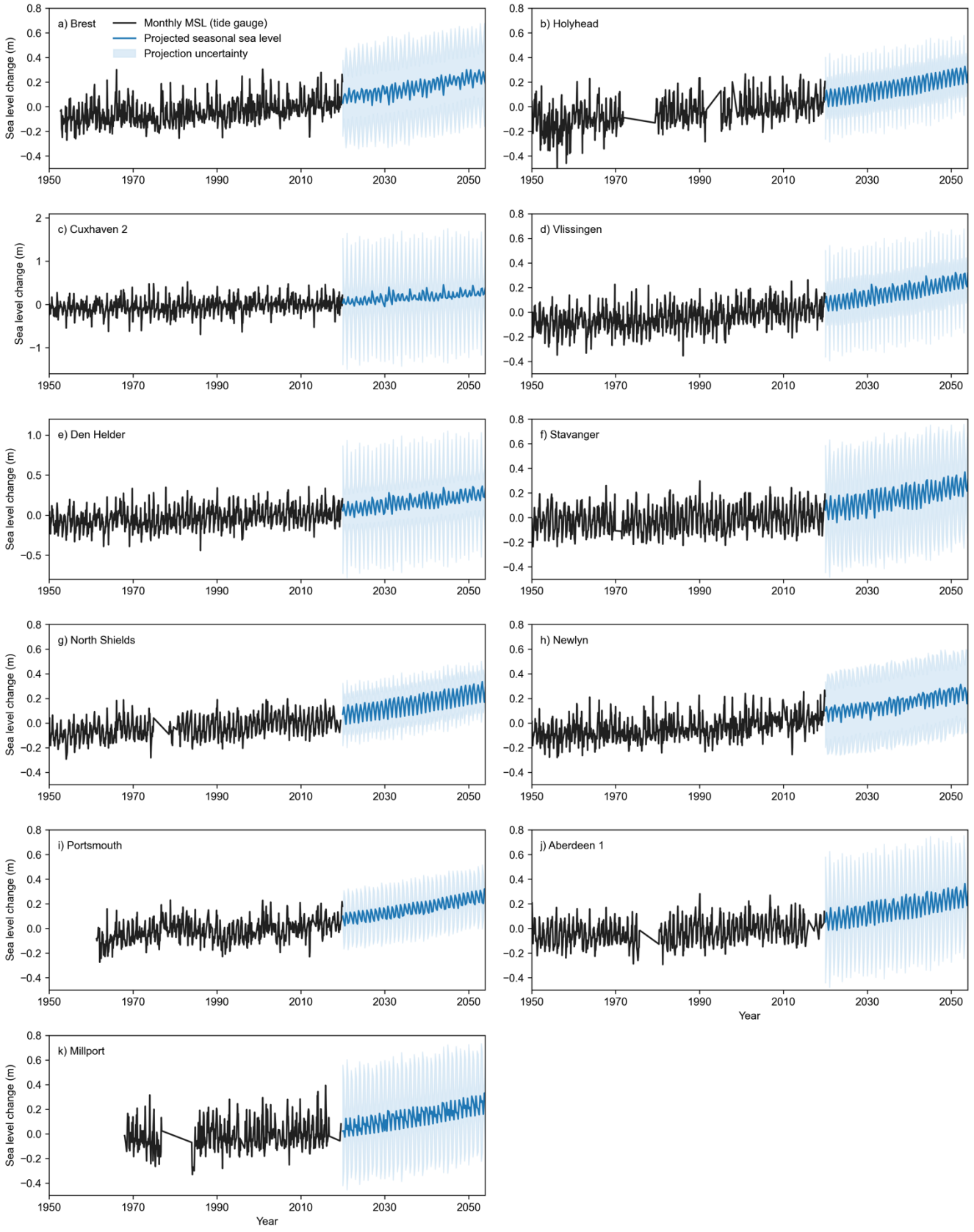

Figure 5.4 Time series of observed monthly MSL from tide gauge data between 1950-2020 (black line) and total projected SLC and the associated uncertainties for 2020-2053 for the 11 tide gauge locations. Gaps in the MSL series are due to missing data at those particular time steps. Note the different y-axis scales for Cuxhaven 2 (c) and Den Helder (e).

GCMs is still an area requiring improvement. The improvements between CMIP generations indicate models are getting closer to resolving the finer-scale features of the NAO (Cusinato *et al.*, 2021), but when these ongoing model challenges are combined with the limitations of how the ensemble mean was calculated, it is reasonable to assume that the NAO projection may lack some finer detail.

The data processing that takes place at the start of the NAO calculation also has a critical effect on the final NAO output. An important factor to consider is the use of the ensemble mean of each individual model to calculate the SLP ensemble mean over all 41 CMIP6 models. This took place at the start of the NAO calculation when determining SLP for the southern and northern boxes (see Appendix A). Using the ensemble mean of each model has several implications for the final output. Extremes and biases emerging from individual model members are mitigated to provide a consistent estimate of SLP from all models. Also, using the individual model means also makes it possible to quantify model uncertainty which emerges as a major contributor to total projection uncertainty (Figure 4.8). However, other factors reduce the effectiveness of using an ensemble mean. The way the ensemble mean was calculated here gives each model mean equal weighting, rather than assessing the ability of each model and assigning each model different weights to reflect ability. Equal weighting also assumes each model is independent which is not true in practice. As highlighted in section 2.3.3, many models within multi-model ensembles such as CMIP5 and CMIP6 share the base model and are therefore not independent of each other. Equally weighting the 42 CMIP6 models in the ensemble mean, despite the presence of these significant shared features and biases, has direct consequences on the ultimate NAO outcome. Accounting for model interdependence in particular could potentially lead to a more highly optimized NAO index when it is calculated using this approach.

The final aspect of the NAO projection to address is the uncertainty on the projection. This was quantified by calculating the standard deviation of the 41 ensemble means and then propagating this estimate of model uncertainty through the NAO calculation (refer to Figures 1-3 in Appendix A). By quantifying model uncertainty in this way, the upper and lower uncertainty bounds represent the maximum and minimum ranges at each stage of the NAO calculation. For example, in the NAO projection (Figure A3) the upper and lower uncertainty bounds represent the maximum and minimum possible NAO index values that could occur across the output of different models. This source of NAO-SL uncertainty dominates over the uncertainties originating from other components (Figure 4.7), which implies that within this particular set of projections, model-based factors are the primary contributors to uncertainty. This finding is consistent with research by McKenna and Maycock (2021), which found that structural

model differences were the predominant source of uncertainty in projections of the NAO made for 2080-2099 using models in the Multimodel Large Ensemble Archive (MMLEA) and CMIP5/6. This again highlights the challenges of making projections at high-resolution temporal and spatial scales using CMIP output, and it is notable that within the methodology in this study, which utilises data and trends from modelled and observed data, the main source of uncertainty is attributed to model-based sources.

5.3.5 Projection uncertainty

Throughout the discussion so far, the importance of projection uncertainty has been emphasised. Here, the projection uncertainty is compared with fractional uncertainty data from the UKCP18 report for Newlyn and Portpatrick (Figure 3.1.6 in Palmer et al., 2018), displayed in Figure 5.5.

Figure 5.5 shows the relative changes in three sources of uncertainty from 2000 to 2100: internal variability, model-based uncertainty, and scenario uncertainty. Between 2020-2060, the relative contributions from these three sources shift; in 2020 natural variability dominates at 50-60% of total uncertainty, followed by model uncertainty with only a small contribution from scenario uncertainty. This pattern agrees with the study's projection uncertainty (Figure 4.8), where highly variable NAO-SL uncertainty also constitutes up to 50% of total uncertainty in 2023 for all TG sites. For direct comparison, annual cycle and NAO-SL uncertainty make up 81% of total uncertainty for Newlyn in 2023 (Figure 4.8h), and similarly natural variability is ~80% of total uncertainty for Newlyn in Figure 5.5. This captures the dominance of natural variability within uncertainty for projections in the short-term. By 2060, Palmer et al. (2018) shows a transition in the dominant source of uncertainty to model and scenario (~80% of total uncertainty, Figure 5.5). The same general pattern is shared in Figure 4.8 as MSL uncertainty becomes more important towards 2053, however for Newlyn NAO-SL uncertainty remains dominant at 63% of total uncertainty, with MSL uncertainty making up 36% and annual cycle uncertainty the remaining 1%. The divergence in total uncertainty towards 2050 between projections in this study and those in UKCP18 is in part related to scenario uncertainty not being included in this study, as projections were only made for SSP2-4.5. If seasonal projections were to be developed for multiple SSP scenarios, then a scenario uncertainty component would be included. Doing so would change the proportions of total uncertainty around 2050 and beyond, as in the long-term scenarios become dominant

over natural variability. In the short term, the consistency between uncertainty sources within the two sets of projections affirms that within this study uncertainty is being treated in a coherent manner.

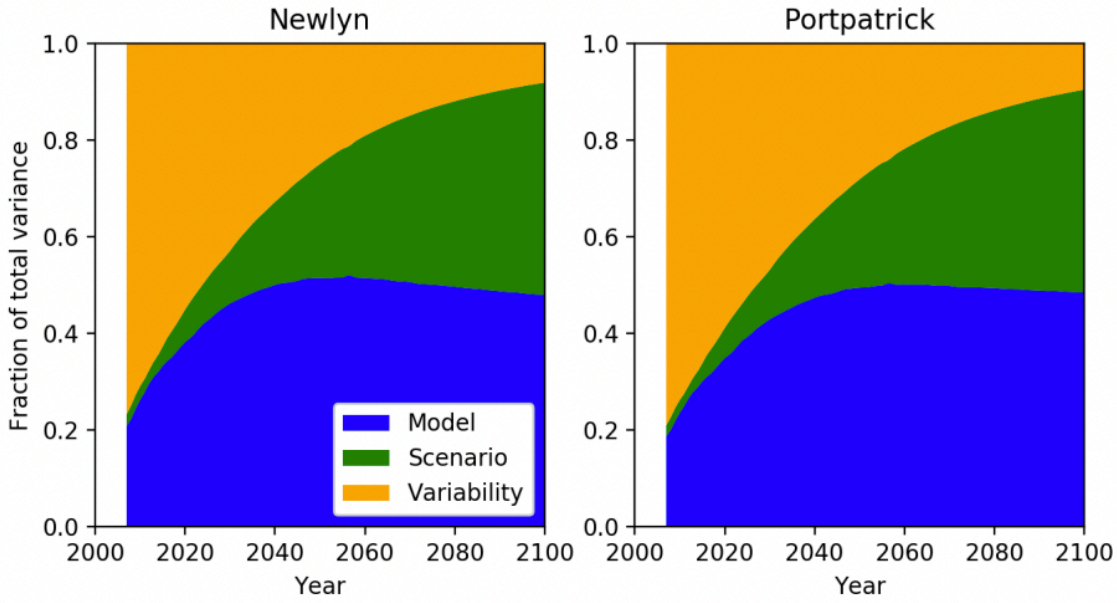

Figure 5.5: The fraction of sea level rise uncertainty for Newlyn (left) and Portpatrick (right) from: sea level variability (yellow); climate change scenario (green); and model uncertainty (blue), following Hawkins and Sutton (2011) based on annual mean data (from Palmer et al., 2018).

It is necessary to address that the uncertainty associated with the MSL component includes model, scenario, and natural variability uncertainty because it directly stems from the SSP2-4.5 projection from AR6. While a true direct comparison would involve separating the MSL uncertainty into individual components, the comparison here is still valuable. A critical point of consideration is that NAO-SL uncertainty represents uncertainty in a highly variable sea-level component, which would typically be incorporated into natural variability uncertainty. However, the approach used in this study produces NAO-SL uncertainty that is predominantly model-based but also highly variable, suggesting high variance in the spread of the model output.

5.4 Limitations and future work

5.4.1 Limitations

When using this type of budget-based approach, consideration should be made of the combination of components included in the projection and also the interactions occurring between those components, both in the physical climate-ocean systems and within the model output. In projection frameworks it can

be common practice for components to be treated as independent of each other (e.g., Kopp et al., 2014), but this does not capture the complex dynamics of sea level and climate systems in reality. By assuming components are independent, the modelling process becomes simpler when making projections. In this study, the individual MSL, annual and NAO-SL components were accordingly treated as independent when combined to form the total seasonal projection, partly for simplicity and also because some interdependencies could not be accounted for. For example, the CMIP6 MSL component is made up of individual elements, described in detail in section 2.3.1, and crucially contains a DSLC component (Slangen *et al.*, 2023). This is the component most likely to interact with the annual and NAO-SL signals, as DSLC captures short-term variations in circulation and density that are driven by oceanic and climatological processes. It is possible that sub-annual changes in DSLC could enhance or dampen SLC represented in both the annual and NAO-SL components, and likewise fluctuations in the NAO could illicit a response in DSLC, because the NAO affects atmospheric pressure patterns over the NWES (Delworth and Zeng, 2016; X. Wang et al., 2017). However, as DSLC here is contained within the MSL component, it is not possible using the methodology in this study to account for the interactions between DSLC and the other components. These complex interactions within the oceanic-atmospheric system are not fully captured within most existing climate models anyway; this is an area that is a work in progress within climate modelling.

Summing the uncertainties in quadrature maintained consistency in the treatment of both the components and their uncertainties, but doing so also carries some assumptions. As with the combining of the sea-level components themselves, combining uncertainties in quadrature assumes that the individual sources of uncertainty are statistically independent and accordingly produces a singular estimate of uncertainty, which does not reflect the cross-correlations that will exist between uncertainties here. An approach that could be taken to improve on this would be to use a probabilistic framework to produce more realistic uncertainty quantiles (e.g., Kopp *et al.*, 2014; Grinsted *et al.*, 2015; Jackson and Jevrejeva, 2016), from which could be sampled to produce uncertainty bounds that better represent the contribution of each source to total uncertainty.

There are a number of stationarity assumptions to consider too. Both the annual cycle and the sea level/NAO coefficients are fixed for each location over the time period, which does not accurately reflect the behaviour of either component. Interannual variations in the annual cycle have been observed in sea-level data and successfully represented in model output (e.g., Amiruddin et al., 2015; Calafat et al., 2018). The potential magnitude of annual cycle fluctuations would increase the relative contribution of the

annual cycle to total seasonal SLC. Using fixed coefficients has the same consequence; assessing whether the coefficients change significantly for stronger or weaker NAO phases would be another step to producing a more detailed picture of future seasonal SLC.

5.4.2 Evaluation of the budget approach and further work

The flexibility of the budget approach lies in its adaptability to region-specific geographical and climatic conditions, making it an adaptable methodology for seasonal sea-level projections. Using large-scale climate oscillations, such as the NAO, as the driver of seasonal SLC is a key aspect of the budget approach which makes it flexible. The method could be applied to other regions in the world where climate oscillations also play a major role in SLC. For example, in regions where ENSO is dominant, an ENSO-driven projection would be a viable and valuable component of the future sea-level 'budget'. This adaptable element of the method allows for regional projections to be made based on the dominant climatic conditions in a region, thus enhancing the accuracy of short-term sea-level predictions.

In addition to the adaptability given by utilizing large-scale climate oscillations, applying a budget-based framework to projections offers a way of generating projections at numerous timescales. By the approach being based on combining components, it can be applied to a specific spatial area and timescale by taking the appropriate components and their uncertainties and combining them in an appropriate way to give a picture of potential water levels.

The versatility offered by this methodology is advantageous for decision-makers and stakeholders, who require region-specific predictions of potential water levels at short timescales in order to implement informed responses to coastal hazards (Miles *et al.*, 2014). Having informed mitigation frameworks to cope with short-term SLC is crucial in key sectors such as coastal infrastructure, urban centres, transport networks, land-use planning, tourism, and agriculture. The utility of seasonal projections for these areas becomes apparent in the prediction of potential extreme water levels. By combining seasonal projections, such as those in Figure 4.7, with predictions of extreme water levels, tidal water levels and the underlying level of MSL rise for a specific region, projections of short-term SLC reflect the influence of all relevant components alongside their uncertainties. The projections produced in this study offer a robust example of this approach, and with some development, particularly when it comes to combining the components to account for interactions between them, could be a useful source of information that allows stakeholders to implement strategies that are relevant to the physical characteristics of different regions.

Chapter 6: Conclusions

This study has produced a comprehensive set of seasonal sea-level projections for the NWES for the period 2023-2053 and contributes to the research effort dedicated to better predicting future patterns of SLC. The projections were developed using a method that projects individual sea-level components and their uncertainties, before integrating the components to provide a projection at seasonal time steps. A key feature of the approach is the use of observed atmospheric-oceanic relationships to quantify and project the seasonal component. Specifically, large-scale climate oscillations are treated as the main driver of seasonal change, which for the NWES is the NAO. The approach is based on elements of the sea-level budget concept, as well as existing projection methods such as the process-based and semi-empirical approaches, and it incorporates observed and modelled climate and sea-level data from TGs, CMIP6 and reanalysis products. The projections were built upon regional MSL projections from CMIP6 under SSP2-4.5. The main findings of the study can be summarised in accordance with the research questions originally outlined in section 1.3:

1. In the first stage of the study, the effect of data availability in TG records on observed relationships between sea level and the NAO index was explored. In an analysis of 82 TG records, it was observed that data gaps do impact correlation coefficients between sea level and the NAO, but the effect is small, only ± 0.15 from the baseline coefficient that represents a 100% complete record. This suggests that in analyses using high-frequency temporal scales, like seasonal or monthly time steps, data gaps have a low impact on the relationships observed within TG records. Further on in the projection phase of the study, this increases confidence in using the observed relationships between sea level and the NAO to quantify the seasonal component.
2. The main aim of the study, namely, to project seasonal SLC, was supported by an assessment of the relationship between sea level and the NAO over two periods: 1950-2021 and 1993-2021. A clear pattern of winter correlations emerges, with a transition from positive correlations between the NAO and MSL for TGs in the north-east to negative correlations for TGs in the south-west. The typically weaker correlations seen in spring and autumn were also valuable for providing insight on the effect of NAO on sea level in the seasonal transitions between the NAO-dominant seasons of winter and summer. The main difference between correlations in the two time periods was a higher number of significant correlations for 1993-2021. This was mainly attributed to the 1950-2021 period being subject to more gaps in data.

3. The projections of seasonal SLC for the 11 TG sites demonstrate a novel way of assessing SLC for high frequency temporal scales and over regional spatial scales. Seasonal amplitudes between ±0.1 m to ±0.4 m across the four defined seasons are predicted across the NWES, and comparison of the projections with existing research, and with the past trajectory of SLC recorded in TG records, reveals similarities in the projected patterns of SLC, which suggests the approach is robust. The uncertainty quantified in the projections reflects uncertainty originating from the data used, the method itself, and inherent variability in the climate system. Uncertainty from the NAO-SL component dominates total uncertainty for sites where the seasonal amplitude is large and creates a seasonal fluctuation present in uncertainty for all sites.

The limitations associated with the projections are also addressed. These include assuming independence between the components in the projection and between the different sources of uncertainty, assumptions of stationarity, and limitations in model output. By refining the method to reduce the impact of these limitations, projections could be produced with reduced uncertainties. Overall, the strength of this adaptable approach is underpinned by its ability to generate regional projections based on the prevailing or dominant climatic conditions in a given region, and it provides decision-makers with a tool to inform appropriate policy and future planning.

Appendix A: Calculation of the projected NAO index using the CRU method

The main adjustment made to the CRU method was in how the NAO was defined. In the CRU method, the NAO is calculated as the difference between a southern station (e.g., Lisbon, Gibraltar, Ponta Delgada) and a northern station (e.g. Reykjavik, SW Iceland). This station- or 'point-' based approach is effective because CRU use observed SLP data to calculate the index. However, in this study, monthly CMIP6-generated SLP data are used to generate an NAO index for future time periods. When using this type of gridded model data, a box-based method is more effective. This is where the NAO is defined using mean SLP spatially averaged over a latitude-longitude defined southern box (90°W–60°E, 20°N–55°N) and northern box (90°W–60°E, 55°N–90°N). This approach was first used by Stephenson et al. (2006) and subsequently used in model-based studies of the NAO (e.g., Baker et al., 2018; McKenna and Maycock, 2021). This area-average definition is effective when using model-based data because it remains robust to changes in the position of centres of action in the observations and models (Hurrell *et al.*, 2003; Stephenson *et al.*, 2006).

For the southern (*S*) and northern (*N*) boxes, the ensemble mean of the monthly SLP data from the 41 CMIP6 ensemble member means were calculated to give S_{μ} and N_{μ} at each time step (Figure A1). $S_{\mu,m,y}$ represents mean SLP in month *m* and year *y* for the southern box and $N_{\mu,m,y}$ represents the same for the northern box.

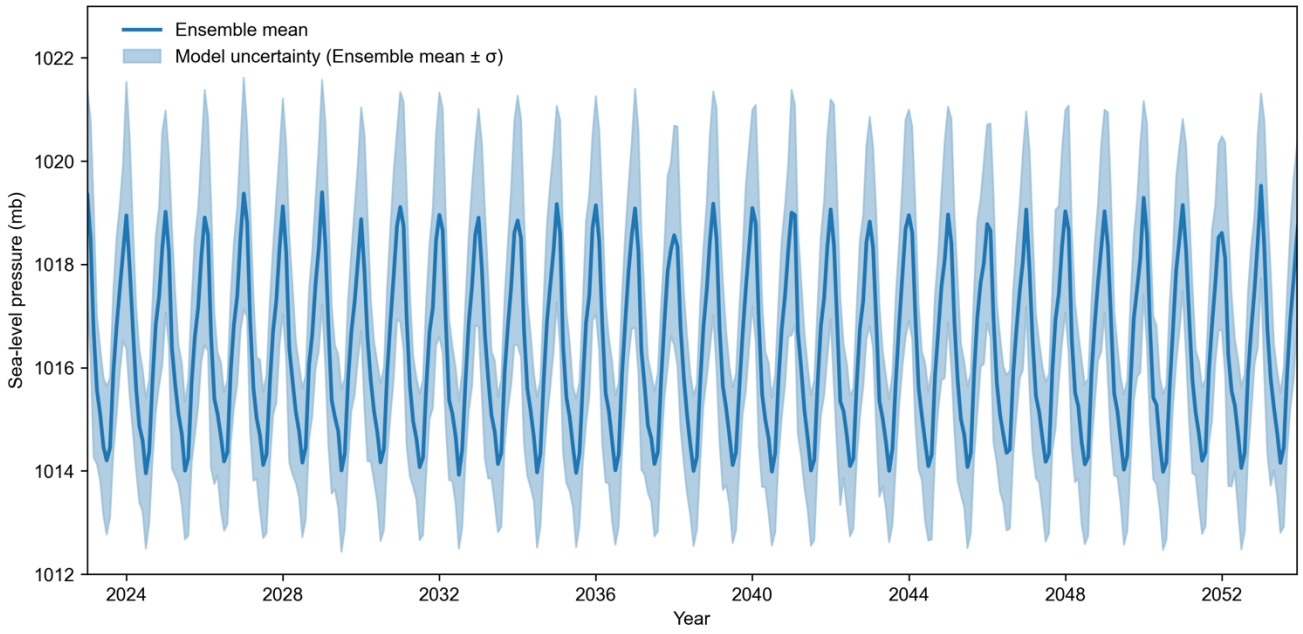

Figure A1: The ensemble mean calculated from the 41 individual CMIP6 SLP ensemble member means for the southern box S_{μ}. The uncertainty bounds are the ensemble mean ± the standard deviation (σ) of the ensemble member means.

To normalise the SLP_μ time series for each box, the mean and standard deviation were computed for each month of the year using values from the reference period 1995-2014 (in line with the reference period used in the CMIP6 sea-level projections). The mean was calculated as follows:

$$\overline{S_{\mu,m}} = \left(\sum_{y=1995}^{y=2014} S_{\mu,m,y} \right) / n$$

(12)

The standard deviation was calculated as:

$$\sigma_{S_{\mu,\mathrm{m}}} = \sqrt{\frac{1}{n-1} \sum_{y=1995}^{y=2014} \left(S_{\mu,m,y} - \overline{S_{\mu,m}} \right)^2}$$

(13)

The same calculations were carried out for N_μ. The SLP_μ time series was then normalised by subtracting the mean and dividing by the standard deviation for the appropriate month:

$$S'_{\mu,m,y} = \left(S_{\mu,m,y} - \overline{S_{\mu,m}} \right) / \sigma_{S_{\mu,m}}$$

(14)

and similarly for N_μ (Figure A2 shows the normalised series for the southern box). The monthly NAO index was then calculated by differencing the two normalised series:

$$NAO_{m,y} = S'_{\mu,m,y} - N'_{\mu,m,y}$$

(15)

Figure A3 shows the time series of the projected NAO index. The time steps in the NAO index then needed to be transformed from monthly values to seasonal values (three-month averages) to allow a seasonal projection to be made later on. The averages were computed according to the month groupings previously outlined in section 3.3.2.

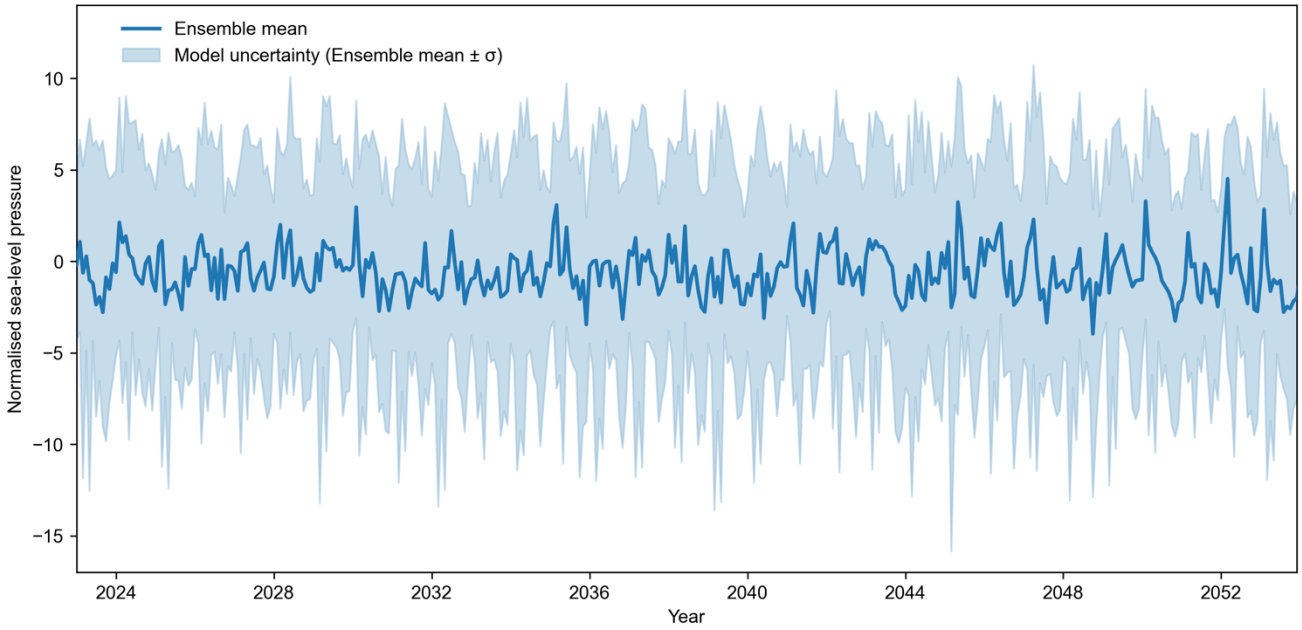

Figure A2: The ensemble mean and uncertainty bounds normalised for the southern box.

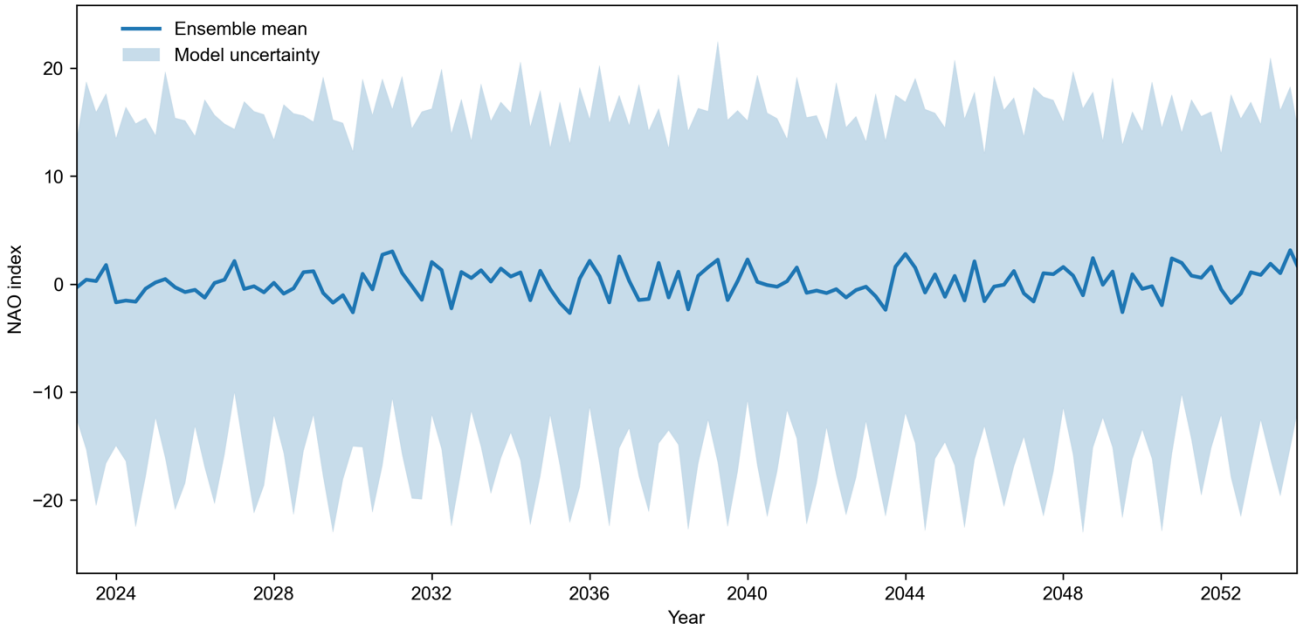

Figure A3: The projected NAO index. The blue line is the NAO index calculated from the SLP ensemble mean. The way in which model uncertainty has been propagated through is described in within the Appendix.

To estimate the uncertainty resulting from the model spread through the process of calculating the NAO, first the standard deviation was calculated across the 41 CMIP6 ensemble member means to give SLP_{σ} at each time step. In order to propagate this model uncertainty through the NAO calculation, two time series were created to represent the upper and lower uncertainty bounds: $SLP_{\mu+\sigma}$ and $SLP_{\mu-\sigma}$. The process completed above was repeated for $SLP_{\mu+\sigma}$ and $SLP_{\mu-\sigma}$ for each box. Each series was normalised using the mean and standard deviation of SLP_{μ}. The normalised upper and lower bounds for each box were then combined in the following manner to calculate upper and lower NAO bounds:

$$NAO + \sigma_{m,y} = S'_{\mu+\sigma,m,y} - N'_{\mu-\sigma,m,y}$$

(16),

$$NAO - \sigma_{m,y} = S'_{\mu-\sigma,m,y} - N'_{\mu+\sigma,m,y}$$

(17)

These upper and lower uncertainty bounds represent the maximum range of sea level driven by the NAO as predicted by the combined magnitude of the coefficient and the projected NAO. Lastly, the mean of $NAO + \sigma$ and $NAO - \sigma$ was computed to find a final value for model uncertainty.

References

Van Alphen, J. (2016) 'The Delta Programme and updated flood risk management policies in the Netherlands', *Journal of Flood Risk Management*. John Wiley & Sons, Ltd, 9(4), pp. 310–319. doi: 10.1111/JFR3.12183.

Amiruddin, A. M., Haigh, I. D., Tsimplis, M. N., Calafat, F. M. and Dangendorf, S. (2015) 'The seasonal cycle and variability of sea level in the South China Sea', *Journal of Geophysical Research: Oceans*. John Wiley & Sons, Ltd, 120(8), pp. 5490–5513. doi: 10.1002/2015JC010923.

Baker, L. H., Shaffrey, L. C., Sutton, R. T., Weisheimer, A. and Scaife, A. A. (2018) 'An Intercomparison of Skill and Overconfidence/Underconfidence of the Wintertime North Atlantic Oscillation in Multimodel Seasonal Forecasts', *Geophysical Research Letters*. John Wiley & Sons, Ltd, 45(15), pp. 7808–7817. doi: 10.1029/2018GL078838.

Bamber, J. L., Westaway, R. M., Marzeion, B. and Wouters, B. (2018) 'The land ice contribution to sea level during the satellite era', *Environmental Research Letters*. IOP Publishing, 13(6), p. 063008. doi: 10.1088/1748-9326/AAC2F0.

Barnston, A. G. and Livezey, R. E. (1987) 'Classification, Seasonality and Persistence of Low-Frequency Atmospheric Circulation Patterns', *Monthly Weather Review*, 115(6), pp. 1083–1126. doi: https://doi.org/10.1175/1520-0493(1987)115<1083:CSAPOL>2.0.CO;2.

Le Bars, D., Drijfhout, S. and De Vries, H. (2017) 'A high-end sea level rise probabilistic projection including rapid Antarctic ice sheet mass loss', *Environmental Research Letters*. IOP Publishing, 12(4), p. 044013. doi: 10.1088/1748-9326/AA6512.

Becker, M., Meyssignac, B., Letetrel, C., Llovel, W., Cazenave, A. and Delcroix, T. (2012) 'Sea level variations at tropical Pacific islands since 1950', *Global and Planetary Change*. Elsevier, 80–81, pp. 85–98. doi: 10.1016/J.GLOPLACHA.2011.09.004.

Boening, C., Willis, J. K., Landerer, F. W., Nerem, R. S. and Fasullo, J. (2012) 'The 2011 La Nina: So strong, the oceans fell', *Geophysical Research Letters*, 39(19), pp. 1–5. doi: 10.1029/2012GL053055.

Bracegirdle, T. J., Lu, H., Eade, R. and Woollings, T. (2018) 'Do CMIP5 Models Reproduce Observed Low-Frequency North Atlantic Jet Variability?', *Geophysical Research Letters*. John Wiley & Sons, Ltd, 45(14), pp. 7204–7212. doi: 10.1029/2018GL078965.

Brands, S. (2022) ‘Common Error Patterns in the Regional Atmospheric Circulation Simulated by the CMIP Multi-Model Ensemble’, *Geophysical Research Letters*. John Wiley & Sons, Ltd, 49(23), p. e2022GL101446. doi: 10.1029/2022GL101446.

Calafat, F. M., Chambers, D. P. and Tsimplis, M. N. (2012) ‘Mechanisms of decadal sea level variability in the eastern North Atlantic and the Mediterranean Sea’, *Journal of Geophysical Research: Oceans*, 117(9), pp. 1–14. doi: 10.1029/2012JC008285.

Calafat, F. M., Wahl, T., Lindsten, F., Williams, J. and Frajka-Williams, E. (2018) ‘Coherent modulation of the sea-level annual cycle in the United States by Atlantic Rossby waves’, *Nature Communications 2018 9:1*. Nature Publishing Group, 9(1), pp. 1–13. doi: 10.1038/s41467-018-04898-y.

Camargo, C. M. L., Riva, R. E. M., Hermans, T. H. J., Schütt, E. M., Marcos, M., Hernandez-Carrasco, I. and Slangen, A. B. A. (2023) ‘Regionalizing the sea-level budget with machine learning techniques’, *Ocean Science*. Copernicus Publications, 19(1), pp. 17–41. doi: 10.5194/OS-19-17-2023.

Carson, M., Lyu, K., Richter, K., Becker, M., Domingues, C. M., Han, W. and Zanna, L. (2019) ‘Climate Model Uncertainty and Trend Detection in Regional Sea Level Projections: A Review’, *Surveys in Geophysics 2019 40:6*. Springer, 40(6), pp. 1631–1653. doi: 10.1007/S10712-019-09559-3.

Chen, X., Dangendorf, S., Narayan, N., O’Driscoll, K., Tsimplis, M. N., Su, J., Mayer, B. and Pohlmann, T. (2014) ‘On sea level change in the North Sea influenced by the North Atlantic Oscillation: Local and remote steric effects’, *Estuarine, Coastal and Shelf Science*. Academic Press, 151, pp. 186–195. doi: 10.1016/J.ECSS.2014.10.009.

Cheng, L. and Zhu, J. (2016) ‘Benefits of CMIP5 Multimodel Ensemble in Reconstructing Historical Ocean Subsurface Temperature Variations’, *Journal of Climate*. American Meteorological Society, 29(15), pp. 5393–5416. doi: 10.1175/JCLI-D-15-0730.1.

Christodoulou, A., Christidis, P. and Demirel, H. (2019) ‘Sea-level rise in ports: a wider focus on impacts’, *Maritime Economics and Logistics*. Palgrave Macmillan Ltd., 21(4), pp. 482–496. doi: 10.1057/S41278-018-0114-Z/FIGURES/5.

Church, J. A., Gregory, J. M., Cazenave, A., Gregory, J. M., Jevrejeva, S., Levermann, A., Merrifield, M. A., Milne, G. A., Nerem, R. S., Nunn, P. D., Payne, A. J., Pfeffer, W. T., Stammer, D., Unnikrishnan, A. S. and Contributing (2013) ‘Sea Level Change. In: Climate Change 2013: The Physical Science Basis.’, *Contribution of Working Group I to the Fifth Assessment Report of the Intergovernmental Panel on Climate Change*.

Church, J. A. and White, N. J. (2011) 'Sea-Level Rise from the Late 19th to the Early 21st Century', *Surveys in Geophysics*, 32(4–5), pp. 585–602. doi: 10.1007/s10712-011-9119-1.

Church, J. A., White, N. J., Coleman, R., Lambeck, K. and Mitrovica, J. X. (2004) *Estimates of the Regional Distribution of Sea Level Rise over the 1950-2000 Period*. Available at: http://www.pol.ac.uk/psmsl/.

Le Cozannet, G., Manceau, J. C. and Rohmer, J. (2017) 'Bounding probabilistic sea-level projections within the framework of the possibility theory', *Environmental Research Letters*. IOP Publishing, 12(1), p. 014012. doi: 10.1088/1748-9326/AA5528.

Cusinato, E., Rubino, A. and Zanchettin, D. (2021) 'Winter Euro-Atlantic Climate Modes: Future Scenarios From a CMIP6 Multi-Model Ensemble', *Geophysical Research Letters*. John Wiley & Sons, Ltd, 48(19), p. e2021GL094532. doi: 10.1029/2021GL094532.

Dangendorf, S., Calafat, F. M., Arns, A., Wahl, T., Haigh, I. D. and Jensen, J. (2014) 'Mean sea level variability in the North Sea: Processes and implications', *Journal of Geophysical Research: Oceans*. John Wiley & Sons, Ltd, 119(10), pp. 6820–6841. doi: 10.1002/2014JC009901.

Dangendorf, S., Hay, C., Calafat, F. M., Marcos, M., Piecuch, C. G., Berk, K. and Jensen, J. (2019) 'Persistent acceleration in global sea-level rise since the 1960s', *Nature Climate Change*. Nature Publishing Group, 9(9), pp. 705–710. doi: 10.1038/s41558-019-0531-8.

Dangendorf, S., Mudersbach, C., Wahl, T. and Jensen, J. (2013) 'Characteristics of intra-, inter-annual and decadal sea-level variability and the role of meteorological forcing: The long record of Cuxhaven', *Ocean Dynamics*. Springer, 63(2–3), pp. 209–224. doi: 10.1007/S10236-013-0598-0/FIGURES/9.

Dangendorf, S., Wahl, T., Hein, H., Jensen, J., Mai, S. and Mudersbach, C. (2012) 'Mean Sea Level Variability and Influence of the North Atlantic Oscillation on Long-Term Trends in the German Bight', *Water 2012, Vol. 4, Pages 170-195*. Molecular Diversity Preservation International, 4(1), pp. 170–195. doi: 10.3390/W4010170.

Davini, P. and Cagnazzo, C. (2014) 'On the misinterpretation of the North Atlantic Oscillation in CMIP5 models', *Climate Dynamics*. Springer Verlag, 43(5–6), pp. 1497–1511. doi: 10.1007/S00382-013-1970-Y/FIGURES/8.

DeConto, R. M., Pollard, D., Alley, R. B., Velicogna, I., Gasson, E., Gomez, N., Sadai, S., Condron, A., Gilford, D. M., Ashe, E. L., Kopp, R. E., Li, D. and Dutton, A. (2021) 'The Paris Climate Agreement

and future sea-level rise from Antarctica', *Nature 2021 593:7857*. Nature Publishing Group, 593(7857), pp. 83–89. doi: 10.1038/s41586-021-03427-0.

Delworth, T. L. and Zeng, F. (2016) 'The Impact of the North Atlantic Oscillation on Climate through Its Influence on the Atlantic Meridional Overturning Circulation', *Journal of Climate*. American Meteorological Society, 29(3), pp. 941–962. doi: 10.1175/JCLI-D-15-0396.1.

Deser, C., Phillips, A., Bourdette, V. and Teng, H. (2012) 'Uncertainty in climate change projections: The role of internal variability', *Climate Dynamics*. Springer, 38(3–4), pp. 527–546. doi: 10.1007/S00382-010-0977-X/FIGURES/17.

Dong, B., Sutton, R. T. and Woollings, T. (2011) 'Changes of interannual NAO variability in response to greenhouse gases forcing', *Climate Dynamics*, 37(7–8), pp. 1621–1641. doi: 10.1007/s00382-010-0936-6.

Eden, C. and Jung, T. (2001) 'North Atlantic Interdecadal Variability: Oceanic Response to the North Atlantic Oscillation (1865-1997)', *Journal of Climate*, 14(5). Available at: www.ifm.uni-kiel.de/to/flame/.

European Commission, Joint Research Centre, Ciscar, J., Feyen, L., Ibarreta, D. and Soria, A. (2018) *Climate impacts in Europe : final report of the JRC PESETA III project*. Edited by A. Soria. Publications Office. doi: doi/10.2760/93257.

Eyring, V., Bony, S., Meehl, G. A., Senior, C. A., Stevens, B., Stouffer, R. J. and Taylor, K. E. (2016) 'Overview of the Coupled Model Intercomparison Project Phase 6 (CMIP6) experimental design and organization', *Geoscientific Model Development*. Copernicus GmbH, 9(5), pp. 1937–1958. doi: 10.5194/GMD-9-1937-2016.

Feliks, Y., Small, J. and Ghil, M. (2021) 'Global oscillatory modes in high-end climate modeling and reanalyses', *Climate Dynamics 2021 57:11*. Springer, 57(11), pp. 3385–3411. doi: 10.1007/S00382-021-05872-Z.

Ferrero, B., Tonelli, M., Marcello, F. and Wainer, I. (2021) 'Long-term Regional Dynamic Sea Level Changes from CMIP6 Projections', *Advances in Atmospheric Sciences*, 38(2), pp. 157–167. doi: 10.1007/s00376-020-0178-4.

Fox-Kemper, B., Hewitt, H. T., Xiao, C., Aðalgeirsdóttir, G., Drijfhout, S. S., Edwards, T. L., Golledge, N. R., M. Hemer, R. E., Kopp, Krinner, G., Mix, A., Notz, D., Nowicki, S., Nurhati, I. S., Ruiz, L., Sallée,

J.-B., Slangen, A. B. A. and Yu, Y. (2022) 'Ocean, Cryosphere and Sea Level Change', in *Climate Change 2021: The Physical Science Basis. Contribution of Working Group I to the Sixth Assessment Report of the Intergovernmental Panel on Climate Change [MassonDelmotte, V., P. Zhai, A. Pirani, S.L. Connors, C. Péan, S. Berger, N. Caud, Y. Chen, L*. Cambridge University Press.

Frederikse, T., Landerer, F. and Caron, L. (2019) 'The imprints of contemporary mass redistribution on local sea level and vertical land motion observations', *Solid Earth*. Copernicus GmbH, 10(6), pp. 1971–1987. doi: 10.5194/SE-10-1971-2019.

Frederikse, T., Landerer, F., Caron, L., Adhikari, S., Parkes, D., Humphrey, V. W., Dangendorf, S., Hogarth, P., Zanna, L., Cheng, L. and Wu, Y. H. (2020) 'The causes of sea-level rise since 1900', *Nature*. Springer US, 584(7821), pp. 393–397. doi: 10.1038/s41586-020-2591-3.

Freitas, A., Bernardino, M. and Guedes Soares, C. (2022) 'The influence of the Arctic Oscillation on North Atlantic wind and wave climate by the end of the 21st century', *Ocean Engineering*. Pergamon, 246, p. 110634. doi: 10.1016/J.OCEANENG.2022.110634.

Gerkema, T. (2019) 'An Introduction to Tides', *An Introduction to Tides*. Cambridge University Press, pp. 1–214. doi: 10.1017/9781316998793.

Gil, E. and de Toro, C. (2005) 'Improving tide-gauge data processing: A method involving tidal frequencies and inverted barometer effect', *Computers & Geosciences*. Pergamon, 31(8), pp. 1048–1058. doi: 10.1016/J.CAGEO.2005.02.006.

Gillett, N. P., Graf, H. F. and Osborn, T. J. (2003) 'Climate Change and the North Atlantic Oscillation', *Geophysical Monograph Series*. American Geophysical Union (AGU), 134, pp. 193–209. doi: 10.1029/134GM09.

Gregory, J. M., Griffies, S. M., Hughes, C. W., Lowe, J. A., Church, J. A., Fukimori, I., Gomez, N., Kopp, R. E., Landerer, F., Cozannet, G. Le, Ponte, R. M., Stammer, D., Tamisiea, M. E. and van de Wal, R. S. W. (2019) 'Concepts and Terminology for Sea Level: Mean, Variability and Change, Both Local and Global', *Surveys in Geophysics*, pp. 1251–1289. doi: 10.1007/s10712-019-09525-z.

Gregory, J. M., White, N. J., Church, J. A., Bierkens, M. F. P., Box, J. E., Van Den Broeke, M. R., Cogley, J. G., Fettweis, X., Hanna, E., Huybrechts, P., Konikow, L. F., Leclercq, P. W., Marzeion, B., Oerlemans, J., Tamisiea, M. E., Wada, Y., Wake, L. M. and Van De Wal, R. S. W. (2013) 'Twentieth-century global-mean sea level rise: Is the whole greater than the sum of the parts?', *Journal of Climate*, 26(13), pp. 4476–4499. doi: 10.1175/JCLI-D-12-00319.1.

Grinsted, A., Jevrejeva, S., Riva, R. E. M. and Dahl-Jensen, D. (2015) 'Sea level rise projections for northern Europe under RCP8.5', *Climate Research*. Inter-Research, 64(1), pp. 15–23. doi: 10.3354/CR01309.

Hague, B. S., Jones, D. A., Trewin, B., Jakob, D., Murphy, B. F., Martin, D. J. and Braganza, K. (2022) 'ANCHORS: A multi-decadal tide gauge dataset to monitor Australian relative sea level changes', *Geoscience Data Journal*. John Wiley & Sons, Ltd, 9(2), pp. 256–272. doi: 10.1002/GDJ3.136.

Hamlington, B. D., Leben, R. R., Nerem, R. S., Han, W. and Kim, K. Y. (2011) 'Reconstructing sea level using cyclostationary empirical orthogonal functions', *Journal of Geophysical Research: Oceans*. John Wiley & Sons, Ltd, 116(C12), p. 12015. doi: 10.1029/2011JC007529.

Hamlington, B. D. and Thompson, P. R. (2015) 'Considerations for estimating the 20th century trend in global mean sea level', *Geophysical Research Letters*. John Wiley & Sons, Ltd, 42(10), pp. 4102–4109. doi: 10.1002/2015GL064177.

Hawkins, E. and Sutton, R. (2009) 'The Potential to Narrow Uncertainty in Regional Climate Predictions', *Bulletin of the American Meteorological Society*. American Meteorological Society, 90(8), pp. 1095–1108. doi: 10.1175/2009BAMS2607.1.

Hawkins, E. and Sutton, R. (2011) 'The potential to narrow uncertainty in projections of regional precipitation change', *Climate Dynamics*. Springer, 37(1), pp. 407–418. doi: 10.1007/S00382-010-0810-6/FIGURES/8.

Hay, C. C., Morrow, E., Kopp, R. E. and Mitrovica, J. X. (2015) 'Probabilistic reanalysis of twentieth-century sea-level rise', *Nature 2015 517:7535*. Nature Publishing Group, 517(7535), pp. 481–484. doi: 10.1038/nature14093.

Hermans, T. H. J., Katsman, C. A., Camargo, C. M. L., Garner, G. G., Kopp, R. E. and Slangen, A. B. A. (2022) 'The Effect of Wind Stress on Seasonal Sea-Level Change on the Northwestern European Shelf', *Journal of Climate*, 35(6), pp. 1745–1759. doi: 10.1175/JCLI-D-21-0636.1.

Hermans, T. H. J., Tinker, J., Palmer, M. D., Katsman, C. A., Vermeersen, B. L. A. and Slangen, A. B. A. (2020) 'Improving sea-level projections on the Northwestern European shelf using dynamical downscaling', *Climate Dynamics*. Springer, 54(3–4), pp. 1987–2011. doi: 10.1007/S00382-019-05104-5/FIGURES/15.

Hersbach, H., Bell, B., Berrisford, P., Hirahara, S., Horányi, A., Muñoz-Sabater, J., Nicolas, J., Peubey, C., Radu, R., Schepers, D., Simmons, A., Soci, C., Abdalla, S., Abellan, X., Balsamo, G., Bechtold, P., Biavati, G., Bidlot, J., Bonavita, M., De Chiara, G., Dahlgren, P., Dee, D., Diamantakis, M., Dragani, R., Flemming, J., Forbes, R., Fuentes, M., Geer, A., Haimberger, L., Healy, S., Hogan, R. J., Hólm, E., Janisková, M., Keeley, S., Laloyaux, P., Lopez, P., Lupu, C., Radnoti, G., de Rosnay, P., Rozum, I., Vamborg, F., Villaume, S. and Thépaut, J. N. (2017) *Complete ERA5 from 1940: Fifth generation of ECMWF atmospheric reanalyses of the global climate*, *Copernicus Climate Change Service (C3S) Data Store (CDS) (Accessed on 12-02-2023)*. John Wiley and Sons Ltd. doi: 10.24381/cds.143582cf.

Hirschfeld, D., Behar, D., Nicholls, R. J., Cahill, N., James, T., Horton, B. P., Portman, M. E., Bell, R., Campo, M., Esteban, M., Goble, B., Rahman, M., Addo, K. A., Chundeli, F. A., Aunger, M., Babitsky, O., Beal, A., Boyle, R., Fang, J., Gohar, A., Hanson, S., Karamesines, S., Kim, M. J., Lohmann, H., McInnes, K., Mimura, N., Ramsay, D., Wenger, L. and Yokoki, H. (2023) 'Global survey shows planners use widely varying sea-level rise projections for coastal adaptation', *Communications Earth & Environment 2023 4:1*. Nature Publishing Group, 4(1), pp. 1–9. doi: 10.1038/s43247-023-00703-x.

Hogarth, P., Hughes, C. W., Williams, S. D. P. and Wilson, C. (2020) 'Improved and extended tide gauge records for the British Isles leading to more consistent estimates of sea level rise and acceleration since 1958', *Progress in Oceanography*. Pergamon, 184, p. 102333. doi: 10.1016/J.POCEAN.2020.102333.

Holgate, S. J., Matthews, A., Woodworth, P. L., Rickards, L. J., Tamisiea, M. E., Bradshaw, E., Foden, P. R., Gordon, K. M., Jevrejeva, S. and Pugh, J. (2013) 'New Data Systems and Products at the Permanent Service for Mean Sea Level', *Journal of Coastal Research*. Allen Press, 29(3), pp. 493–504. doi: 10.2112/JCOASTRES-D-12-00175.1.

Howard, T., Palmer, M. D. and Bricheno, L. M. (2019) 'Contributions to 21st century projections of extreme sea-level change around the uk', *Environmental Research Communications*. IOP Publishing, 1(9). doi: 10.1088/2515-7620/ab42d7.

Humphrey, V. and Gudmundsson, L. (2019) 'GRACE-REC: A reconstruction of climate-driven water storage changes over the last century', *Earth System Science Data*. Copernicus GmbH, 11(3), pp. 1153–1170. doi: 10.5194/ESSD-11-1153-2019.

Hurrell, J. W. (1995) 'Decadal Trends in the North Atlantic Oscillation: Regional Temperatures and Precipitation', *Science*, 269(5224), pp. 676–679.

Hurrell, J. W. (2003) *NAO Index Data provieded by the Climate Analysis Section, NCAR, Boulder, USA. Updated regularly.*

Hurrell, J. W., Kushnir, Y., Ottersen, G. and Visbeck, M. (2003) 'An overview of the north atlantic oscillation', *Geophysical Monograph Series*, 134, pp. 1–35. doi: 10.1029/134GM01.

Huthnance, J., Hopkins, J., Berx, B., Dale, A., Holt, J., Hosegood, P., Inall, M., Jones, S., Loveday, B. R., Miller, P. I., Polton, J., Porter, M. and Spingys, C. (2022) 'Ocean shelf exchange, NW European shelf seas: Measurements, estimates and comparisons', *Progress in Oceanography*. Pergamon, 202, p. 102760. doi: 10.1016/J.POCEAN.2022.102760.

Jackson, L. P., Grinsted, A. and Jevrejeva, S. (2018) '21st Century Sea-Level Rise in Line with the Paris Accord', *Earth's Future*. John Wiley & Sons, Ltd, 6(2), pp. 213–229. doi: 10.1002/2017EF000688.

Jackson, L. P. and Jevrejeva, S. (2016) 'A probabilistic approach to 21st century regional sea-level projections using RCP and High-end scenarios', *Global and Planetary Change*. The Authors, 146, pp. 179–189. doi: 10.1016/j.gloplacha.2016.10.006.

Jevrejeva, S., Frederikse, T., Kopp, R. E., Le Cozannet, G., Jackson, L. P. and van de Wal, R. S. W. (2019) 'Probabilistic Sea Level Projections at the Coast by 2100', *Surveys in Geophysics 2019 40:6*. Springer, 40(6), pp. 1673–1696. doi: 10.1007/S10712-019-09550-Y.

Jevrejeva, S., Matthews, A. and Slangen, A. (2017) 'The Twentieth-Century Sea Level Budget: Recent Progress and Challenges'. Springer, Cham, pp. 301–313. doi: 10.1007/978-3-319-56490-6_13.

Jevrejeva, S., Palanisamy, H. and Jackson, L. P. (2020) 'Global mean thermosteric sea level projections by 2100 in CMIP6 climate models', *Environmental Research Letters*. IOP Publishing, 16(1), p. 014028. doi: 10.1088/1748-9326/ABCEEA.

Jones, P. D., Jonsson, T. and Wheeler, D. (1997) 'Extension to the North Atlantic Oscillation using early instrumental pressure observations from gibraltar and south-west Iceland', *International Journal of Climatology*, 17(13), pp. 1433–1450. doi: 10.1002/(sici)1097-0088(19971115)17:13<1433::aid-joc203>3.3.co;2-g.

Kim, H. J., An, S. Il, Park, J. H., Sung, M. K., Kim, D., Choi, Y. and Kim, J. S. (2023) 'North Atlantic Oscillation impact on the Atlantic Meridional Overturning Circulation shaped by the mean state', *npj Climate and Atmospheric Science 2023 6:1*. Nature Publishing Group, 6(1), pp. 1–13. doi: 10.1038/s41612-023-00354-x.

Knutti, R., Masson, D. and Gettelman, A. (2013) 'Climate model genealogy: Generation CMIP5 and how we got there', *Geophysical Research Letters*. John Wiley & Sons, Ltd, 40(6), pp. 1194–1199. doi: 10.1002/GRL.50256.

Kopp, R. E., Hay, C. C., Little, C. M. and Mitrovica, J. X. (2015) 'Geographic Variability of Sea-Level Change', *Current Climate Change Reports*. Springer, 1(3), pp. 192–204. doi: 10.1007/S40641-015-0015-5/FIGURES/4.

Kopp, R. E., Horton, R. M., Little, C. M., Mitrovica, J. X., Oppenheimer, M., Rasmussen, D. J., Strauss, B. H. and Tebaldi, C. (2014) 'Probabilistic 21st and 22nd century sea-level projections at a global network of tide-gauge sites', *Earth's Future*. John Wiley & Sons, Ltd, 2(8), pp. 383–406. doi: 10.1002/2014EF000239.

Kopp, R. E., Kemp, A. C., Bittermann, K., Horton, B. P., Donnelly, J. P., Gehrels, W. R., Hay, C. C., Mitrovica, J. X., Morrow, E. D. and Rahmstorf, S. (2016) 'Temperature-driven global sea-level variability in the Common Era', *Proceedings of the National Academy of Sciences of the United States of America*. National Academy of Sciences, 113(11), pp. E1434–E1441. doi: 10.1073/PNAS.1517056113/SUPPL_FILE/PNAS.1517056113.SD03.XLS.

Krivec, T., Kocijan, J., Perne, M., Grašic, B., Božnar, M. Z. and Mlakar, P. (2021) 'Data-driven method for the improving forecasts of local weather dynamics', *Engineering Applications of Artificial Intelligence*. Pergamon, 105, p. 104423. doi: 10.1016/J.ENGAPPAI.2021.104423.

Leduc, M., Laprise, R., de Elía, R. and Šeparović, L. (2016) 'Is Institutional Democracy a Good Proxy for Model Independence?', *Journal of Climate*. American Meteorological Society, 29(23), pp. 8301–8316. doi: 10.1175/JCLI-D-15-0761.1.

Legge, O., Johnson, M., Hicks, N., Jickells, T., Diesing, M., Aldridge, J., Andrews, J., Artioli, Y., Bakker, D. C. E., Burrows, M. T., Carr, N., Cripps, G., Felgate, S. L., Fernand, L., Greenwood, N., Hartman, S., Kröger, S., Lessin, G., Mahaffey, C., Mayor, D. J., Parker, R., Queirós, A. M., Shutler, J. D., Silva, T., Stahl, H., Tinker, J., Underwood, G. J. C., Van Der Molen, J., Wakelin, S., Weston, K. and Williamson, P. (2020) 'Carbon on the Northwest European Shelf: Contemporary Budget and Future Influences', *Frontiers in Marine Science*. Frontiers Media S.A., 7. doi: 10.3389/fmars.2020.00143.

Little, C. M., Horton, R. M., Kopp, R. E., Oppenheimer, M. and Yip, S. (2015) 'Uncertainty in Twenty-First-Century CMIP5 Sea Level Projections', *Journal of Climate*. American Meteorological Society, 28(2), pp. 838–852. doi: 10.1175/JCLI-D-14-00453.1.

Mangiarotti, S. (2007) ‘Coastal sea level trends from TOPEX-Poseidon satellite altimetry and tide gauge data in the Mediterranean Sea during the 1990s’, *Geophysical Journal International*. Oxford Academic, 170(1), pp. 132–144. doi: 10.1111/J.1365-246X.2007.03424.X/2/170-1-132-FIG009.JPEG.

Marcos, M., Marzeion, B., Dangendorf, S., Slangen, A. B. A., Palanisamy, H. and Fenoglio-Marc, L. (2017) ‘Internal Variability Versus Anthropogenic Forcing on Sea Level and Its Components’. Springer, Cham, pp. 337–356. doi: 10.1007/978-3-319-56490-6_15.

Masson, D. and Knutti, R. (2011) ‘Climate model genealogy’, *Geophysical Research Letters*. John Wiley & Sons, Ltd, 38(8), p. 8703. doi: 10.1029/2011GL046864.

Mathis, M., Elizalde, A. and Mikolajewicz, U. (2018) ‘Which complexity of regional climate system models is essential for downscaling anthropogenic climate change in the Northwest European Shelf?’, *Climate Dynamics*. Springer Verlag, 50(7–8), pp. 2637–2659. doi: 10.1007/S00382-017-3761-3/TABLES/5.

McEvoy, S., Haasnoot, M. and Biesbroek, R. (2021) ‘How are European countries planning for sea level rise?’, *Ocean & Coastal Management*. Elsevier, 203, p. 105512. doi: 10.1016/J.OCECOAMAN.2020.105512.

McIntosh, P. C., Church, J. A., Miles, E. R., Ridgway, K. and Spillman, C. M. (2015) ‘Seasonal coastal sea level prediction using a dynamical model’, *Geophysical Research Letters*. John Wiley & Sons, Ltd, 42(16), pp. 6747–6753. doi: 10.1002/2015GL065091.

McKenna, C. M. and Maycock, A. C. (2021) ‘Sources of Uncertainty in Multimodel Large Ensemble Projections of the Winter North Atlantic Oscillation’, *Geophysical Research Letters*. John Wiley & Sons, Ltd, 48(14), p. e2021GL093258. doi: 10.1029/2021GL093258.

McKenna, C. M., Maycock, A. C., Forster, P. M., Smith, C. J. and Tokarska, K. B. (2021) ‘Stringent mitigation substantially reduces risk of unprecedented near-term warming rates’, *Nature Climate Change*. Springer US, 11(2), pp. 126–131. doi: 10.1038/s41558-020-00957-9.

Mengel, M., Levermann, A., Frieler, K., Robinson, A., Marzeion, B. and Winkelmann, R. (2016) ‘Future sea level rise constrained by observations and long-term commitment’, *Proceedings of the National Academy of Sciences of the United States of America*. National Academy of Sciences, 113(10), pp. 2597–2602. doi: 10.1073/PNAS.1500515113/SUPPL_FILE/PNAS.201500515SI.PDF.

Merrifield, A. L., Brunner, L., Lorenz, R., Humphrey, V. and Knutti, R. (2023) 'Climate model Selection by Independence, Performance, and Spread (ClimSIPS v1.0.1) for regional applications', *Geoscientific Model Development*. Copernicus GmbH, 16(16), pp. 4715–4747. doi: 10.5194/GMD-16-4715-2023.

Miles, E. R., Spillman, C. M., Church, J. A. and McIntosh, P. C. (2014) 'Seasonal prediction of global sea level anomalies using an ocean–atmosphere dynamical model', *Climate Dynamics*. Springer Verlag, 43(7–8), pp. 2131–2145. doi: 10.1007/S00382-013-2039-7/FIGURES/7.

Moore, J. C., Jevrejeva, S. and Grinsted, A. (2011) 'The historical global sea-level budget', *Annals of Glaciology*. Cambridge University Press, pp. 8–14. doi: 10.3189/172756411799096196.

Neill, S. P., Hashemi, M. R. and Lewis, M. J. (2016) 'Tidal energy leasing and tidal phasing', *Renewable Energy*. Pergamon, 85, pp. 580–587. doi: 10.1016/J.RENENE.2015.07.016.

Nerem, R. S., Beckley, B. D., Fasullo, J. T., Hamlington, B. D., Masters, D. and Mitchum, G. T. (2018) 'Climate-change–driven accelerated sea-level rise detected in the altimeter era', *Proceedings of the National Academy of Sciences of the United States of America*. National Academy of Sciences, 115(9), pp. 2022–2025. doi: 10.1073/PNAS.1717312115/ASSET/7B2ADB67-3200-4483-939B-EFE5698F7511/ASSETS/GRAPHIC/PNAS.1717312115FIG03.JPEG.

Nerem, R. S., Chambers, D. P., Leuliette, E. W., Mitchum, G. T. and Giese, B. S. (1999) 'Variations in global mean sea level associated with the 1997–1998 ENSO event: Implications for measuring long term sea level change', *Geophysical Research Letters*. John Wiley & Sons, Ltd, 26(19), pp. 3005–3008. doi: 10.1029/1999GL002311.

Nicholls, R. J., Hanson, S. E., Lowe, J. A., Warrick, R. A., Lu, X. and Long, A. J. (2014) 'Sea-level scenarios for evaluating coastal impacts', *Wiley Interdisciplinary Reviews: Climate Change*. John Wiley & Sons, Ltd, 5(1), pp. 129–150. doi: 10.1002/WCC.253.

Nieves, V., Radin, C. and Camps-Valls, G. (2021) 'Predicting regional coastal sea level changes with machine learning', *Scientific Reports 2021 11:1*. Nature Publishing Group, 11(1), pp. 1–6. doi: 10.1038/s41598-021-87460-z.

O'Neill, B. C., Kriegler, E., Riahi, K., Ebi, K. L., Hallegatte, S., Carter, T. R., Mathur, R. and van Vuuren, D. P. (2014) 'A new scenario framework for climate change research: The concept of shared socioeconomic pathways', *Climatic Change*. Kluwer Academic Publishers, 122(3), pp. 387–400. doi: 10.1007/S10584-013-0905-2/TABLES/2.

Oppenheimer, M., Glavovic, B., Hinkel, J., van de Wal, R., Magnan, A. K., Abd-Elgawad, A., Cai, R., Cifuentes-Jara, M., DeConto, R. M., Ghosh, T., Hay, J., Isla, F., Marzeion, B., Meyssignac, B. and Sebesvari, Z. (2019) 'Sea Level Rise and Implications for Low Lying Islands, Coasts and Communities.', *IPCC Special Report on the Ocean and Cryosphere in a Changing Climate*, 355(6321), pp. 126–129.

Palmer, M. D., Gregory, J. M., Bagge, M., Calvert, D., Hagedoorn, J. M., Howard, T., Klemann, V., Lowe, J. A., Roberts, C. D., Slangen, A. B. A. and Spada, G. (2020) 'Exploring the Drivers of Global and Local Sea-Level Change Over the 21st Century and Beyond', *Earth's Future*. John Wiley & Sons, Ltd, 8(9), p. e2019EF001413. doi: 10.1029/2019EF001413.

Palmer, M., Howard, T., Tinker, J., Lowe, J., Bricheno, L., Calvert, D., Edwards, T., Gregory, J., Harris, G. and Krijnen, J. (2018) *UKCP18 marine report*. Met Office Hadley Centre.

Pelling, H. E., Mattias Green, J. A. and Ward, S. L. (2013) 'Modelling tides and sea-level rise: To flood or not to flood', *Ocean Modelling*, 63, pp. 21–29. doi: 10.1016/j.ocemod.2012.12.004.

Pezzulli, S., Stephenson, D. B. and Hannachi, A. (2005) 'The Variability of Seasonality', *Journal of Climate*. American Meteorological Society, 18(1), pp. 71–88. doi: 10.1175/JCLI-3256.1.

Piecuch, C. G. and Ponte, R. M. (2015) 'Inverted barometer contributions to recent sea level changes along the northeast coast of North America', *Geophysical Research Letters*. John Wiley & Sons, Ltd, 42(14), pp. 5918–5925. doi: 10.1002/2015GL064580.

Pinto, J. G. and Raible, C. C. (2012) 'Past and recent changes in the North Atlantic oscillation', *Wiley Interdisciplinary Reviews: Climate Change*, 3(1), pp. 79–90. doi: 10.1002/wcc.150.

Ponte, R. M. (2006) 'Low-frequency sea level variability and the inverted barometer effect', *Journal of Atmospheric and Oceanic Technology*, 23(4), pp. 619–629. doi: 10.1175/JTECH1864.1.

Ranger, N., Reeder, T. and Lowe, J. (2013) 'Addressing "deep" uncertainty over long-term climate in major infrastructure projects: four innovations of the Thames Estuary 2100 Project', *EURO Journal on Decision Processes*. Springer, 1(3–4), pp. 233–262. doi: 10.1007/S40070-013-0014-5/TABLES/4.

Richter, K., Nilsen, J. E. Ø. and Drange, H. (2012) 'Contributions to sea level variability along the Norwegian coast for 1960-2010', *Journal of Geophysical Research: Oceans*, 117(5), pp. 1–12. doi: 10.1029/2011JC007826.

Roberts, C. D., Calvert, D., Dunstone, N., Hermanson, L., Palmer, M. D. and Smith, D. (2016) 'On the Drivers and Predictability of Seasonal-to-Interannual Variations in Regional Sea Level', *Journal of Climate*. American Meteorological Society, 29(21), pp. 7565–7585. doi: 10.1175/JCLI-D-15-0886.1.

Robson, J., Aksenov, Y., Bracegirdle, T. J., Dimdore-Miles, O., Griffiths, P. T., Grosvenor, D. P., Hodson, D. L. R., Keeble, J., MacIntosh, C., Megann, A., Osprey, S., Povey, A. C., Schröder, D., Yang, M., Archibald, A. T., Carslaw, K. S., Gray, L., Jones, C., Kerridge, B., Knappett, D., Kuhlbrodt, T., Russo, M., Sellar, A., Siddans, R., Sinha, B., Sutton, R., Walton, J. and Wilcox, L. J. (2020) 'The Evaluation of the North Atlantic Climate System in UKESM1 Historical Simulations for CMIP6', *Journal of Advances in Modeling Earth Systems*. John Wiley & Sons, Ltd, 12(9), p. e2020MS002126. doi: 10.1029/2020MS002126.

Roy, K. and Peltier, W. R. (2015) 'Glacial isostatic adjustment, relative sea level history and mantle viscosity: reconciling relative sea level model predictions for the U.S. East coast with geological constraints', *Geophysical Journal International*. Oxford Academic, 201(2), pp. 1156–1181. doi: 10.1093/GJI/GGV066.

Royston, S., Vishwakarma, B. D., Westaway, R., Rougier, J., Sha, Z. and Bamber, J. (2020) 'Can We Resolve the Basin-Scale Sea Level Trend Budget From GRACE Ocean Mass?', *Journal of Geophysical Research: Oceans*. John Wiley & Sons, Ltd, 125(1), p. e2019JC015535. doi: 10.1029/2019JC015535.

Rummukainen, M. (2010) 'State-of-the-art with regional climate models', *Wiley Interdisciplinary Reviews: Climate Change*. John Wiley & Sons, Ltd, 1(1), pp. 82–96. doi: 10.1002/WCC.8.

Skinner, D. T., Matthews, A. J. and Stevens, D. P. (2022) 'North Atlantic Oscillation response to the Madden–Julian Oscillation in a coupled climate model', *Weather*. John Wiley & Sons, Ltd, 77(6), pp. 201–205. doi: 10.1002/WEA.4215.

Slangen, A. B. A., Katsman, C. A., van de Wal, R. S. W., Vermeersen, L. L. A. and Riva, R. E. M. (2012) 'Towards regional projections of twenty-first century sea-level change based on IPCC SRES scenarios', *Climate Dynamics*. Springer, 38(5–6), pp. 1191–1209. doi: 10.1007/S00382-011-1057-6/FIGURES/10.

Slangen, A. B. A., Palmer, M. D., Camargo, C. M. L., Church, J. A., Edwards, T. L., Hermans, T. H. J., Hewitt, H. T., Garner, G. G., Gregory, J. M., Kopp, R. E., Santos, V. M. and Wal, R. S. W. van de (2023) 'The evolution of 21st century sea-level projections from IPCC AR5 to AR6 and beyond', *Cambridge Prisms: Coastal Futures*. Cambridge University Press, 1, p. e7. doi: 10.1017/CFT.2022.8.

Slangen, A. B. A., Van De Wal, R. S. W., Wada, Y. and Vermeersen, L. L. A. (2014) 'Comparing tide gauge observations to regional patterns of sea-level change (1961-2003)', *Earth System Dynamics*, 5(1), pp. 243–255. doi: 10.5194/ESD-5-243-2014.

Song, J., Tong, G., Chao, J., Chung, J., Zhang, M., Lin, W., Zhang, T., Bentler, P. M. and Zhu, W. (2023) 'Data driven pathway analysis and forecast of global warming and sea level rise', *Scientific Reports 2023 13:1*. Nature Publishing Group, 13(1), pp. 1–14. doi: 10.1038/s41598-023-30789-4.

Stammer, D., Cazenave, A., Ponte, R. M. and Tamisiea, M. E. (2013) 'Causes for Contemporary Regional Sea Level Changes', *https://doi.org/10.1146/annurev-marine-121211-172406*. Annual Reviews , 5, pp. 21–46. doi: 10.1146/ANNUREV-MARINE-121211-172406.

Stephenson, D. B., Pavan, V., Collins, M., Junge, M. M. and Quadrelli, R. (2006) 'North Atlantic Oscillation response to transient greenhouse gas forcing and the impact on European winter climate: A CMIP2 multi-model assessment', *Climate Dynamics*. Springer, 27(4), pp. 401–420. doi: 10.1007/S00382-006-0140-X/METRICS.

Tinker, J., Krijnen, J., Wood, R., Barciela, R. and Dye, S. R. (2018) 'What are the prospects for seasonal prediction of the marine environment of the North-west European Shelf?', *Ocean Science*. Copernicus GmbH, 14(4), pp. 887–909. doi: 10.5194/OS-14-887-2018.

Tinker, J., Palmer, M. D., Copsey, D., Howard, T., Lowe, J. A. and Hermans, T. H. J. (2020) 'Dynamical downscaling of unforced interannual sea-level variability in the North-West European shelf seas', *Climate Dynamics*. Springer Berlin Heidelberg, 55(7–8), pp. 2207–2236. doi: 10.1007/s00382-020-05378-0.

Tsimplis, M. N., Shaw, A. G. P., Flather, R. A. and Woolf, D. K. (2006) 'The influence of the North Atlantic Oscillation on the sea-level around the northern European coasts reconsidered: The thermosteric effects', *Philosophical Transactions of the Royal Society A: Mathematical, Physical and Engineering Sciences*, 364(1841), pp. 845–856. doi: 10.1098/rsta.2006.1740.

Tsimplis, M. N., Woolf, D. K., Osborn, T. J., Wakelin, S., Wolf, J., Flather, R., Shaw, A. G. P., Woodworth, P., Challenor, P., Blackman, D., Pert, F., Yan, Z. and Jevrejeva, S. (2005) 'Towards a vulnerability assessment of the UK and northern European coasts: The role of regional climate variability', *Philosophical Transactions of the Royal Society A: Mathematical, Physical and Engineering Sciences*, 363(1831), pp. 1329–1358. doi: 10.1098/rsta.2005.1571.

Uehara, K., Scourse, J. D., Horsburgh, K. J., Lambeck, K. and Purcell, A. P. (2006) 'Tidal evolution of the northwest European shelf seas from the Last Glacial Maximum to the present', *Journal of Geophysical Research: Oceans*. Blackwell Publishing Ltd, 111(9). doi: 10.1029/2006JC003531.

Ullmann, A. and Monbaliu, J. (2010) 'Changes in atmospheric circulation over the North Atlantic and sea-surge variations along the Belgian coast during the twentieth century', *International Journal of Climatology*. John Wiley & Sons, Ltd, 30(4), pp. 558–568. doi: 10.1002/JOC.1904.

Visbeck, M. H., Hurrell, J. W., Polvani, L. and Cullen, H. M. (2001) 'The North Atlantic oscillation: Past, present, and future', *Proceedings of the National Academy of Sciences of the United States of America*, 98(23), pp. 12876–12877. doi: 10.1073/pnas.231391598.

Vousdoukas, M. I. , Mentaschi, L., Voukouvalas, E., Verlaan, M., Jevrejeva, S., Jackson, L. P. , and Feyen, L. (2018) 'Global probabilistic projections of extreme sea levels show intensification of coastal flood hazard', *Nature Communications 2018 9:1*. Nature Publishing Group, 9(1), pp. 1–12. doi: 10.1038/s41467-018-04692-w.

Vousdoukas, M. I., Mentaschi, L., Hinkel, J., Ward, P. J., Mongelli, I., Ciscar, J. C. and Feyen, L. (2020) 'Economic motivation for raising coastal flood defenses in Europe', *Nature Communications*. Springer US, 11(1), pp. 1–11. doi: 10.1038/s41467-020-15665-3.

Vousdoukas, M. I., Mentaschi, L., Voukouvalas, E., Bianchi, A., Dottori, F. and Feyen, L. (2018) 'Climatic and socioeconomic controls of future coastal flood risk in Europe', *Nature Climate Change 2018 8:9*. Nature Publishing Group, 8(9), pp. 776–780. doi: 10.1038/s41558-018-0260-4.

Wakelin, S. L., Holt, J. T., Blackford, J. C., Allen, J. I., Butenschön, M. and Artioli, Y. (2012) 'Modeling the carbon fluxes of the northwest European continental shelf: Validation and budgets', *Journal of Geophysical Research: Oceans*. Blackwell Publishing Ltd, 117(5). doi: 10.1029/2011JC007402.

Wakelin, S. L., Woodworth, P. L., Flather, R. A. and Williams, J. A. (2003) 'Sea-level dependence on the NAO over the NW European continental shelf', *Geophysical Research Letters*, 30(7), pp. 1–4. doi: 10.1029/2003GL017041.

Wang, L., Ting, M. and Kushner, P. J. (2017) 'A robust empirical seasonal prediction of winter NAO and surface climate', *Scientific Reports 2017 7:1*. Nature Publishing Group, 7(1), pp. 1–9. doi: 10.1038/s41598-017-00353-y.

Wang, X., Li, J., Sun, C. and Liu, T. (2017) 'NAO and its relationship with the Northern Hemisphere mean surface temperature in CMIP5 simulations', *Journal of Geophysical Research: Atmospheres*. John Wiley & Sons, Ltd, 122(8), pp. 4202–4227. doi: 10.1002/2016JD025979.

Woodworth, P. L., Flather, R. A., Williams, J. A., Wakelin, S. L. and Jevrejeva, S. (2007) 'The dependence of UK extreme sea levels and storm surges on the North Atlantic Oscillation', *Continental Shelf Research*, 27(7), pp. 935–946. doi: 10.1016/j.csr.2006.12.007.

Yan, Z., Tsimplis, M. N. and Woolf, D. (2004) 'Analysis of the relationship between the North Atlantic oscillation and sea-level changes in northwest Europe', *International Journal of Climatology*, 24(6), pp. 743–758. doi: 10.1002/JOC.1035.

Zemp, M., Huss, M., Thibert, E., Eckert, N., McNabb, R., Huber, J., Barandun, M., Machguth, H., Nussbaumer, S. U., Gärtner-Roer, I., Thomson, L., Paul, F., Maussion, F., Kutuzov, S. and Cogley, J. G. (2019) 'Global glacier mass changes and their contributions to sea-level rise from 1961 to 2016', *Nature 2019 568:7752*. Nature Publishing Group, 568(7752), pp. 382–386. doi: 10.1038/s41586-019-1071-0.